Copyright Warning & Restrictions

The copyright law of the United States (Title 17, United States Code) governs the making of photocopies or other reproductions of copyrighted material.

Under certain conditions specified in the law, libraries and archives are authorized to furnish a photocopy or other reproduction. One of these specified conditions is that the photocopy or reproduction is not to be "used for any purpose other than private study, scholarship, or research." If a, user makes a request for, or later uses, a photocopy or reproduction for purposes in excess of "fair use" that user may be liable for copyright infringement,

This institution reserves the right to refuse to accept a copying order if, in its judgment, fulfillment of the order would involve violation of copyright law.

Please Note: The author retains the copyright while the New Jersey Institute of Technology reserves the right to distribute this thesis or dissertation

Printing note: If you do not wish to print this page, then select "Pages from: first page # to: last page #" on the print dialog screen

NJIT New Jersey's Science & Technology University

The Van Houten library has removed some of the personal information and all signatures from the approval page and biographical sketches of theses and dissertations in order to protect the identity of NJIT graduates and faculty.

INFORMATION TO USERS

This manuscript has been reproduced from the microfilm master. UMI films the text directly from the original or copy submitted. Thus, some thesis and dissertation copies are in typewriter face, while others may be from any type of computer printer.

The quality of this reproduction is dependent upon the quality of the copy submitted. Broken or indistinct print, colored or poor quality illustrations and photographs, print bleedthrough, substandard margins, and improper alignment can adversely affect reproduction.

In the unlikely event that the author did not send UMI a complete manuscript and there are missing pages, these will be noted. Also, if unauthorized copyright material had to be removed, a note will indicate the deletion.

Oversize materials (e.g., maps, drawings, charts) are reproduced by sectioning the original, beginning at the upper left-hand corner and continuing from left to right in equal sections with small overlaps. Each original is also photographed in one exposure and is included in reduced form at the back of the book.

Photographs included in the original manuscript have been reproduced xerographically in this copy. Higher quality 6" x 9" black and white photographic prints are available for any photographs or illustrations appearing in this copy for an additional charge. Contact UMI directly to order.

U·M·I

University Microfilms International
A Bell & Howell Information Company
300 North Zeeb Road, Ann Arbor, MI 48106-1346 USA
313/761-4700 800/521-0600

Reproduced with permission of the copyright owner. Further reproduction prohibited without permission.

Reproduced with permission of the copyright owner. Further reproduction prohibited without permission.

Order Number 9401733

Tensile behavior of concrete and mortar under direct impact tensile load

Emad, Kayumars, Ph.D.

New Jersey Institute of Technology, 1993

Copyright ©1993 by Emad, Kayumars. All rights reserved.

U·M·I
300 N. Zeeb Rd.
Ann Arbor, MI 48106

Reproduced with permission of the copyright owner. Further reproduction prohibited without permission.

Reproduced with permission of the copyright owner. Further reproduction prohibited without permission.

TENSILE BEHAVIOR OF CONCRETE AND MORTAR UNDER DIRECT IMPACT TENSILE LOAD

by
Kayumars Emad

A Dissertation
Submitted to the Faculty of
New Jersey Institute of Technology
in Partial Fulfillment of the Requirement for the Degree of
Doctor of Philosophy

Department of Civil and Environmental Engineering

May 1993

Reproduced with permission of the copyright owner. Further reproduction prohibited without permission.

ABSTRACT

Tensile Behavior of Concrete and Mortar Under Direct Impact Tensile Load

by

Kayumars Emad

Structures are often subjected to impact loadings during their lifetime. Most structural specifications including the special provisions for seismic design in the current ACI building codes, have been developed on the basis of quasi-static assumptions. Cement composites are strain rate sensitive materials therefore, their properties determined under quasi-static condition should not be used to predict their performance under high strain rates.

The objectives of this investigation are:

- to develop a standard test set-up for direct tensile testing of cementitious composites.
- to study the tensile behavior of mortar and concrete under direct impact tensile load.
- to develop a simplified formula to predict the behavior of mortar and concrete under direct tensile impact loading.

A unique specimen was developed for this study based on a coaxial cylindrical design and is used to investigate

Reproduced with permission of the copyright owner. Further reproduction prohibited without permission.

the direct tensile behavior of cementitious composites. A specially instrumented drop weight testing apparatus was used for this study.

Wave propagation analysis was carried out on the proposed test specimen using the ANSYS finite element program to verify the uniform stress distribution across the specimen thickness. Strain rates of 0.03 to 0.97 1/Sec were achieved during these experiments by varying the instrumented drop-hammer height and the rubber-pad thickness at the contact zone between the drop-hammer and the specimen.

It was found that tensile properties of mortar and concrete were strain rate sensitive. The peak tensile loads and strains under direct impact tensile load were 1.9 and 1.7 times those obtained under static loading respectively. By increasing the strain rate, the stress-strain curve becomes less non-linear. Dynamic energy absorption to failure was found to be 3.9 times the energy absorbed under static loads. Cracking pattern was found to be one of the major differences for the observed strain rate effects in concrete composites.

A model is proposed based on the constitutive law to evaluate the response of the test specimen subjected to an impact load. The model is capable of predicting the rate sensitivity behavior of mortar and concrete under impact loading.

Reproduced with permission of the copyright owner. Further reproduction prohibited without permission.

Copyright © 1993 by Kayumars Emad

ALL RIGHTS RESERVED

Reproduced with permission of the copyright owner. Further reproduction prohibited without permission.

APPROVAL PAGE

Tensile Behavior of Concrete and Mortar Under Direct Impact Tensile Load

Kayumars Emad

Dr. Methi Wecharatana, Dissertation Advisor (date)
Professor of Civil Engineering, Department of Civil and Environmental Engineering, New Jersey Institute of Technology.

Dr. William Spillers, Committee Member (date)
Chairperson and Professor of Civil Engineering, Department of Civil and Environmental Engineering, New Jersey Institute of Technology.

Dr. Dorairaja Raghu, Committee Member (date)
Professor of Civil Engineering, Department of Civil and Environmental Engineering, New Jersey Institute of Technology.

Dr. Namunu Meegoda, Committee Member (date)
Associate Professor of Civil Engineering, Department of Civil and Environmental Engineering, New Jersey Institute of Technology.

Dr. Samer A. Ezeldin, Committee Member (date)
Associate Professor of Civil Engineering, Department of Civil, Environmental and Coastal Engineering, Stevens Institute of Technology.

Reproduced with permission of the copyright owner. Further reproduction prohibited without permission.

BIOGRAPHICAL SKETCH

Author: Kayumars Emad

Degree: Doctor of Philosophy in Civil Engineering

Date: May 1993

Undergraduate and Graduate Education:

- Master of Science in Civil Engineering,
  State University of New York at Buffalo, 1982
- Bachelor of Science in Civil Engineering,
  State University of New York at Buffalo, 1981

Major: Civil Engineering

Presentation and Publications:

Emad, Kayumars. and Manolis, George D. "Shallow Trenches and Propagation of Surface Waves" Journal of Engineering Mech. Vol. 111, No. 2, Feb. 1985, pp. 279-282.

Reproduced with permission of the copyright owner. Further reproduction prohibited without permission.

DEDICATION

To my loving parents, Dr. Aziz Emad and Khadijeh Karboor, whose love and nurturing have directed my life.

To my wife, Ferzaneh Sabahi, for her love, patience and never-failing support in my work.

To my daughter, Fatemeh who has patiently realized a home without a father for some time.

Reproduced with permission of the copyright owner. Further reproduction prohibited without permission.

ACKNOWLEDGMENT

As always, I am most grateful for God Almighty for rewarding my efforts with a successful completion. And I hope that this work will be of benefit for the advancement of human civilization.

I would like to thank Dr. Methi Wecharatana, my dissertation advisor, for his direction and insight throughout my graduate education.

I would like to thank Dr. William Spillers, Dr. Dorairaja Raghu, Dr. Namunu Meegoda and Dr. Samer A. Ezeldin for being a supportive committe members, as well as my friend, Dr. Sanjay qMehta for his enthusiastic help and collaboration. My deepest appreciation is for Mr. Anas Alkassem, Dr. Asghar Kharrazi and Mr. Allyn Luke for their assistance and friendship.

Finally, I must acknowledge the management of Parsons Brinckerhoff for their support and advice especially Mr. Farzin Lackpour.

Reproduced with permission of the copyright owner. Further reproduction prohibited without permission.

TABLE OF CONTENTS

Reproduced with permission of the copyright owner. Further reproduction prohibited without permission.

Reproduced with permission of the copyright owner. Further reproduction prohibited without permission.

Reproduced with permission of the copyright owner. Further reproduction prohibited without permission.

Reproduced with permission of the copyright owner. Further reproduction prohibited without permission.

LIST OF TABLES

Reproduced with permission of the copyright owner. Further reproduction prohibited without permission.

LIST OF FIGURES

Reproduced with permission of the copyright owner. Further reproduction prohibited without permission.

Reproduced with permission of the copyright owner. Further reproduction prohibited without permission.

Reproduced with permission of the copyright owner. Further reproduction prohibited without permission.

Reproduced with permission of the copyright owner. Further reproduction prohibited without permission.

Reproduced with permission of the copyright owner. Further reproduction prohibited without permission.

Reproduced with permission of the copyright owner. Further reproduction prohibited without permission.

Reproduced with permission of the copyright owner. Further reproduction prohibited without permission.

Reproduced with permission of the copyright owner. Further reproduction prohibited without permission.

Reproduced with permission of the copyright owner. Further reproduction prohibited without permission.

NOTATION

A	: Cross-sectional area of the beam specimen.
A_1	: Cross-sectional area of the cylindrical specimen at the wall.
A_2	: Cross-sectional area of the cylindrical specimen at the base.
D_1	: Inner diameter of the cylindrical specimen.
D_2	: Outer diameter of the cylindrical specimen.
E	: Modulus of elasticity.
e_{ij}	: Components of the strain deviation.
$\dot{e}_{ij}$	: Strain rate deviation component.
F	: Statical yield function.
h	: Length of the overhang in the beam specimen.
I	: Moment of inertia of the beam specimen.
I_2^D	: The second invariant of inelastic strain rate tensor.
J_2	: Second invariant of the stress deviation.
K	: Elastic constant.
L	: Length of the beam span or height of the cylindrical specimen.
P	: Material constant.
p	: Material constant.
P_i	: Generalized inertial load.
P_r	: Equivalent material resistance load.
P_t	: Observed tup load.
Q	: Material constant.
S_{ij}	: Stress deviation components.

Reproduced with permission of the copyright owner. Further reproduction prohibited without permission.

$\dot{S}_{ij}$: Stress deviation rate component.

U : Displacement of the specimen.

U_o : Displacement at the center of the beam specimen, or at the bottom of the cylindrical specimen.

Üo : Acceleration at midspan of the beam specimen, or bottom plate of the cylindrical specimen.

Y : Distance from the neutral axis.

α : Material constant.

β : Material constant.

γ : Material constant.

$\overset{o}{\sigma}$: Physical constant of materials.

δU_o : Virtual displacement at the mid span of the beam specimen, or at the bottom plate of the cylindrical specimen.

ε_{ij}^{e} : Elastic strain tensor.

ε_{ij}^{p} : Inelastic strain tensor.

$\dot{\varepsilon}_{ij}$: Strain rate tensor.

$\dot{\varepsilon}_{ij}^{e}$: Elastic strain rate tensor.

$\dot{\varepsilon}_{ij}^{p}$: Inelastic strain rate tensor.

η : Coefficient of viscosity.

κ : Yield stress in simple shear.

λ : Material constant.

μ : Elastic constant.

ρ : Mass density of the specimen material.

σ : Strength of the material under strain rate.

σ_o : Quasi-static strength of the material.

σ_{ij} : Stress tensor.

Reproduced with permission of the copyright owner. Further reproduction prohibited without permission.

$\Phi(F)$	:	Shape function to represent the results on the behavior of Materials under dynamic loading.
MOR	:	Modulus of Rupture.
SHPB	:	Split Hopkinson Pressure Bar.

Reproduced with permission of the copyright owner. Further reproduction prohibited without permission.

CHAPTER 1

INTRODUCTION

1.1 Introduction

During their lifetime many structures are not only subjected to long-term static loads but short-term dynamic loads as well. In general, the behavior of materials under dynamic loads is vastly different from the behavior under static conditions. Material behavior is exceedingly complex in most cases of dynamic loading conditions. Often, no exact analytical solution can be found due to the large number of unknown factors. For example, in a punching operation, if the punch is slowly applied to the material, calculations of punch pressure can be made on a static basis. On the other hand, if a bullet is fired at a plate, it is necessary to consider the mechanical and material properties of both target and projectile, velocity of the bullet, the attack angle, and the geometry of both target and projectile. Most dynamic loads fall into one of three categories defined by the impact of: heavy masses, air blasts (wind gusts), and earthquake[1-3]. In an impact, the ultimate strength and its variation with time depend on, among other things, the masses involved (including that of the structure that is hit and set in motion by the impact), the dimensions and stiffness, applied strain rate, and velocity of the

Reproduced with permission of the copyright owner. Further reproduction prohibited without permission.

impacting object as well as, the properties of the contact zone. In air blast (wind gust), magnitude and variation with time of the load is independent of the mass and the stiffness of the structure, while in case of earthquake and collision of two materials, mass has a large role in defining the stiffness of the structure.

Most materials are significantly stronger when loaded or strained at the very high rate associated with impact or explosion than they are when tested in the laboratory at normal rate or subjected to long duration loads in service. Some are also significantly stiffer. Clearly, these changes in properties should be taken into account both in the interpretation of the results of impact and similar tests on structural elements and for predictions of structural responses for purposes of design. Some note should also be taken of possible accompanying embattlement or reduction in ductility.

At a time when a concrete structure comes under impact, two different modes of failure should be distinguished: local effects and the global effects on the structure. The local impact response of concrete is characterized by intense dynamic stresses producing crushing, shear failure and split tensile fracturing. The global effect of structures are studied by researchers using single and repeated impact loadings. The majority of

Reproduced with permission of the copyright owner. Further reproduction prohibited without permission.

tests conducted on concrete have studied the effect of single impact loadings.

Because of the complex nature of local responses of structures to an impact load, no entirely rational computational model is available. Therefore, design procedures have often been based on various empirical formulas prepared for the behavior of the concrete contact zone under impact load [4-9].

In case of global effects of impact loads, few studies have been performed utilizing repeated impact loads [10,11]. These results were superficial since the quantity measured contained no relationship between the energy input to the test specimen and energy losses or inertial effects. In the case of global effect of impact heads, the majority of research has been conducted on single impact loads [1,4,6-9,12-18]. The flexural and compressive behavior of cement based materials under different strain-rates have been studied rather extensively [19-23]. But because of difficulties in the test set up and instrumentation, little attempt was made to measure the direct tensile behavior of cement composites under impact loads and thus little data is available[13,24].

For cement based materials determining the strength-to-mass ratio, inherent brittleness and the problems associates with inertial effects are very critical. Often

Reproduced with permission of the copyright owner. Further reproduction prohibited without permission.

the inertial response of the specimen may completely overshadow the material response.

To overcome these difficulties, a new specimen configuration has been developed at New Jersey Institute of Technology for this study. Sophisticated testing techniques combined with the new specimen configuration have produced better test results which leads to a better understanding of the impact behavior of cement based materials subjected to direct tension.

1.2 Objective

The effect of strain rate (impact load) on tensile behavior of mortar and concrete are studied. A standard test set-up to study the direct tensile behavior of cement based materials is developed. Utilizing the results from this study and from other investigators, a simplified formula to predict the behavior of cement composites under different strain rates is developed.

A drop weight test set-up is used in this study to apply an impact load. A new specimen configuration and proper instrumentation were needed to apply this direct tensile impact load. A closed bottom, hollow cylinder specimen is developed as shown on Figure 1.1. A new

Reproduced with permission of the copyright owner. Further reproduction prohibited without permission.

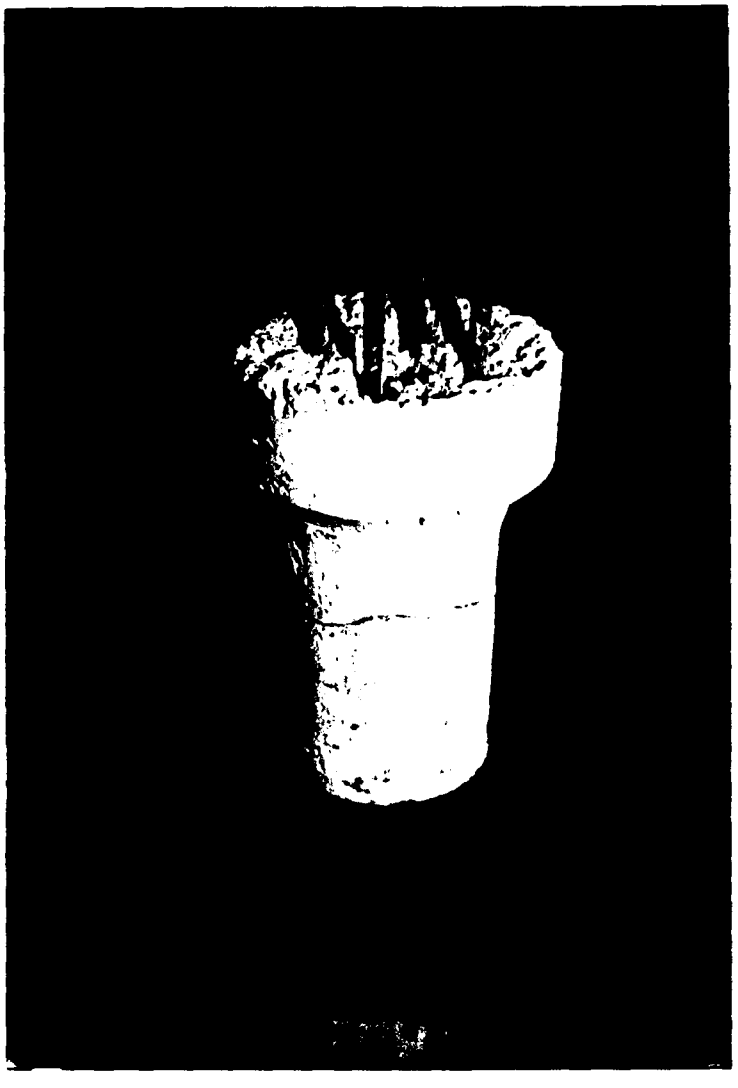

Figure 1.1 View of the proposed bottom closed hollow cylindrical specimen configuration.

Reproduced with permission of the copyright owner. Further reproduction prohibited without permission.

instrumentation set-up, consisting of an instrumented column load cell and strain gage set-up, is designed and calibrated.

Parameters affecting behavior of cement based materials under impact loading are modulus of elasticity, ultimate tensile strength, strain rate and energy absorption under static and dynamic loads. These properties will be studied in this investigation using the proposed new direct tension specimen. An MTS closed-loop servo-controlled hydraulic testing system is used to evaluate the static properties of the materials. These static properties will be compared with the observed dynamic behaviors. In order to apply different strain rates and eliminate the inertial effects in an impact test, the drop height and weight of the hammer as well as the thickness of the rubber pad at the tip of the hammer are varied. Effect of these variables is also investigated.

Reproduced with permission of the copyright owner. Further reproduction prohibited without permission.

CHAPTER 2

LITERATURE REVIEW

2.1 Background

2.1.1 Impact loads

An impact loading is generated by different causes including both artificial and natural events. Their effects should identify the circumstances in which structures may be subjected to input loadings and which may be important for design.

In recent years, vibration due to human activity has become an important factor for structural design. In buildings there is an increasing use of lightweight elements, especially as panels or infillings in framed structures. These elements and components do not always have enough resistance to failure or perforation due to impact caused by human actions.

The density of traffic on roads has increased dramatically recently. Therefore, the probability of the impact of a vehicle for structures on and along side traffic routes must be considered. It will be necessary in the future to pay attention to the problem of repeated impact loadings on their supports, columns, guardrails and, on their railings or guide barriers[25-27]. It is also necessary to consider the possibility of vehicle

Reproduced with permission of the copyright owner. Further reproduction prohibited without permission.

collisions with load-bearing elements of houses situated near traffic routes.

In an attempt to consider the effect of impact on bridge elements, the American Association of State Highway and Transportation Office (AASHTO) specifies the following equation[28]:

$$I = \frac{50}{125 + L} \qquad (2.1)$$

where:
L = Span length (ft).
I = Impact fraction.

for determining the "Impact Factor". It covers wheel falls into "chuck holes", application of live load for a very short duration, vehicle vibration on its springs and the contribution of uneven roadway surfaces[29].

Since air traffic has also increased recently, more attention to the structural consequences of possible collisions of this type is needed i.e., collisions with power plant reactors, water supply reservoirs and dams, chemical plants, rooftop helicopter platforms and bridges(Fig. 2.1). Particular attention must be given to facilities which cannot be damaged or destroyed without serious dangerous consequences to people living nearby.

For example, in nuclear facility design, safety class of structures, components and equipment shall be protected

Reproduced with permission of the copyright owner. Further reproduction prohibited without permission.

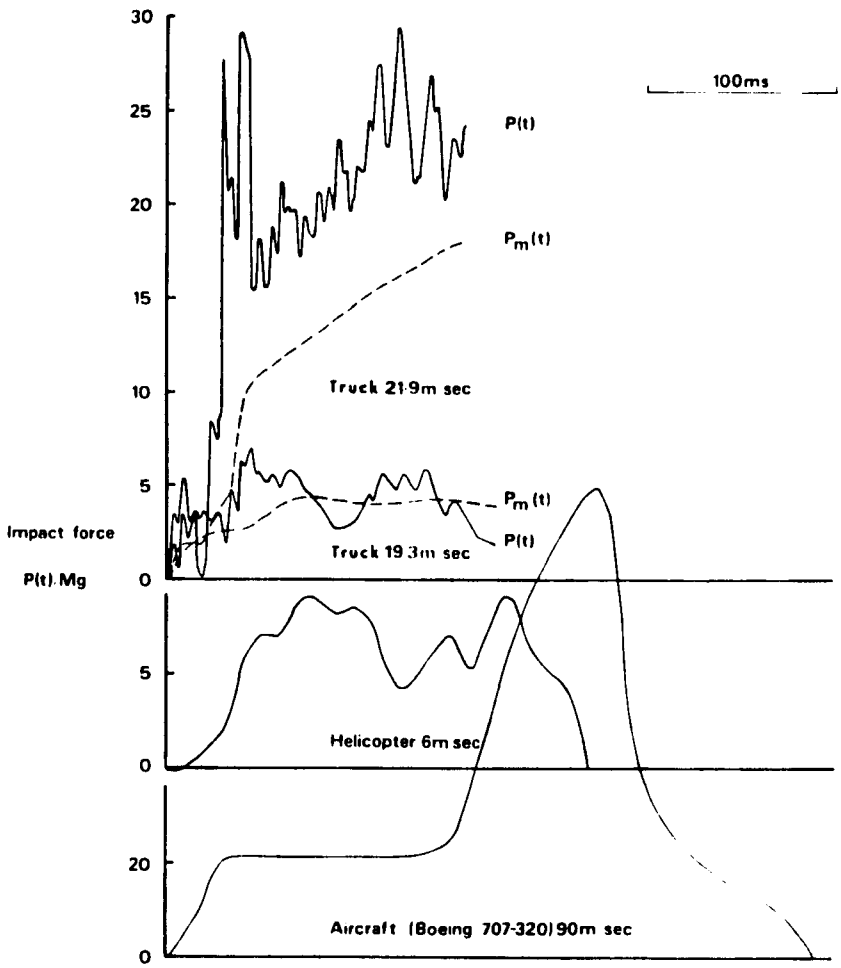

Figure 2.1 Measured (upper curves) and estimated (bottom curve) loads due to horizontal impact by heavily loaded truck and aircraft and vertical impact by helicopter.

Reproduced with permission of the copyright owner. Further reproduction prohibited without permission.

against loss of function due to postulated plant generated and extreme environmental missiles[26,27].

Raised platforms on rooftops may be built to serve as heliports in central urban areas. These platforms must resist the impact loadings caused by emergency landings of helicopters.

Consideration should be given to impact loads during construction or from erection of equipment, such as those from cranes, forklifts, shorings, forms and transport and temporary storage of major mechanical and electrical components[19].

Impact loading by floating objects must be considered for embankments, bridge piers, dock walls and gates, barrages, guaywalls, and for impacts caused by docking ships[30].

Knowing the precise locations of explosions is considered fortuitous. Even in so-called peace time, detonations of highly explosive materials are possible; for instance explosive caused by saboteurs, have to be considered for high-risk plants such as power plant reactors, etc. Bombs planted by saboteurs could be carefully sited to cause maximum damage[31-33].

Considerable turbulence and pressure are generated by gaseous explosion. Leaking gas mains or service pipes, defective appliances, and negligent or deliberate misuse of appliances have resulted in a number of serious

Reproduced with permission of the copyright owner. Further reproduction prohibited without permission.

explosions in recent years[34]. Pressure waves resulting from detentions of gas-air-mixtures, as well as fragments of materials can cause damage in chemical plants and oil refineries. In recent years many people have been injured or killed and much damage done by such accidents.

Hurricane, storm and tornado occur frequently. Gust wind loading is on the borderline between single and repeated dynamic loads. In reality the wind in the boundary layer just above the earth's surface is in turbulent flow and its speed is a random time function[35,36].

As a rough approximation one can assume wind gusts to have static and dynamic components and assign the latter to be impulsive loadings.

2.1.2 Materials

Materials behave differently under an impact loading than the static one. Most materials are significantly stronger when loaded or strained at the very high rates associated with impacts explosions than they are when tested in the laboratory at normal rates or subjected to a longer duration of applied loads in service.

A considerable amount of literature is available on the dynamic properties of steel and the influence of various chemical compositions and physical micro-

Reproduced with permission of the copyright owner. Further reproduction prohibited without permission.

structures. The stress-strain diagrams indicate an enhanced dynamic strength at all values of strain until just before failure, see Figure 2.2,[27,37]. It is reported that:

- The dynamic yield strength is increased by increasing the loading rate.
- The elastic modulus seems to be unaffected by the rate of straining.
- The stronger the steel when tested statically, the less enhancement of strength there is under dynamic conditions[38-40].
- The sensitivity increases for very high rates of straining in double shear and in punching[41].

There is a reasonable amount of data on aluminium and its alloys. Only a few aluminium alloys allow a sharp yield point. Stress-strain diagrams for aluminium show that the fast-rate diagrams are all closely parallel to the static diagrams,[42-45] indicating that the rate of straining aluminium has little, if any, effect on its stiffnesses except over a narrow range of strains within which linear elastic behavior gives way to plastic flow. It has also been observed that aluminium is rate sensitive at room temperature[5,46].

Brittle materials like glass have a simple microstructure. Its tensile strength has been found to

Reproduced with permission of the copyright owner. Further reproduction prohibited without permission.

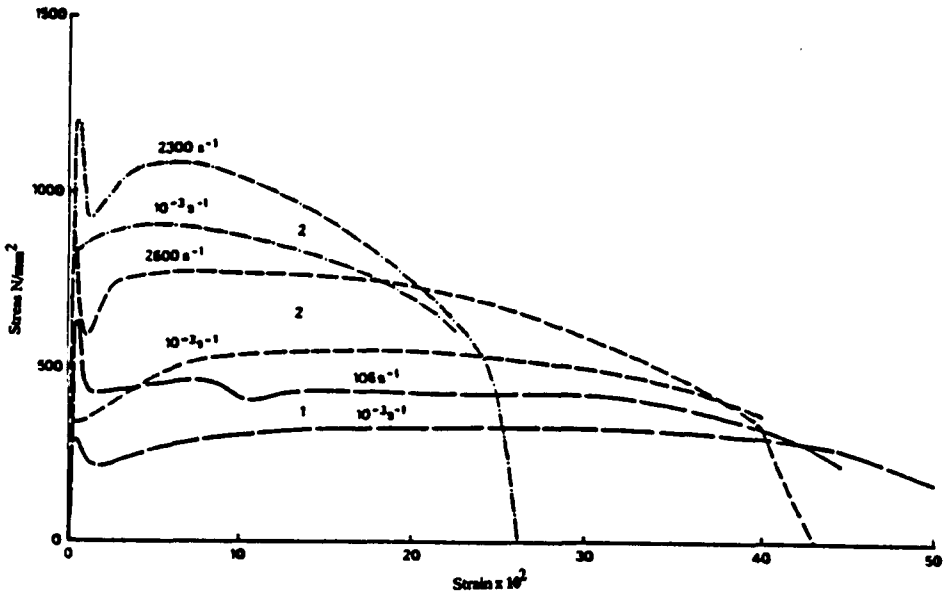

Figure 2.2 Stress-strain diagrams for three steels at different rates of straining. sources: 1. Campbell and Cooper(63), 2. Harding(59).

Reproduced with permission of the copyright owner. Further reproduction prohibited without permission.

decrease with time and increase by increasing rate of straining[47-50] as illustrated on Figure 2.3.

There are a relatively large amount of data[51] on the effects of time under duration load, rate of straining, and temperature for plastic materials. The dynamic property of Perspex at 100 degrees Celsius(Figure 2.4) shows increases in strength about twice as large as for the same increase in the loading rate[52-54].

The structures of wood varies from one species to another. The major shared characteristic for all species is that they are all highly non-isotropic. The strength in bending or direct compression with stresses acting parallel to the grain (Fig. 2.4) has been shown[55-58] to increase directly with the rate of loading.

Brick is a highly heterogeneous material. Unfortunately, there is very little data available on the dynamic properties of brick. The only known tests on the compressive strengths of individual bricks[59] were also inconclusive.

Concrete is the most widely used construction material which offers suitable engineering properties at low cost, combined with energy-saving and ecological benefits. Due to inadequate information on the effects of strain rate of cement based materials, most structural

Reproduced with permission of the copyright owner. Further reproduction prohibited without permission.

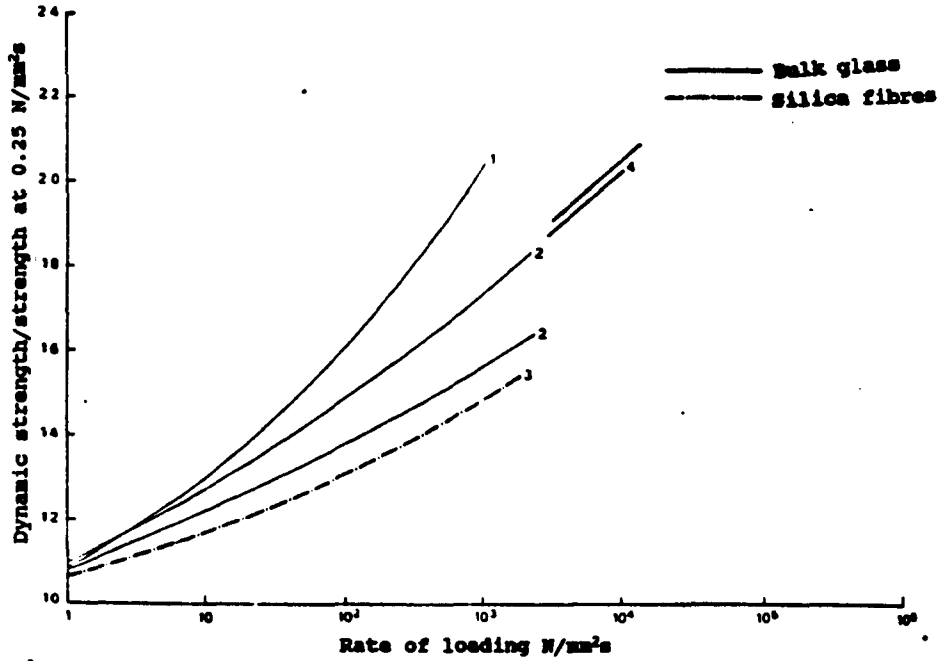

Figure 2.3 Variation of tensile strength of glass with duration of loading (at constant stress). sources: 1. Baker and Preston(47) 2. Mould and Southwick(48), 3. Proctor, Whitney and Jnhnson(49), 4. Thompson and Cousins(50).

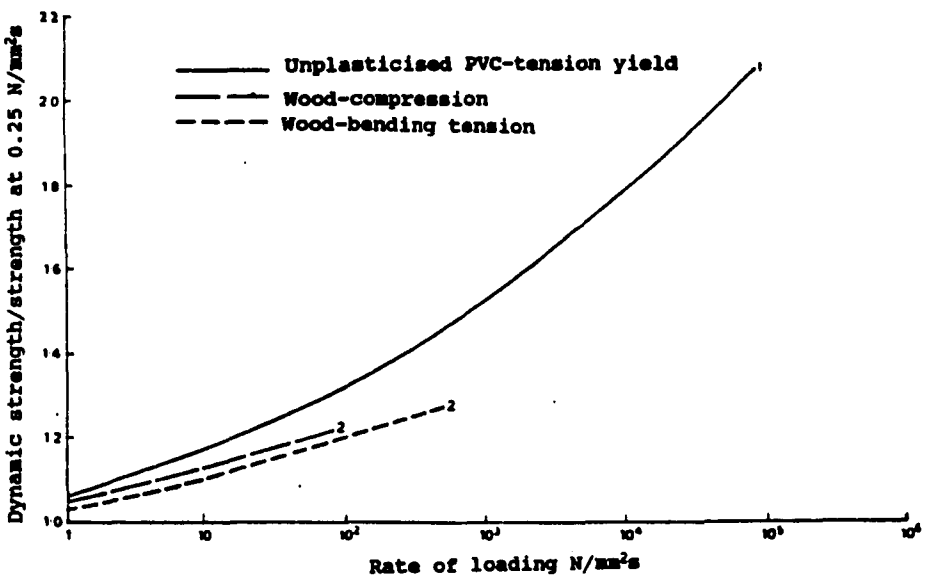

Figure 2.4 Variations of strengths of PVC and wood with rate of loading or straining. sources: 1. Ogorkiewicz(51), 2. Liska(58).

Reproduced with permission of the copyright owner. Further reproduction prohibited without permission.

design specifications, including the special provision for seismic design in the current ACI Building code[60] and CSA building codes[61], have been developed based on the results obtained from quasi-static tests[62]. The loading rates from which these codes specify are substantially lower than those expected during an earthquake. The study on the flexural and compressive behavior of concrete under different strain rates have been reported, however very little investigation has been done on the tensile behavior of cement based composites under impact loads.

2.2 Testing Methods

Impact loading has been studied by researchers using different testing set-ups. These tests include Projectile Impact Test, Multiple-Cycle Drop-Weight Test, Triaxial Test, Explosive Test, the Charpy Impact Test, Instrumented Low Blow, Modified Instrumented Charpy Test, Split Hopkinson Bar, and the Instrumented Drop-Weight Test.

2.2.1 Projectile Impact Tests

The response of concrete to projectile impact has been studied by Anderson, W.F., et al. [6]. Armor piercing bullets travelling at approximately 800 m/s were employed as projectiles. A measure of damage due to impact was

Reproduced with permission of the copyright owner. Further reproduction prohibited without permission.

obtained in these tests by measuring the crater volume and the normal penetration depth.

Projectile impact tests, where planar shock-wave loads were generated, were also carried out by Hulsewig, M. et.al [9]. They employed 3.5 inch diameter by 1 inch thick (90 mm X 25 mm) cylindrical projectiles which were made out of fiber reinforced concrete and measured the cumulative damage of cement based materials subjected to impact loads.

In another study by Knob, L.I., and Clifton, J.R. [4], 610 mm X 610 mm, 76 mm thick concrete slabs were placed on a square steel frame with a continuous ledge supporting all four edges, as illustrated on Figure 2.5. The ledge provided about 35 mm width of support. A tube with an inside diameter of about 64 mm was used to guide the projectile so as to strike the slab center. The projectile was released at the top of the tube resulting in a drop height of about 1.7 m. Two steel projectiles were used. Each projectile had a mass of 5.0 kg and was 215 mm long. One projectile head was hemispherical with a head radius of 32 mm while the other projectile head was flat-nosed. They both had cylindrical bodies with a radius of about 31 mm.

The maximum approximate depth of the crater caused by the repeated drop impact of the projectile was measured

Reproduced with permission of the copyright owner. Further reproduction prohibited without permission.

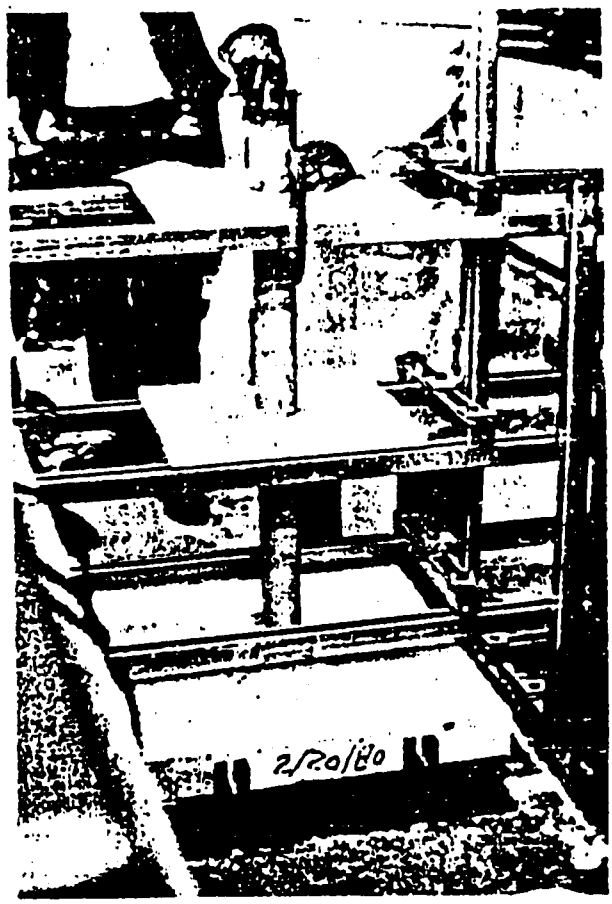

Figure 2.5 Test setup for repeated drop impact tests.

Reproduced with permission of the copyright owner. Further reproduction prohibited without permission.

periodically throughout the test by using a 0.0254 mm (0.001 inch) dial indicator. A general trend of increasing crater depth with increasing number of impacts was evident. The crater depth appeared to be a good indication of cumulative impact damage.

In another experiment, Gueraud, R. and Sokolovsky, A. [7] tightened a similar slab in place with nuts screwed on the threaded rods. They hoisted the missile to its upper position and then released by cutting with a flame a small supporting steel rod. The fall was guided by the three long vertical rods. Just before contact, the speed of the missile was measured by a device prepared specially for these tests. The velocity was measured as it passed two light beams, separated by a vertical distance of 202 mm, placed as close as possible to the upper surface of the photo-sensitive cells. The light beams reacted to the occultation by the passage of the missile. The timing of the two successive occultations were registered by an electronic quartz chronometer.

The missile, in some cases, completely transpierced the slab; it was then stopped by a small steel ball placed on a steel cylinder under the center of the slab. The print left by the sphere in the cylinder gave an indication of the energy left in the missile after going

Reproduced with permission of the copyright owner. Further reproduction prohibited without permission.

through the slab. The missile generally rebounded after the impact.

Accelerations were measured with an accelerometer fixed in the upper surface of the slab near the impact zone. In some case an attempt was made to register the deformations using strain gages attached to the reinforcement bars or, the concrete.

This testing set up was useful for measuring the amount of destruction caused by collision of a mass with a structure. It lacks, however, a precise measurement of energy absorbed. Also, the failure was a combination of compression, as well as lateral splitting tension and shear through, which are hard to separate and measure individually.

2.2.2 Multiple-Cycle Drop-Weight Test

A multiple-cycle drop-weight technique developed by Schrader [10] and recommended by the American Concrete Institute committee 544 on Fiber Reinforced Concrete[66] is another way to evaluate the impact resistance of concrete composites. It is simple in terms of the procedural and equipment requirements. The tests are to be conducted by dropping a 10 lb. hammer repeatedly from a 18 inch height onto a hardened steel ball resting on a 6 inch diameter, 2.5 inch height cylindrical specimen. The number

Reproduced with permission of the copyright owner. Further reproduction prohibited without permission.

of blows required to produce the first visible crack is considered to be an indication of the impact resistance of the material.

The problem with multiple-cycle drop-weight test is that the result is superficial since the quantity measured bears no relationship to the energy input to the testing specimen, energy losses or inertial effects[123]. Also, unlike the single-cycle high-rate testing techniques which produce true impact conditions, this technique produces some combination of impact and fatigue loadings. Another disadvantage of this drop-weight technique is that the stress condition of axial compression combined with lateral splitting tension bears little resemblance to the situation encountered in most applications. But, the most serious difficulty with the test is the inherently high variability of results which far exceed normally acceptable levels.

2.2.3 Triaxial Test

Takeda, J., Tachikawa, H., and Fujimoto, M.,[12] performed dynamic axial tests on concrete cylinders loaded by compressive and tensile axial loads. At the first stage of the test a prescribed confining pressure was applied statically. Then the axial load was applied with one of

Reproduced with permission of the copyright owner. Further reproduction prohibited without permission.

the three different axial straining rates of $2X10^{-5}$ 1/Sec, $2X10^{-2}$ 1/Sec and 2 1/Sec.

This testing technique has rarely been used. And there is not enough information available on its accuracy.

2.2.4 Explosive Test

Mayhofer, C. and Thor, H.J.[8] carried out tests in a blast load simulator. A pressure chamber divided the slab into two parts. A resultant force was applied on the test plate by venting the two chambers with different flow rates. The fastest rise-time of the pressure pulse was 3-5 ms and for the simulation of static loads this rise-time was lengthened to 4 minutes. During the tests, pressure measurements were taken employing pressure transducers and the plate deflection was monitored by an inductive displacement transducer.

Since the mode of failure was a combination of tension, compression and shear along with fragmentation, a precise measurement of the load versus strain was difficult to obtain. Therefore, expensive and sophisticated instrumentation is needed which is not readily available.

Reproduced with permission of the copyright owner. Further reproduction prohibited without permission.

2.2.5 Charpy Impact Test

For many materials, the most common method of obtaining their impact resistance is by Charpy Impact Test, as illustrated on Figure 2.6 [64]. In this test, a three point bend specimen is struck at the center by a pendulum. Knowing the height of the pendulum before and after impact and assuming that all the energy lost by the striker is absorbed breaking the beam, one can calculate the energy absorbed due to impact test.

This testing set-up requires small specimens. In general, the minimum dimensions of a specimen is a function of the size of its material composition. In case of concrete materials, the size of aggregate is relatively large therefore, a large specimen with the least dimension in excess of three times the maximum size of aggregate is required. This makes the normal Charpy Testing set-up inappropriate for concrete testing.

2.2.6 Instrumented Low Blow

Low-blow testing originally meant hitting the test specimen with two successive blows in the Charpy apparatus. The first blow does not have enough energy to fracture the specimen while the second blow provides an impact using the total available energy. Low-blow testing has been employed for various purposes; for instance,

Reproduced with permission of the copyright owner. Further reproduction prohibited without permission.

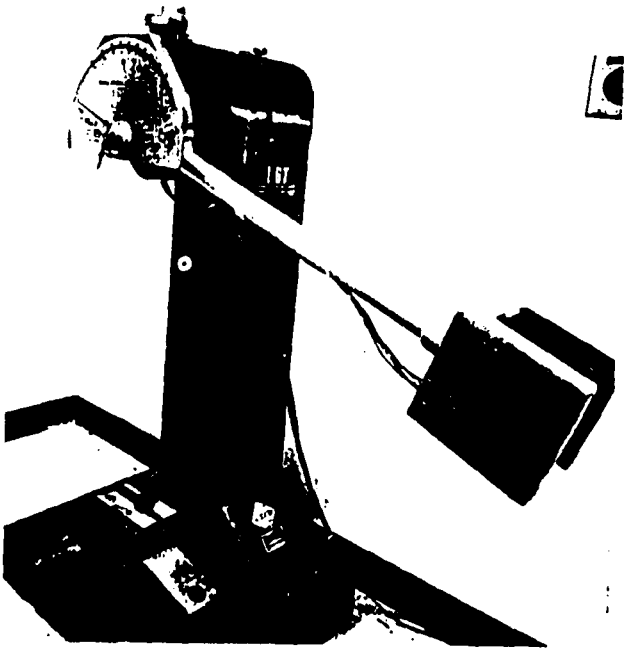

Figure 2.6 Sonntag model SI-1 240-ft.lb-capacity charpy impact machine initially instrumented to measure dynamic properties.

Reproduced with permission of the copyright owner. Further reproduction prohibited without permission.

Orner and Hartbower [18] used low-blow testing to induce a type of "pre-crack" in Charpy specimens. Tardif and Marquis[65] extended the low-blow technique to instrumented impact testing.

By further extending these initial ideas, a new configuration for low-blow testing can be defined in which increasing levels of energy are applied. The energy level at which first damage is observed can then be used as a threshold value that might later be used in design as a damage tolerance criteria.

2.2.7 Modified Instrumented Charpy Set-up

A conventional Charpy tester can be modified and instrumented to facilitate tests on concrete specimens at different impact velocities[20]. Among the three primary modifications are:

a) Instrumentation of the striker and the two supporting anvils,
b) Seating arrangement to accommodate large-size specimens,
c) Low-blow fixture to enable tests at different impact velocities, as shown on Figure 2.7 [20].

It is felt that simultaneous recording of anvil and striker loads are essential both for a proper interpretation of inertial loads, and to assess the

Reproduced with permission of the copyright owner. Further reproduction prohibited without permission.

Reproduced with permission of the copyright owner. Further reproduction prohibited without permission.

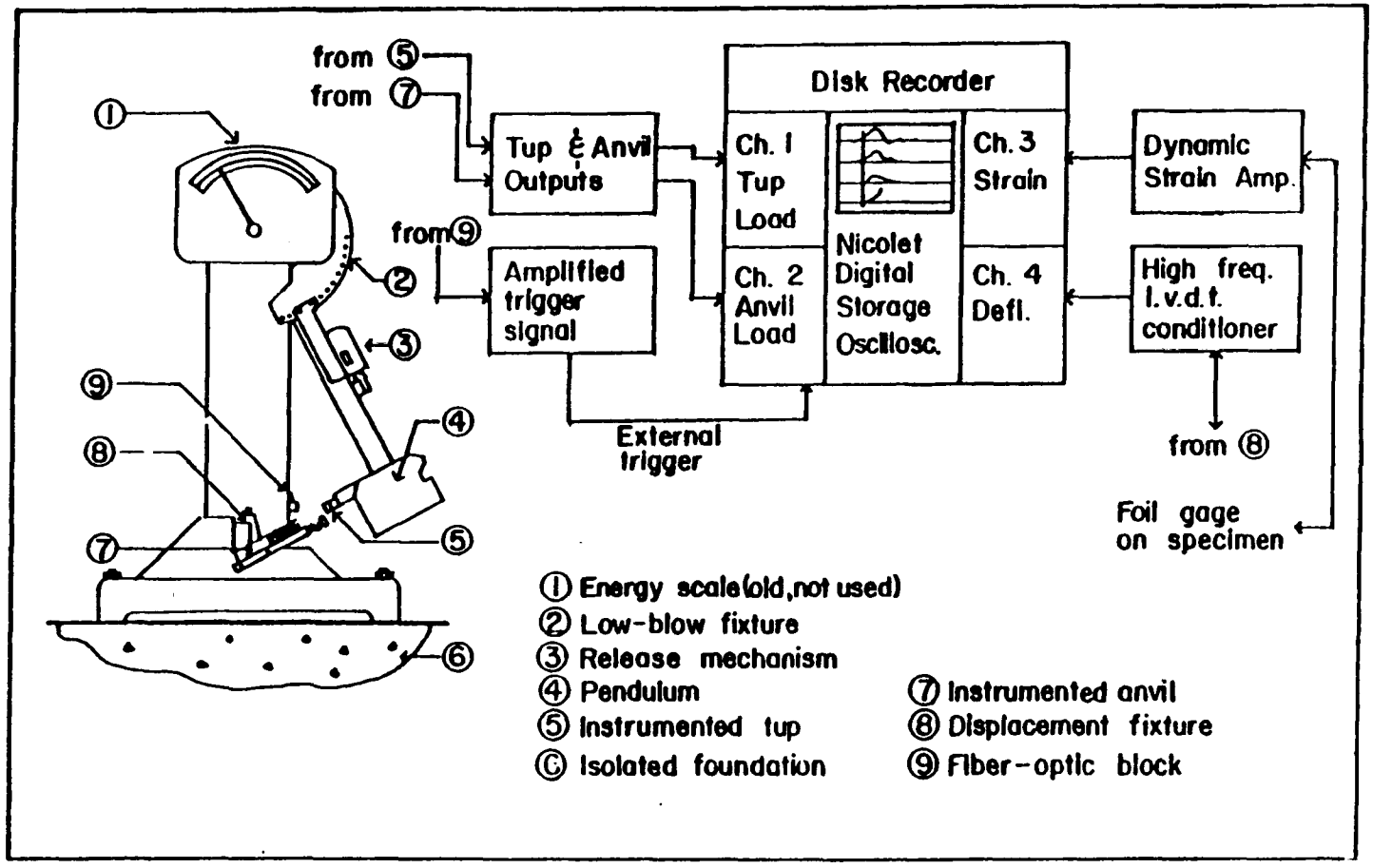

Figure 2.7 A Schematic diagram showing the general features of modified instrumented charpy test.

influence of parameters such as test-system compliance, specimen size and impact velocities on the test results. The anvil and the striker are designed to serve as compression load cells capable of recording dynamic loads transmitted through them during an impact event. They are sufficiently rounded at the specimen contact points so as to avoid local compressive damage to the specimen on impact, and at the same time facilitate smooth specimen rotation during bending. Semiconductor gages are used in a full-bridge configuration within protective recesses provided on either side of all the load cells (two anvils and the striker). Besides providing a high signal-to-noise ratio, the configuration allows temperature compensation. The load cells are calibrated statically after having been subjected to low-amplitude cyclic pre-loading to eliminate initial gage-seating effects. A 10-volt DC bridge excitation is used for all the load cells. Output from the two anvils are tied in series to monitor total load recorded by the supports.

In original Charpy testing the dimensions of the support and the depth of the specimen did not allow impact to occur when the pendulum reached its lowest position. As a result, the beam and its supports were adequately inclined to ensure a flush contact between the beam and the striker at the moment of impact. While designing the striker, it is ensured that the center of percussion of

Reproduced with permission of the copyright owner. Further reproduction prohibited without permission.

the pendulum is retained at the center of the striking face so that adverse vibrations of the pendulum were avoided. For larger specimens the pendulum can not clear the broken halves of the specimen, unlike a normal Charpy test. A hydraulic shock-absorber mechanism facilitates arresting the motion of the pendulum after the beam has deflected about 50 mm.

To allow for impacting the specimen at different velocities, a low-blow fixture is designed. This allows impact velocities in the range of 0.5-0.3 m/s with safety lock-latching mechanism to hold the hammer in its raised position to assure a vibration-free release when activated.

The disadvantages of the Instrumented Charpy testing are: The test does not measure the direct tensile impact behavior of the material since three-point-bend testing is used and only the modulus of rupture can be calculated. When testing specimens with low strength/weight ratio the material response is completely overshadowed by the inertial response in the load readings[21]. For concrete materials, the beam specimens which are used in the Charpy testing have low strength/weight ratio. Therefore, large errors in material response measurements are expected. It is also difficult to use different specimen configuration and sizes. And the pendulum mass can not be changed easily as a testing variable parameter.

Reproduced with permission of the copyright owner. Further reproduction prohibited without permission.

2.2.8 Split Hopkinson Bar

The test equipment consists of two elastic bars between which the specimen is sandwiched[1]. A stress pulse propagating through the first bar is partly transmitted and partly reflected at the interface between elastic bar and specimen. The ratio between transmission and reflection depends upon the mechanical impedance of the materials involved. Zielinski, et al.,[1] found that in the case of an aluminium bars and a concrete specimen, about 80 to 95 percent of the stress pulse is transmitted. The transmitted pulse is measured on the second bar and because of equilibrium, immediately gives the force which acted on the specimen. Figure 2.8 [24] shows the set-up of a Split Hopkinson Bar which Zielinski, et al. used in the Stevin Laboratory at the Delft University of Technology. The tensile pulse is generated by drop weight hitting the anvil at the bottom of the lower bar. Layers of rubber or cardboard between drop weight and anvil cause different contact and lead to different stress rates in the range from 2 to 60 N/mm^2per ms. By the variation of the drop weight and height, the stress rate can be varied systematically. The bars must have a certain length in

Reproduced with permission of the copyright owner. Further reproduction prohibited without permission.

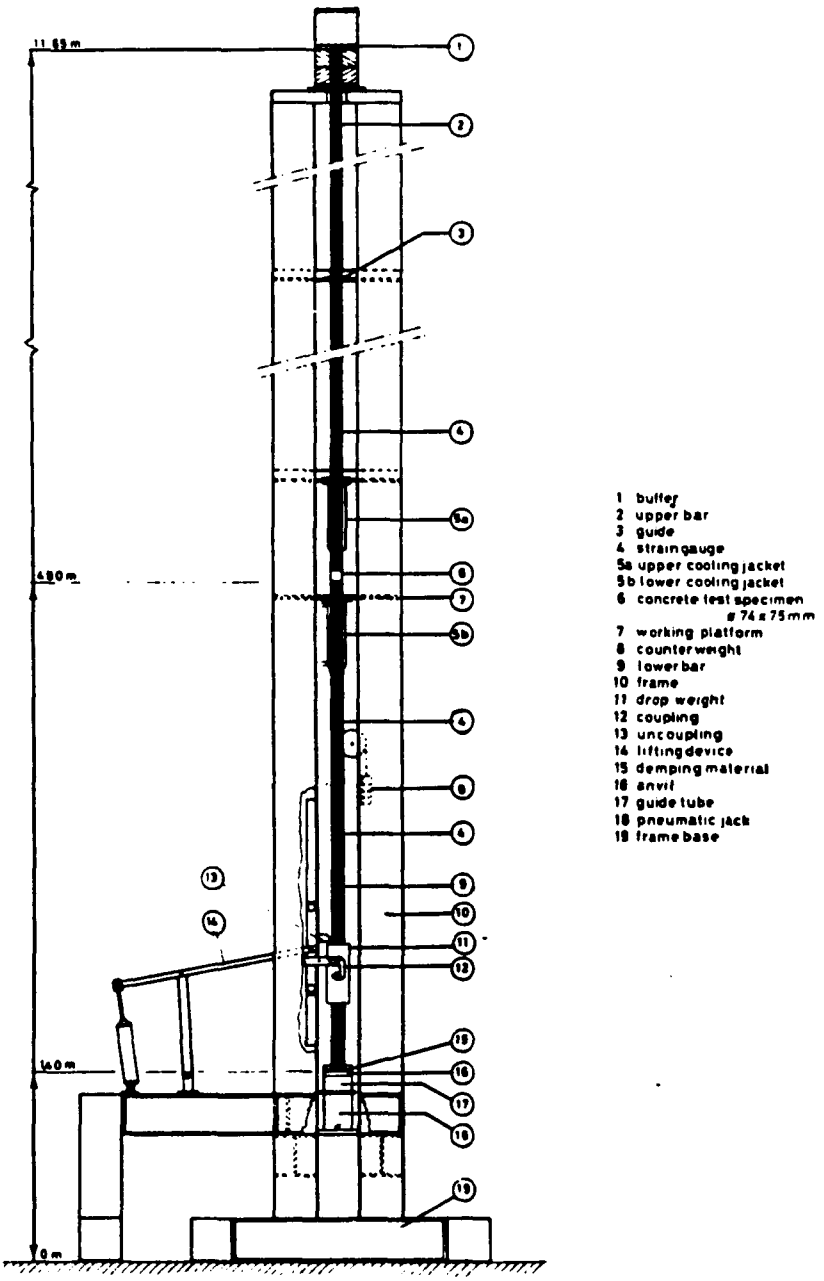

Figure 2.8 Schematic of split-hopkinson bar testing set-up at Stevin laboratory.

Reproduced with permission of the copyright owner. Further reproduction prohibited without permission.

order to provide a uniformly distributed stress pluses. Zielinski A.J., and Reinhardt H.W.[1] have concluded that a length of about 20 times the diameter is necessary to keep the specimen and the measuring point force free from unintended reflection. It turned out that for a given wave propagation velocity of about 5000 m/s and a maximum pulse duration of about 2 ms, the bars should be about 5 m long. In this experiment, the specimen should be glued to the aluminium bars and for the whole duration of an experiment the strains can be measured on the specimen by strain gages or contactless LVDT's. The strain of the upper bar can be measured by strain gages giving the loading force, calculated from a known value of the modulus of elasticity for aluminium.

Another version of Split-Hopkinson bar was used by Ross, C.A., Kuennen, S.T. and Tedesco, J. as illustrated on Figure 2.9 [15]. It was driven by compressed nitrogen [16,17]. In the direct tensile test, a striker bar slides on the incident bar and hits the tup at the bar end causing stress on the specimen. The length of the stress pulse is proportional to twice the length of the striker bar, and the magnitude of the impact is proportional to its velocity. Assuming uniform stress along the length of the specimen, dynamic stress-strain curve is generated. To ensure a uniform stress condition, Ross et al.[15]

Reproduced with permission of the copyright owner. Further reproduction prohibited without permission.

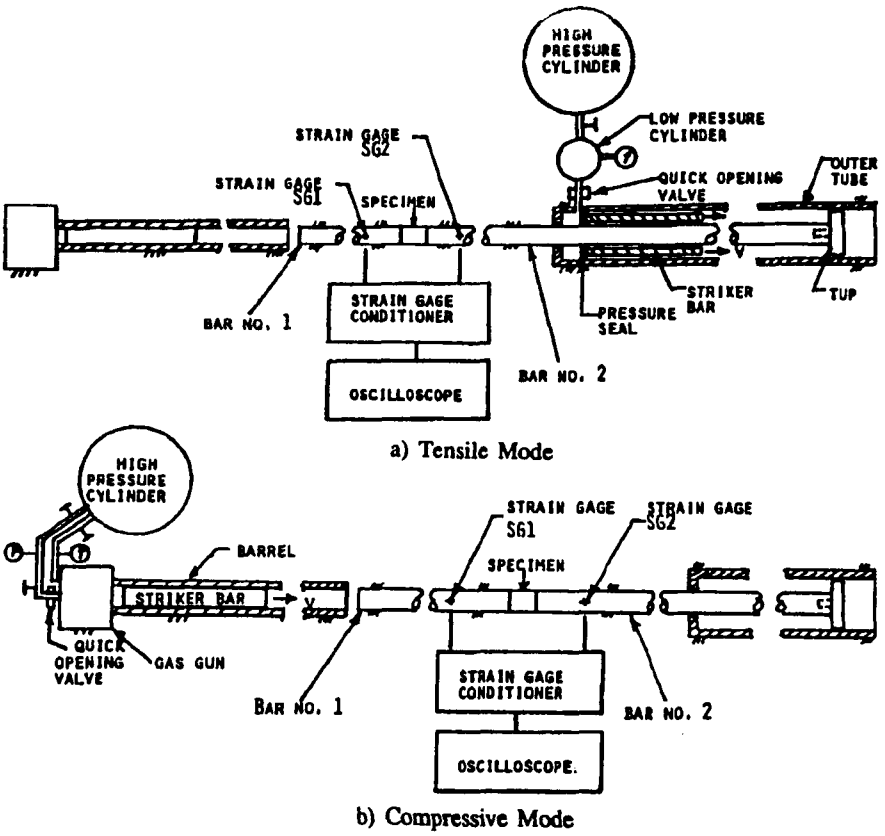

Figure 2.9 Schematic of AFESC split-hopkinson pressure bar.

Reproduced with permission of the copyright owner. Further reproduction prohibited without permission.

selected the length of the specimen so that multiple stress reflections occur during the passage of the stress wave through the specimen. With a small adjustment to the testing set-up it can be changed to apply compressive loads to the specimen, as can be seen on Figure 2.9.

One of the difficulties with this test is that since the specimens are glued to the bars, the bond and material behavior of glue will introduce distortions in the measurement readings. The inherent limitation of the split Hopkinson bar method precludes its use for determining material behavior in the elastic region because of the stress-wave reflection and stress nonuniformity. Another difficulty is that if the material of the specimen varies in each test, in order to have a uniform stress condition, the aluminium bars and specimen length have to be varied for each test. Also because stress pulse is partly transmitted and partly reflected at the interface between specimen and aluminium bars and since the applied load is analyzed by measuring the strain on the aluminum bars, it could lead to error in load readings.

2.2.9 Instrumented Drop-Weight Set-up

This instrumented impact system consists of the hammer and the striker(tup) assembly and a three-point-bend specimen. In the study by Suaris, W., and Shah,

Reproduced with permission of the copyright owner. Further reproduction prohibited without permission.

S.P.,[67] the striker is instrumented with two semi-conductor strain gages which enable the measurement of the compressive load interaction between the tup and the specimen during testing, as illustrated on Figure 2.10. Power supply, amplifying the tup-load signal and contained signal display components for receiving permanent records of the load and energy absorption during impact, is provided by a Dynamic Response Module. The impact velocity is measured and the storage oscilloscope is triggered by using a fiber-optic system.

The advantages of this testing set-up are:

- The velocity of impact test can be controlled by varying the height of the drop hammer.
- The drop mass can be changed by attaching more mass to the tup.
- Different specimen configurations and sizes can be used readily with few modifications.
- It is easy to apply new instrumentations for a particular testing set-up.

The disadvantages of Instrumented Drop Weight set-up are: the test does not measure the direct tensile behavior of cement based materials. A large inertial response is introduced due to the low strength/weight ratio specimen of cementitious composites which will be further discussed in the Theoretical Model section

Reproduced with permission of the copyright owner. Further reproduction prohibited without permission.

Reproduced with permission of the copyright owner. Further reproduction prohibited without permission.

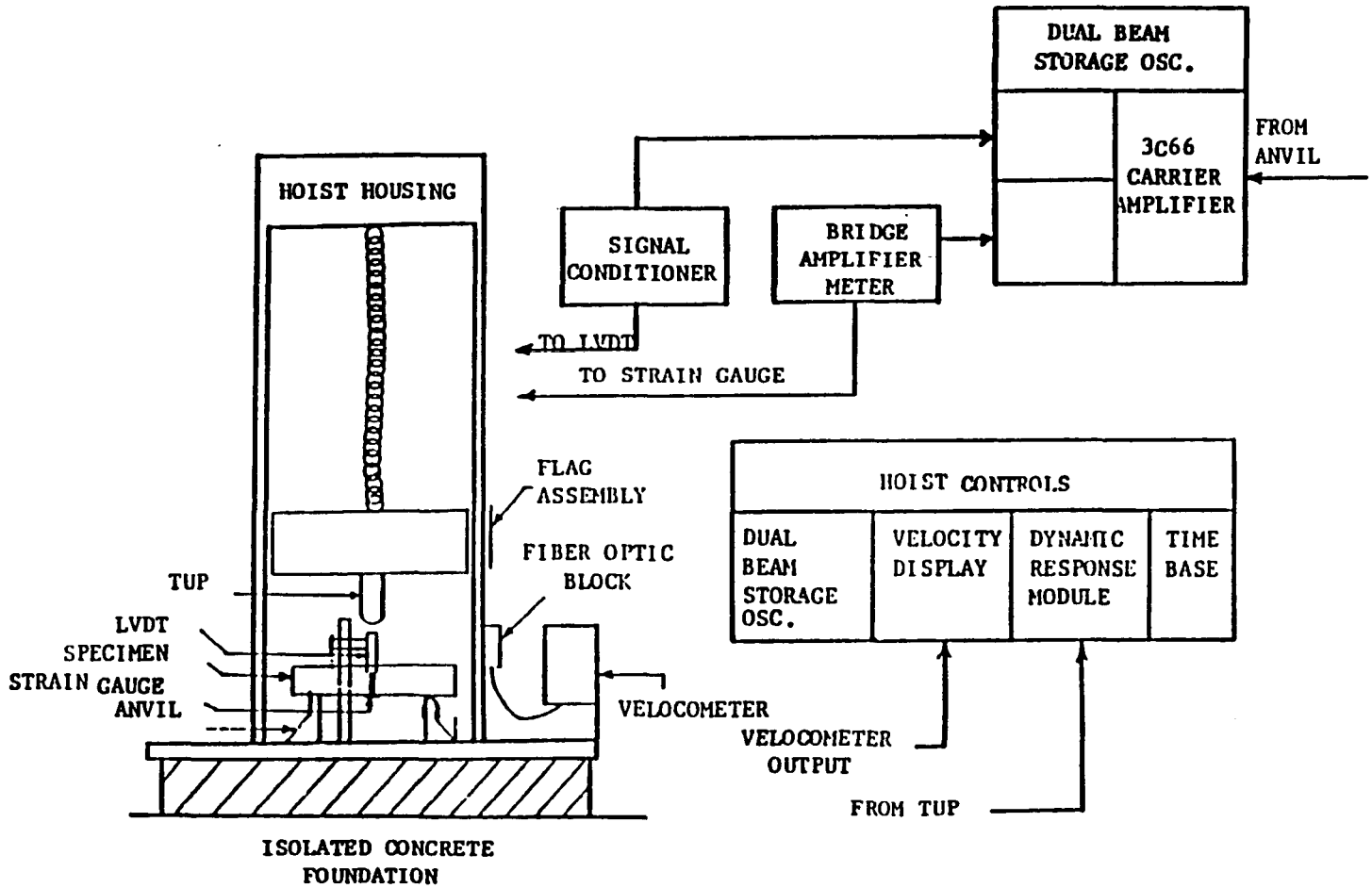

Figure 2.10 Layout diagram of the instrumented drop-weight set-up.

There are different impact testing set-ups. Some of them such as projectile impact tests, explosion test and multiple-cycle drop-weight test produce indication of a specific material behavior and lack a level of precision appropriate for standardization.

Charpy Impact test requires small specimens. In cement based materials, large specimens are needed due to material composition. Therefore, this testing apparatus is not suitable for concrete materials under impact loadings.

In the Modified Instrumented Charpy set-up the following shortcomings exist. It does not measure the direct impact behavior of material. Because of three-point-bend test set-up, the strength/weight ratio is small which leads to large inertial response in the load readings. It is difficult to use different specimen configurations and sizes. Also, strain rate along the specimen depth varies for a specific impact load.

In Split Hopkinson Bar, existence of glue material and bond between the specimen and the bars plus the need for proper alignment causes some errors in observing the specimen material behavior under direct tensile impact test. Also, since the load reading is performed on the bar and the stress pulse is partly reflected and partly transmitted, errors in load readings can be introduced.

Instrumented drop hammer weight has the following disadvantages: high inertial response on load readings,

Reproduced with permission of the copyright owner. Further reproduction prohibited without permission.

and indirect measurement of tensile behavior of materials under impact test. It, however, has the following advantages: readily use of different specimen configurations and sizes, easy application of new instrumented devices, ability to change drop hammer mass and velocity of impact.

One of the objectives of the present research was to develop a new specimen configuration with high strength/weight ratio and proper instrumentation to overcome the inertial response in load readings.

The advantages of Drop Hammer testing setup which were employed in this section are the simplicity of the testing apparatus combined with a new specimen configuration. These combinations make this test set up one of the most suitable means to be used for direct tensile impact test of cementitious composites.

Reproduced with permission of the copyright owner. Further reproduction prohibited without permission.

2.3 Effect of impact on tensile behavior of concrete composites

Concrete materials are highly heterogeneous in their internal structures both on the macroscopic and microscopic scales. This heterogeneity, compared to steel and aluminium, leads to several differences in the characteristic of deformation. In particular, the development of microcracks at small fractions of the ultimate strain and their progressive growth must be a major reason for the early departure from linearity of the stress-strain diagram at any rate of straining.

The effect of impact on concrete performance can be characterized by the local effect of the impact on the specimen, such as the penetration depth of projectile into the impacted target, the number of loading cycles to failure and, global effect of impact on the structures.

2.3.1 Local Response Study

Knob and Clifton[4] conducted a study concerned primarily with low projectile velocities and shallow penetration. By comparing the crater depth versus the number of impacts in seven tests, they observed a general trend of increasing crater depth with increasing number of impacts. They concluded that crater depth appears to be the indication of cumulative impact damage.

Reproduced with permission of the copyright owner. Further reproduction prohibited without permission.

The local impact response of concrete is characterized by intense dynamic stresses producing crushing, shear failure and split tensile fracturing. Because of the complex nature of this response no entirely rational computational model is available and design procedures have been based on various empirical formulas proposed for the behavior of concrete at the contact zone under impact[29].

2.3.2 Repeated Impact Loading

Hughes, B.P., and Gregory, R.,[68] performed impact splitting tests on concrete cubes by employing a ballistic pendulum. They measured the impact strength in terms of number of blows or average energy absorbed per blow to failure.

In general these results are valid only for their particular impact test conditions. The test results are greatly influenced by test variables such as mass, stiffness of impact loading set up and test specimen. Also, it is difficult to obtain any typical measures, like stress or strain values, for further analysis. Therefore, such test results, eventhough useful in providing information on the relative behavior of different concrete, lack correlation with other impact tests. They

Reproduced with permission of the copyright owner. Further reproduction prohibited without permission.

can not be directly used for the design of structures subjected to impact loading.

2.3.3 Single Impact Loading

There are three common methods to study the tensile behavior of cement based materials under single impact loading: split tension tests, direct tension tests, and flexural tests.

2.3.3.1 Split Tensile Impact Study

Cowell, W.[70] conducted tensile impact tests on concrete cylinders using split-cylinder technique. A pneumatic-hydraulic machine with an adjustable load velocity was used in this test. By applying strain gauges in the center of each end face of the specimen and normal to the axis of load application, tensile strains were measured.

Ross, C.A., Kuennen, S.T., and Tedesco, J.W.,[15] studied the direct tension response of cementitious composites under impact load using a Split Hopkinson Pressure Bar (SHPB). But, due to problems such as proper alignment and specimen connection, they also performed splitting tension tests under impact load using the same testing apparatus in the compressive mode where the

Reproduced with permission of the copyright owner. Further reproduction prohibited without permission.

specimen is loaded diametrically. They studied the tensile behavior of concrete under high strain rates. Three different types of concrete specimens were used. In the direct tension experiments both square-notched and saddle-notched specimens were tested. Plain 2-inch diameter cylinders were used for the splitting tensile tests. All specimens types were tested at all strain rates. In the splitting tension study, the peak transmitted compressive stress was assumed to be proportional to the tensile strength through a relation similar to the static equation[71,72] as shown on Figures 2.11 and 2.12. The slope of the transmitted stress versus time was considered to be an indication of the loading or stress rate. Using the stress rate and assuming a linear elastic material, they obtained the strain rate by dividing the stress rate by the static Young's modulus. In this study, the quasi-static strength was determined at a strain rate of 2.5×10^{-7} 1/sec. The fracture of the splitting tensile cylinders for the quasi-static and dynamic tests were very similar for strain rates between 10^{-7} to 5 1/sec. At this point, some bifurcation of the crack appeared near the center of the specimens. They reported that for the direct tension specimens, the quasi-static and dynamic failure appear to be very similar for strain rates between 1 to 5 1/sec. However, above this strain rate, double fracture

Reproduced with permission of the copyright owner. Further reproduction prohibited without permission.

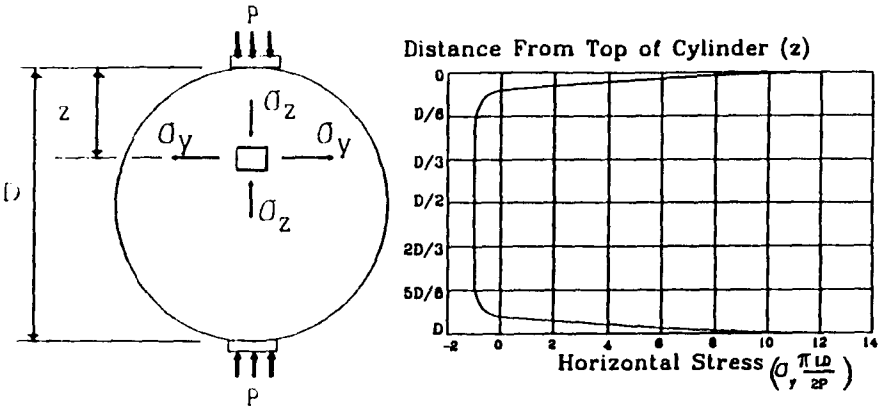

Figure 2.11 Stress distribution for a static splitting tensile cylinder.

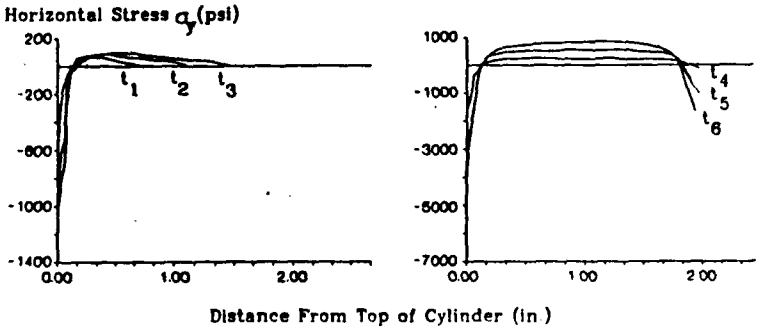

Figure 2.12 Elastic stress distribution for a dynamic splitting tensile cylinder.

Reproduced with permission of the copyright owner. Further reproduction prohibited without permission.

appeared and the strength was lower than that for the single fracture specimens.

One of the shortcomings of the split tension test is that only the tensile strength is recorded and no stress-strain curve is generated from which to determine the modulus of elasticity. Also, the assumption that the modulus of elasticity under static test is equal to that of dynamic test is questionable [11,75,76,96].

2.3.3.2 Direct Tensile Impact Study

In another experiment, Ross, C.A., and Kuennen, S.T.,[73] studied the tensile strength of concrete at strain rates ranging from $3x10^{-7}$ to 10^{2} 1/sec on 2 inches diameter by 2 inches long concrete specimens. SHPB testing was used for tension and compression tests. For the direct tensile test, specimens were glued between the two bars. The direct tensile strength was found to be 530 psi when the compressive strength was 8700 psi. They reported that the tensile strength data showed abrupt increase at a strain rate of about approximately 1.0 1/sec. The concrete strengths obtained at strain rates above this value were found to be a function of the cube of the strain rate.

Zielinski, A.J., and Reinhardt, H.W.,[1] also used the Split-Hopkinson-Bar technique to investigate the tensile stress-strain behavior of concrete, microconcrete

Reproduced with permission of the copyright owner. Further reproduction prohibited without permission.

and mortar at different stress rates. Mortar and microconcrete cylinders were subjected to single uniaxial impact tests at stress rates ranging from 6 to 28 N/mm^2 per millisecond and 20 to 31 N/mm^2 per millisecond. They found a 130% increase in strength for mortar and 150% increase for microconcrete specimens subjected to the tensile impact load. A model was developed for an idealized particulate composite consisting of spherical particles dispersed and embedded within a matrix. Furthermore, it was assumed that the degree of multiple cracking of a material is stress-rate dependent and, overall cracking was also found to increase with increasing stress rate. The path of a single crack was assumed to be influenced by the rate of stress in such a way that, for a given configuration of aggregate particles within the matrix, more particles would be fractured and fewer interfacial bond fractures would occur at higher stress rates as compared with static fracture. They found that more energy is absorbed in impact than in static loadings.

For normal operation of a SHPB, it is assumed that the stress is uniform along the length of the specimen. In order to ensure uniform stress condition, the length of the specimen must be chosen in such a way that multiple stress reflections occur during the passage of the pulse

Reproduced with permission of the copyright owner. Further reproduction prohibited without permission.

across the specimen[15]. For direct tension this is difficult to achive due to large discrepancy between the tensile and the compressive strengths. This difficulty along with problems of proper alignment and specimen connection make the SHPB a method not completely suitable for evaluating the impact behavior of concrete materials under direct tension.

2.3.3.3 Bending Tensile Impact Study

A Modified Instrumented Charpy test was used by Gopalaratnam, V.S., Shah, S.P., and Reji, J.,[20] on a 1:2:2:0.5 (C:S:A:W) concrete mix. They performed the flexural tests at four different impact velocities, 70, 130, 185, and 240 cm/Sec. The velocity was measured using a fiber-optic block/flag assembly. Tests were performed with and without 1/8 inch thick rubber pads(shore hardness of about 70) placed between the striker and the specimen. They recorded peak load increases of 60% when the strain rate increased from 10^{-6} 1/Sec to 0.3 1/Sec. Using analysis based on elastic beam theory, they reported a 60% increase for the modulus for rupture of the same concrete.

In a study by Brooks and Samaraie [74], flexural and direct tensile behavior of concrete were tested at three stress rates ranging from 0.025 to 250 MPa/sec. Four sizes of prisms, 100x100x300, 75x150x450, 50x50x450 and

Reproduced with permission of the copyright owner. Further reproduction prohibited without permission.

150x150x450 mm were tested under three-point and four point loadings. For the direct tension tests a concrete mix of 1:1.8:3.5 with a water/cement ratio of 0.5, ordinary portland cement, quartzite gravel and one size bobbin-shaped specimen were selected. The tests were performed on a servo-controlled hydraulic test machine. Using electrical resistance gages embedded in the specimen for direct tension and installed on the surface of the flexural test specimens, the stresses were determined. They found that the tensile strength consistently increased as the stress rate increased. Also, that the direct tensile strength is more sensitive to the stress rate than the flexural strength.

Some of the shortcomings of studying the direct tensile behavior of cement based materials using the flexural tests are: 1) that variable strain rate exists along the depth of the beam, 2) the assumption of elastic beam theory for the impact test in order to evaluate the modulus of rupture and, 3) the inherently low strength/mass ratio of cementitious composites which leads to a large inertial effect in load readings.

2.3.3.4 Effect of Tensile Impact on Strength

Cowell, W.,[70] studied the behavior of concrete under tensile impact loading using a Dynamic Split

Reproduced with permission of the copyright owner. Further reproduction prohibited without permission.

Cylinder test. He observed an increase of between 50% to 75% in tensile strength with a strain rate increase of $2x10^{-1}$ 1/sec.

Using a high speed loading apparatus, Takeda, J., and Tachikawa, H.[75] conducted tensile tests on concrete as shown on Figure 2.13 [95]. The apparatus, driven by compressed air, produced strain rates from $5x10^{-6}$ to $5x10^{-2}$ 1/sec. They found a 70% increase in tensile strength due to that increase in the strain rate.

Kormeling, H.A., et al.[11] studied tensile behavior of concrete by Split Hopkinson Bar method. They found that the impact strength at a stress rate of 30 N/mm^2 per millisecond (strain rate of 0.75 1/sec) to be 2.11 times higher than the static strength which was measured at 10^{-4} N/mm^2 per millisecond.

Mellinger, F.M. and Birkimer, D.L.,[76] conducted tensile test on concrete cylinder by the Pallet Technique. The shock wave generally had a rise of about 20-30 microseconds. They recorded the dynamic tensile strengths of over five times the static strength.

Ross, C.A., et al.,[15,73] reported that the tensile strength of concrete showed significant strain-rate effects at strain-rate of approximately 1.0 1/sec. Above this strain rate, the concrete tensile strength is

Reproduced with permission of the copyright owner. Further reproduction prohibited without permission.

proportional to strain rate to the one-third power. They also found that at logarithm of strain rates between 1 and 1.1 1/sec the ratio of static to dynamic stress increased between 2.7 to 3.6 in the splitting tests and, between 1.6 to 2.4 in the direct tensile test. Grady, E.E., et al.,[77-79] and Birkimer, D.L.,[98] reported the same results on brittle materials either from the flaw size study or the energy method.

The split cylinder tests by Wakabayashi, M., et al.,[80] and the direct uniaxial tests performed by Komlos, K.,[81] also indicate the increase in tensile strength of cement based materials under impact loading.

Suaris, W., and Shah, S.P.,[14] performed impact tests on mortar and concrete by using a drop weight impact tester. They recorded that by increasing the strain rate from 0.67×10^{-6} 1/Sec. to 0.27 1/Sec, in mortar and concrete, modulus of rupture increased by 1.67 times in mortar and 1.46 in concrete. They also found that the higher the value of the static flexural strength, the lower the relative increase in the flexural strength with increasing strain rate will be.

Brooks, J.J., and Samarai, N.H.,[74] found that increasing stress rate by 10^4 in direct tension tests resulted in an increase of 82% for the tensile strength,

Reproduced with permission of the copyright owner. Further reproduction prohibited without permission.

while the same stress rate increase in three-point bending tests would lead to only a 41%-62% increase in the flexural strength.

Weerheijm, J., and Reinhardt, H.W.,[83] studied the extension of penny-shaped cracks in linear elastic materials. They concluded that the moderate and steep increase in the tensile strength for low response high loading rates were caused by two different phenomenon.

For loading rates up to about 10 GPa/sec the strength increase was caused by an increasing energy demand to form the final fracture plane. Beyond 10 GPa/sec, aggregate and multiple fracture occurred as well as changes in the mechanical response of the material around the crack tips caused the steep increase. A decreasing crack propagation velocity resulting in a strength increase was caused by the distribution of the applied energy over the various types of energy changes.

The reported results from the three most common tests, namely the uniaxial tensile, flexural and compressive tests show that tensile strength is the most sensitive while compressive strength is the least of the three properties to changes in strain rate[21] as shown in Figure 2.14. This means that cracking plays an important role in determining the effects of strain rate on the properties of concrete. In particular, it appears

Reproduced with permission of the copyright owner. Further reproduction prohibited without permission.

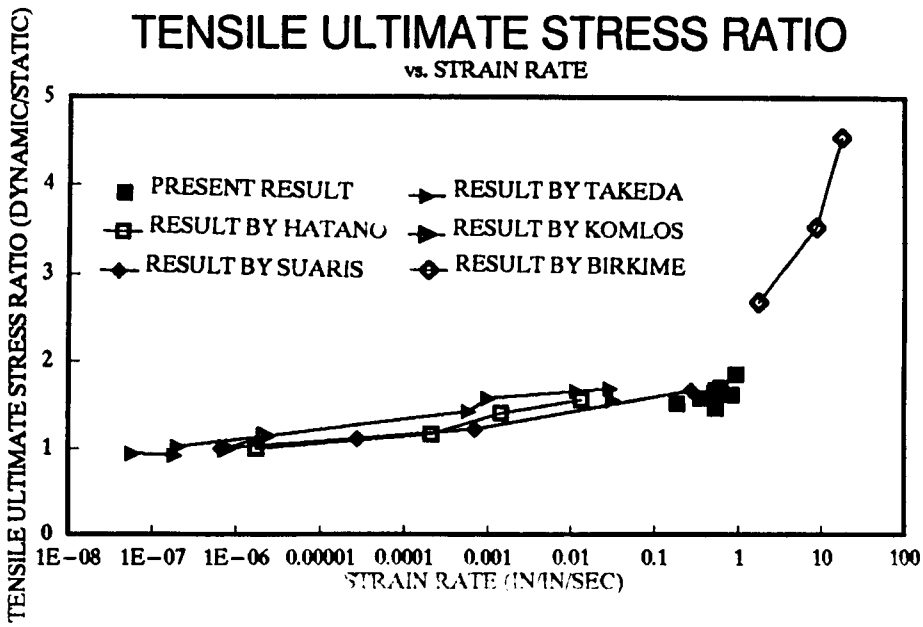

Figure 2.13 Survey of results of experiments on tensile strength related to loading rate.

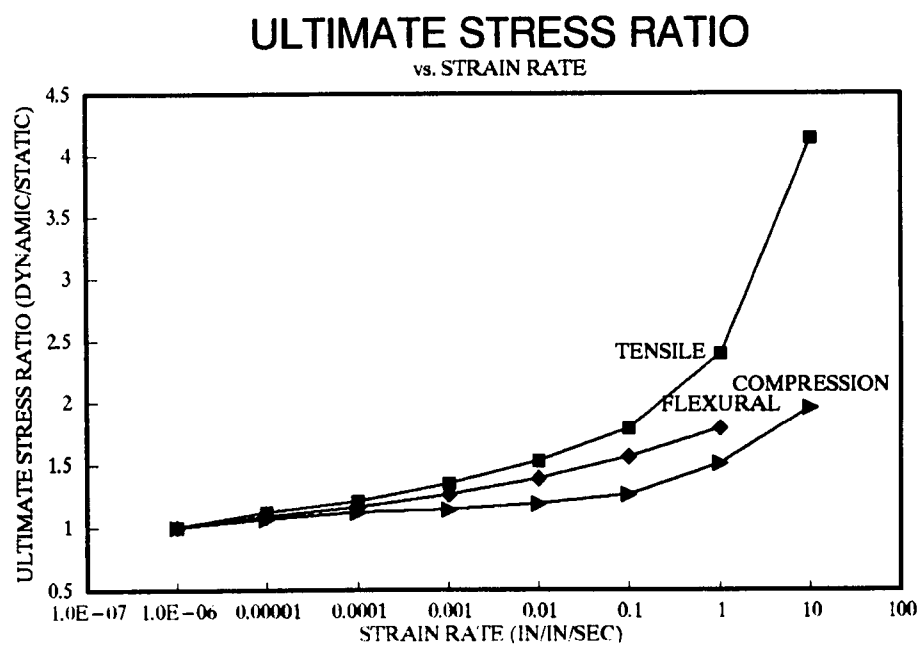

Figure 2.14 Relative increase in strength vs. strain rate for plain concrete specimens in tension, flexure and compression.

Reproduced with permission of the copyright owner. Further reproduction prohibited without permission.

that with an increase in strain rate, the extent of internal microcracking decreases and, as a result, the stress-strain curve becomes less nonlinear at a higher strain rate.

Slower loading rates allow more subcritical crack growth to occur, leading to the formation of larger flaws and hence, smaller fracture loads.

Microcracks are believed to be the source of fracture initiation, since at their tips local stress concentration can lead to the extension of these microcracks under existing externally applied loads. Stiff aggregate particles embedded in the cement matrix also cause local stress concentrations in the zones around the particles which may be intensified by the presence of bond cracks at the interfacial zone.

Earlier studies[64,22] have shown that due to differences in the extent of micro-cracking in the specimens, the weaker cement based composites exhibit greater strain rate sensitivity.

For higher impact tensile strength, cracks are forced to develop along shorter paths of higher resistance. Cracks may be arrested due to the heterogeneity of the materials considered from both the micro and macro levels, or the crack tip encounters material zones of either lower

Reproduced with permission of the copyright owner. Further reproduction prohibited without permission.

stress intensity or higher capacity which take up the local concentration of tensile stresses.

It has been observed that cracks usually passed under aggregate particles in statically loaded concretes, but for impact, the fracture surfaces often have many fractured aggregate particles. The fracture process normally starts at the interface of the aggregate particles and propagates in the direction perpendicular to the tensile load.

2.3.3.5 Modeling of Concrete Composites Under Tensile Impact

In order to incorporate the effect of strain rate in to the design of structures, a model is needed to predict the material behavior under impact loading.

In the study by Kormeling, Zielinski, and Reinhardt [11] on impact fatigue tensile tests, four concrete mixes of microconcrete and mortar were tested. The observed experimental data indicated that tensile fatigue of concrete, like compressive fatigue, was progressive in character[84-86]. The following linear relationships between upper stress limit σ_{max} and the number of loading cycle (N) were proposed:

for concrete mix,

$$\sigma_{max} = 4.30 - 0.318 \ln N \qquad (2.2)$$

Reproduced with permission of the copyright owner. Further reproduction prohibited without permission.

for microconcrete,

$$\sigma_{max} = 5.21 - 0.439 \ln N \qquad (2.3)$$

for mortar,

$$\sigma_{max} = 2.82 - 0.268 \ln N \qquad (2.4)$$

The predicted responses from these equations were found to be in a fairly good agreement with the experimental results

Heilmann, Hilsdorf, and Finsterwalder[87] studied the influence of strain rate on concrete using specimens of three different concrete qualities (compressive strength of 14, 22.4 and 35 N/mm^2). The strain rates used in their tests were $1.3x10^{-9}$, $2.1x10^{-8}$, $1.7x10^{-7}$ and $1.3x10^{-6}$ 1/sec.

An empirical relation between the tensile strength and the static compressive strength was proposed:

$$\sigma = b\ e\ [\ (\ \sigma_o\ )^2\ ]^{1/3} \qquad (2.5)$$

Where:

- σ = Tensile strength of concrete under impact.
- σ_o = Static tensile strength of concrete.
- b = 0.55 for axial loading.
- e = The influence factor due to strain rate as given in table(2.1)

Reproduced with permission of the copyright owner. Further reproduction prohibited without permission.

Table(2.1): STRAIN RATE INFLUENCE FACTOR

$\dot{\varepsilon}$, 1/s	1.3×10^{-6}	1.7×10^{-7}	2.1×10^{-8}	1.3×10^{-9}
β	1.13	1.00	0.98	0.96

Several investigators have proposed models for brittle materials such as concrete, rocks, glass and ceramic based on thermally activated flaw growth. Charles, R.J.,[88,89] proposed the following equation:

$$V = D\,(\sigma_m)^n\,(\exp)^{-A/RT} \qquad (2.6)$$

where:

V = Velocity of flaw in the direction of maximum tensile stress.
σ_m = Stress at the flaw tip.
A = Activation energy.
R = Gas constant.
T = Absolute temperature.
D,n = Constants.

Through a stress concentration relationship, he proposed:

$$\sigma_f \propto (\dot{\sigma})^{1/n+1} \qquad (2.7)$$

where:

σ_f = Ultimate stress
$\dot{\sigma}$ = Stress rate
n = Constant.

By fitting experimental data, "n" was found to be 16 for static fatigue tests[89]. The value of "n" for strain rate below 10^{-4} 1/sec remained the same and no data was checked for strain rate higher than 10^{-4} 1/sec.

Reproduced with permission of the copyright owner. Further reproduction prohibited without permission.

In order to predict the sensitivity of material properties due to strain rate, Evans, A.G.,[91] conducted studies on cement based materials. He confirmed the conclusions reported by Charles, R.J.,[88,89] that the ultimate strength of cement paste, changed with the applied stress rate. He proposed an empirical formula similar to equation(2.7).

From the available experimental results, Suaris and Shah[14] concluded that the commonly used equation (2.7) is not an accurate expression since the value of "n" decreases with the increase in strain rate. They reported the "n" values from 47 to 16 as the strain rate increased from 10^{-6} to 10^{-1} 1/sec as illustrated in Figure 2.15.

Mihashi, H., and Wittmann, F.H.,[69] studied the influence of rate of loading on the strength of concrete. Using a stochastic approach, they developed expressions to predict the strain-rate sensitivity of the fracture strength in the form of:

$$\sigma_f \propto (\dot{\varepsilon})^{1/n+1} \qquad (2.8)$$

where:

σ_f = Ultimate strength.
$\dot{\varepsilon}$ = Strain rate.
n = Constant.

Reproduced with permission of the copyright owner. Further reproduction prohibited without permission.

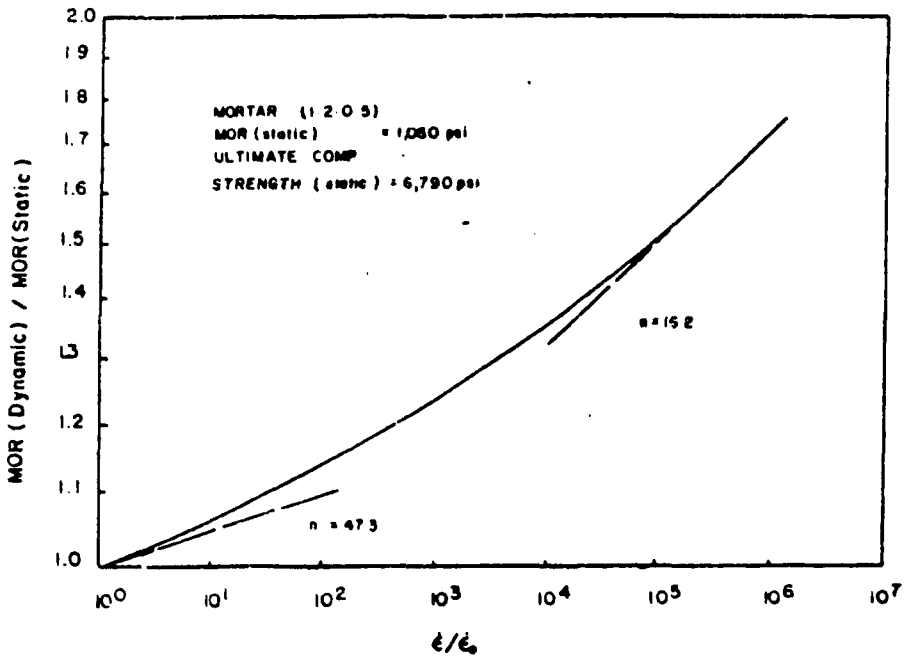

Figure 2.15 Relative MOR versus strain rate for plain concrete.

Reproduced with permission of the copyright owner. Further reproduction prohibited without permission.

Mindess, S., and Nadeau, J.S.,[23] performed experiments at a high strain rate of 0.3 1/sec and found that the "n" value for equation (2.8) to be 17.7 in mortar.

Mellinger, F.M., and Birkimer, D.L.,[76] found that the "n" value in equation (2.8) decreased to 2 at a higher strain rate. Results reported by Mindess, S., et al.,[23,90] indicated different values for "n" at low and high strain rates. This is partly due to different crack velocities in these two cases.

Komlos, K.,(93) studied the strain rate effect on the tensile behavior of different concrete. Conducting tests at the stress rates of 2.5×10^{-5} and 8.3×10^{-5} N/mm^2 per millisecond and, by varying the aggregate to cement ratio, in conjunction with the results reported by Sneikin, Nikolab, Hatano, and Kvirikadze[94], they developed an experimental formula as follow:

$$\sigma / \sigma_0 = 1.0 + 0.1 \log(\dot{\sigma}/\dot{\sigma}_0) \qquad (2.9)$$

Where:

σ = Dynamic ultimate stress.
σ_0 = Static ultimate stress.
$\dot{\sigma}$ = Dynamic stress rate.
$\dot{\sigma}_0$ = Static stress rate.

Mihashi and Izumi[92] studied the behavior of concrete under tensile impact loading using the stochastic

Reproduced with permission of the copyright owner. Further reproduction prohibited without permission.

theory for fracture of concrete. They proposed the following formula:

$$\sigma_{td}/\sigma_{ts} = (\dot{\sigma}_d/\dot{\sigma}_s)^{1/1+L} \qquad (2.10)$$

Where:

σ_{td} = Mean value of dynamic strength at stress rate of $\dot{\sigma}_d$.
σ_{ts} = Mean value of the quasi-static strength at stress rate of $\dot{\sigma}_s$.
$\dot{\sigma}$ = Stress rate.
L = Material parameter.

Mihashi and Wittmann[69] assumed: 1) the micro-crack length depends on the elastic modulus, 2) the surface energy of the material has a given statistical distribution and, 3) the material defects and the characteristic properties of each element in addition to the micro-crack have the same statistical distribution in the whole region. They also assumed the theory of rate process is a function of the activation energy of the stressed media and, the rate of the crack nucleation is proportional to the number of molecules in the vicinity of the tip of the pre-existing cracks, and concluded that:

$$\sigma/\sigma_0 = (\dot{\sigma}/\dot{\sigma}_0)^{L} \qquad (2.11)$$

Where:

σ = Dynamic ultimate strength.
$\sigma 0$ = Quasi-static ultimate strength.
$\dot{\sigma}$ = Stress rate.
L = Material parameter.

Reproduced with permission of the copyright owner. Further reproduction prohibited without permission.

They reported that the above relationship is valid for compressive loading, but is not applicable to tensile behavior.

Split tension testing under impact load was conducted by Ross,C.A., et al.,[15] using Split Hopkinson Pressure Bar technique. The specimens were compressed diametrically. The peak transmitted compressive stress was assumed to be proportional to the tensile strength through a relation similar to the static equation:

$$\sigma_{td} = \frac{2\ P_t}{\pi\ D\ L} \qquad (2.12)$$

and,

$$P_t = A_B\ \sigma_t$$

Where;
σ_{td} = Dynamic tensile strength.
A_B = Cross-sectional area of the bar.
σ_t = Peak transmitted compressive stress.
D = Cylinder diameter.
L = Cylinder length.
π = Constant(3.14)

The slope of the transmitted stress versus time was considered to be the stress rate. To find the strain rate, they used the stress rate, assumed a linear elastic material and, divided the stress rate by static modulus of elasticity. They found that for logarithm of strain rate between 1 to 1.1 1/sec, the dynamic to static stress ratio was between 2.7 to 3.6 in split test, and 1.6 to 2.4 in

Reproduced with permission of the copyright owner. Further reproduction prohibited without permission.

direct tensile test. The large variation of dynamic to static stress ratio between split tensile and direct tensile tests are indications of an error in the original assumption that the peak transmitted compressive stress is proportional to the tensile strength through a relation similar to static condition. Another shortcoming of this test was that there is no way to evaluate the modulus of elasticity during the impact test. Finally, the assumption that the modulus of elasticity under static test is equal to that of dynamic test is questionable [11,75,76,96].

In the study by Mindess[97], it was found that in the following equation:

$$\sigma_d = A + B \log R \qquad (2.13)$$

Where;

σ_d = Impact strength(in tension, compression, or flexural).
R = Stress rate, (or strain rate, or rate of cross-head deflection of the testing machine).
A,B = Material Constants.

the data are not particularly consistent quantitatively from different studies. Also material constants "A" and "B" are varied in different reported researches.

2.3.3.6 Effect of Tensile Impact on Strain

To predict the strain at failure of cementitious composite materials under tensile impact loads, Birkimer,

Reproduced with permission of the copyright owner. Further reproduction prohibited without permission.

D.L.,[98,99] has proposed the following formula based on critical fracture strain energy concept.

$$\varepsilon_f = [\ 6\ U_f / A\ E_d\ C_l\ ]\ x\ \dot{\varepsilon}^{1/3} \qquad (2.14)$$

where:

ε_f = Strain at failure.
U_f = Strain energy at failure.
A = Cross-sectional area of specimen.
C_l = Longitudinal wave velocity
$\dot{\varepsilon}$ = Strain rate.

Although the above equation was verified for the strain rates between 2 to 35 1/Sec, it was found not to be valid for wide range of other strain rates[82].

In the study conducted by Kormeling, H.A., et al.,[11] it was found that the mean value of the strain at the peak stress was 1.46 times higher in impact than in static cases.

Based on experimental results Zielinski[95] concluded that the impact strain at maximum tensile stress was larger than that of the static strain.

An increase of strain at maximum stress was also reported by Birkimer[98]. He proposed the following formula using data regression technique:

$$\varepsilon_{cr} = 0.1 + 0.01\ \dot{\varepsilon} + 0.26\ (1 - \exp^{-\dot{\varepsilon}}) \qquad (2.15)$$

Reproduced with permission of the copyright owner. Further reproduction prohibited without permission.

Compared to the static test where critical strain was roughly 0.1 0/00, the critical strain at strain rate of 4 1/sec was about 4 times than that of the static test. This result is much larger than the results reported by other investigators.

Therefore, it can be concluded that ultimate strain increases under tensile impact load, but there is disagreement as to the magnitude of the increase in the different studies reported.

2.3.3.7 Effect of Tensile Impact on Modulus of Elasticity

Kormeling, H.A., et al.,[11], studied the concrete behavior under impact tensile loading. They found the secant modulus increased for higher strain rates.

Takeda and Tachikawa[75] also observed that the secant modulus (at peak stress) increased with an increased rate of straining. They developed the relationship between the stress and strain rates as follow:

$$\dot{\sigma}/\dot{\varepsilon} = a\ (\ \dot{\varepsilon}\ )^{B-1} \qquad (2.16)$$

where:

$\dot{\sigma}$ = Stress rate
$\dot{\varepsilon}$ = Strain rate
B = 1.032

Reproduced with permission of the copyright owner. Further reproduction prohibited without permission.

Zielinski, A.J.,[95] used the Split Hopkinson Bar technique and found a slight increase in modulus of elasticity due to increasing strain-rate.

Mellinger and Birkimer[76] conducted impact tensile tests on concrete using the "Pallet Technique",[100,101]. They obtained a value for the static modulus of elasticity of 4.6×10^6 psi and the dynamic modulus of elasticity of 4.8×10^6 psi which indicated that the modulus of elasticity increased due to the higher strain-rate.

The study performed by Brooks, J.J., and Samarai, N.H.,[74] using three-point bending tests and direct tensile tests on concrete, found that the strain at peak stress increased with stress rate. However, this increase was less than that of the peak stress so he was concluded that the secant modulus at peak stress increased with stress rate.

Rusch, H.,[102], Wright, P.J.F.,[103], and Heilmann, A., et al.,[87] found that in flexural tests the modulus of elasticity increased as the rate of loading increased.

Suaris, W., and Shah, S.P.,[14] performed impact tests on mortar and concrete by using a drop weight impact tester on three-point-bend specimens. They recorded that by increasing the strain rate from 0.67×10^{-6} 1/Sec to 0.27

Reproduced with permission of the copyright owner. Further reproduction prohibited without permission.

1/Sec in mortar and concrete, modulus of elasticity increased by 1.17 in mortar and 1.21 in concrete.

The above studies indicate that the modulus of elasticity increased during impact tensile tests. But the reported magnitude of the increase varied in different studies.

2.3.3.8 Effect of Tensile Impact Load on Energy Absorption

Zielinski, A.J.,[95] found that there was more energy involved in impact loadings than for static loadings for mortar and microconcrete. He found the ratio of energy absorption of impact loading to energy absorption of static loading to be 5.6 for mortar, and 6.3 in case of microconcrete.

Suaris, W., et al.[14] performed impact tests on mortar and concrete using a drop weight testing set-up for three-point-bending tests. They recorded that by increasing the strain rate from 0.67x10-6 1/sec. to 0.7x10-3 1/sec., energy absorption up to peak load increased by 1.19 for mortar and 1.60 in concrete.

Reinhardt, H.W.[105] recorded energy absorption at the highest strain rate to be about 2-3 times higher than the lowest strain rate for mortar and concrete.

Reproduced with permission of the copyright owner. Further reproduction prohibited without permission.

It can be concluded that the energy absorption of cement based materials is strain rate sensitive. Additionally, concrete absorbed more energy than mortar. But, again the level of rate sensitivity varied in different studies.

2.3.3.9 Effect of Tensile Impact Load on Stress-Strain Relation

Zielinski[95] observed that the normalized stress strain curve for static and dynamic loading are very similar. This is illustrated in Figures 2.16 and 2.17. it can be seen that they are similar in shape, but the characteristic points of discontinuity are shifted according to the absolute value of maximum stress and corresponding strain.

Suaris, W., and Shah, S.P.,[82] noticed that with an increase in strain rate, the extent of internal microcracking decreased, and as a result, the stress-strain curve become less nonlinear at a higher strain rates.

2.4 Dissertation Problem

Structures are often subjected to impact loads during their lifetime. In general, the behavior of materials

Reproduced with permission of the copyright owner. Further reproduction prohibited without permission.

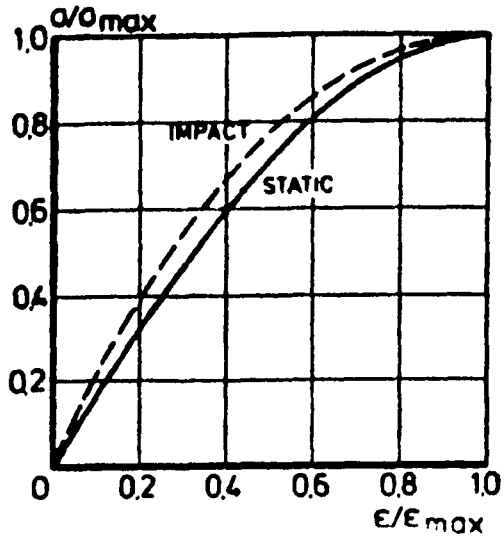

Figure 2.16 Normalized static and impact stress-strain lines for microconcrete.

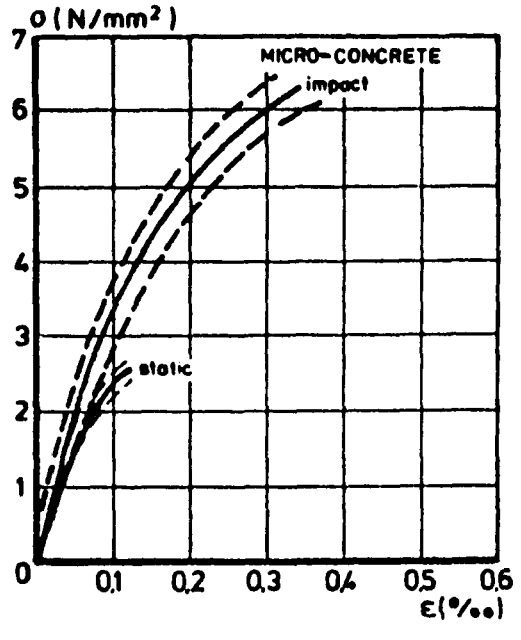

Figure 2.17 Static and impact stress-strain curves for microconcrete.

Reproduced with permission of the copyright owner. Further reproduction prohibited without permission.

under impact loads is vastly different from behavior under static conditions.

A large amount of literature is available on the dynamic properties of steel and the influence of various properties such as chemical composition and physical microstructures. This information is also available for aluminium and its alloys, and many plastic materials as well. Eventhough concrete is one of the most common building materials there is little research on its behavior under impact loadings.

Among concrete characteristics, compressive strength is the most studied, while tensile behavior under impact loading received lesser attention. In cementitious materials, cracking behavior under shear forces, and bond properties of reinforcing steel are influenced by tensile strength of concrete. Therefore, it is of great importance to study the tensile behavior of concrete materials under impact.

The effect of tensile impact loads on properties of cement based materials are studied as local effects and global effects. The local response of structures are complex in nature, therefore, no entirely rational computational model is available. In case of the global effects of tensile impact loads, two approaches are used. They are repeated tensile impact loads and single impact tensile loads. In case of repeated impact loads, the

Reproduced with permission of the copyright owner. Further reproduction prohibited without permission.

result is superficial since it contains no relationship between energy input, energy losses and inertial effects. But, for single tensile impact loads, there has been few studies because of difficulties in the testing set-ups and instrumentation.

There have been three approaches to study the tensile behavior of concrete under single impact loading, i.e. split tension, direct tension and flexural tests. In case of splitting tension impact loads, the solid cylindrical specimen is loaded diametrically. The main problem with split tensile test is that only the tensile strength is recorded and no stress-strain curve can be produced directly. In the SHPB direct tension test, there are several points to consider. Since the specimens are glued to the bars, the bond and material behavior of glue will introduce distortion in the measurement readings. Also, it is hard to produce uniform stress along the length of the specimens. Finally, it is difficult to achieve proper alignment. Therefore, a new specimen configuration is needed in order to accurately study the tensile behavior of cementitious materials under impact loading. In case of flexural tests, the data is analyzed assuming simple beam theory under static loading would apply to a dynamic loading condition. Some of the shortcomings of flexural tests are that the specimen cross section is under different strain rates during a specific loading rate.

Reproduced with permission of the copyright owner. Further reproduction prohibited without permission.

Specimen failure is due to a combined tensile and compressive mode. Also, since the strength/mass ratio of concrete is low, a large inertial response is introduced into the load readings.

One of the objectives of the present research is to develop a new specimen configuration with a high strength/mass ratio and proper instrumentation to overcome the inertial response in the load readings. The configuration should allow to study the direct tensile behavior of cementitious materials. The advantages of the drop hammer testing set up were mentioned previously combined with the new specimen configuration, this testing set up is a more suitable means to study the behavior of cement based materials under direct tensile impact loads.

Reproduced with permission of the copyright owner. Further reproduction prohibited without permission.

CHAPTER 3

EXPERIMENTAL PROGRAM

3.1 Selection Criteria

In developing the new test system, the following criteria were considered:

1- The system should produce results which quantitatively define material behavior relative to some readily understandable and fundamentally significant reference level of behavior.

2- The system should clearly distinguish levels of performance of different materials with satisfactory repeatability.

3- The results should reflect material behavior independent of specimen size and shape.

4- The test system should be cost effective with particular attention to utilizing the existing equipment already employed for testing by others.

3.2 System Description

A typical instrumented impact test system consists of three major components, the dynamic load cell, the load cell display system, and signal data acquisition unit. The dynamic load cell is the tup (or striker) which produces an electrical signal of the interaction force between the

Reproduced with permission of the copyright owner. Further reproduction prohibited without permission.

specimen and the machine. The data display system is usually an oscilloscope which records force on the specimen as a function of time. The signal conditioning unit balances the strain-gage bridge, amplifies the bridge output, filters the signal, and provides a calibration function to determine the bridge amplification.

The output signal(the load signal) is inherently filtered to some degrees by the signal conditioning unit. However, at times additional filtering is employed to eliminate a high-frequency noise in the output signal to make data interpretation easier. This increased filtering prolongs the response time of the testing system.

High-speed tape recorders, transient signal recorders, computers and an oscilloscope are some of the signal display components. The oscilloscope is most commonly used signal display component which provides a better signal resolution relative to the other display units.

3.3 Strain Rate Experimental Set-up

An impact testing system was developed in order to study the direct tensile properties of mortar and concrete under high strain rates. The design of the system required the development and selection of the testing frame,

Reproduced with permission of the copyright owner. Further reproduction prohibited without permission.

specimen configurations, transducers, and data recording devices as described below.

3.3.1 Testing Frame Description

The dynamic testing apparatus utilizes a drop weight that impacts the specimen to produce the required high rate of straining. A drop weight configuration guided by two columns as shown in figures 3.1 and 3.2, was selected for these tests as opposed to a pendulum impact mass and arm assembly due to its simplicity and inherent stiffness.

The hammer weighs 50 pounds. This weight can be increased to 110 pounds by the addition of steel plates to the top of the weight. The drop weight is raised by a motor driven cable. The weight is released by a solenoid activated jaw. The testing bed is constructed from a 2-inch thick steel plate. This is bolted to a 9 inches by 9 inches steel box member having a 5/8 inch wall thickness. The box member is in turn grouted and bolted to the laboratory's 3 foot thick reinforced concrete load floor. This method of construction was intended to provide maximum rigidity for the testing bed.

3.3.2 Specimens for Impact Tensile Tests

The load-time response of a specimen during impact testing is usually measured using strain gages attached to

Reproduced with permission of the copyright owner. Further reproduction prohibited without permission.

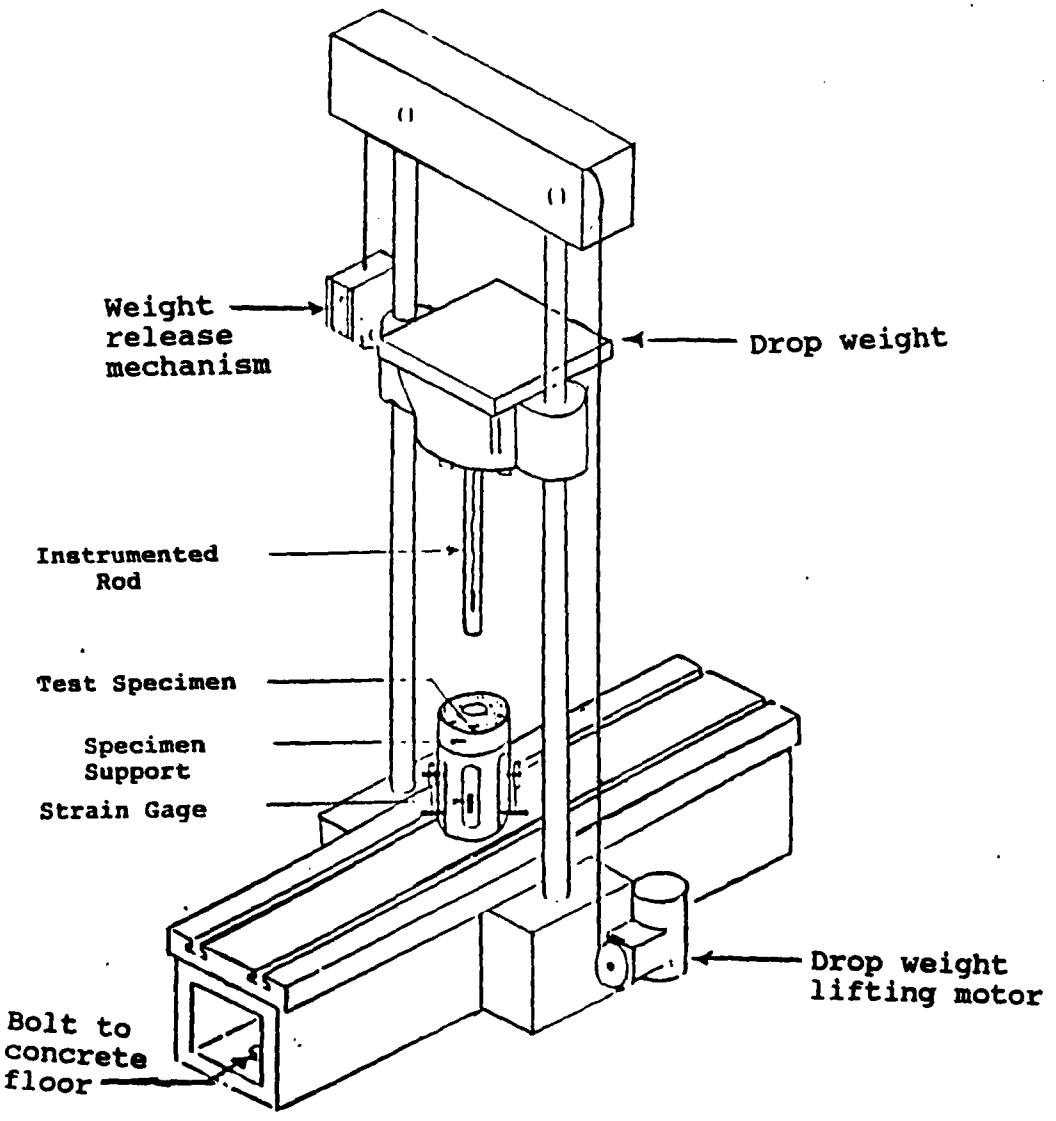

Figure 3.1 A Schematic showing the general features of instrumented drop hammer test.

Reproduced with permission of the copyright owner. Further reproduction prohibited without permission.

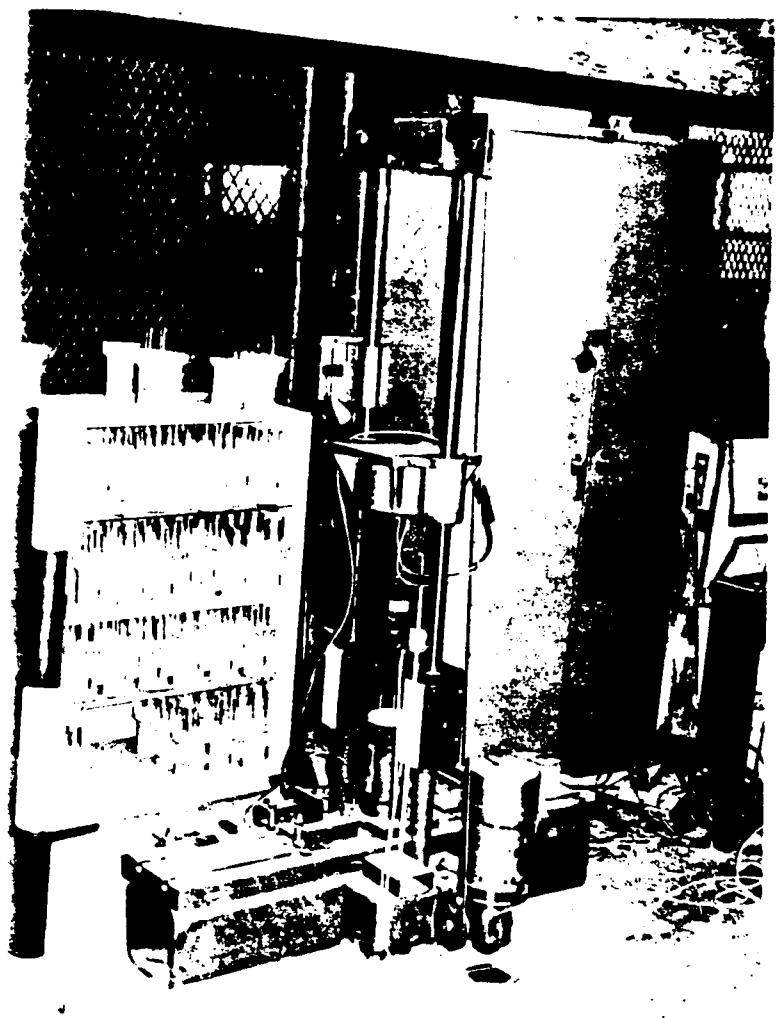

Figure 3.2 Overall view of drop-hammer weight testing system.

Reproduced with permission of the copyright owner. Further reproduction prohibited without permission.

the tup or the load cell portion of the impact hammer. The signal generated by strain gages consists of the following components:

a) The mechanical response of the specimen
b) The inertial effect due to acceleration of the specimen from rest [106-108].
c) Stored elastic energy and reflected stress waves in low frequency fluctuations [107,109].
d) High frequency noise produced by the amplifier system [107,110].

To isolate the mechanical response of the specimen, high gain strain gages are used to generate a relatively large signal to noise ratio and, at times, electronic filtering is supplied to suppress noise. A new specimen type is used and a rubber pad is introduced at the contact zone between the load cell and the specimen to minimize the inertial effect. Furthermore, the new specimen is analyzed to check the effect of wave propagation along the specimen.

3.3.2.1 Specimen Configuration

To study the tensile behavior of cement based materials under impact loadings, solid cylindrical specimens[24] and a beam specimens[67] are frequently used by the researchers.

Reproduced with permission of the copyright owner. Further reproduction prohibited without permission.

Cylindrical specimens which are used in the "Split Hopkinson Bar" testing set-up, has four deficiencies[15]:

1) Error in material behavior readings. Since glue is used between the specimen and aluminium bars, interference from the material behavior of the glue is inevitable.

2) Introduction of error in load readings due to stress reflection at the contact zone between the specimen and the bars- Since the load is analyzed by measuring the strain in the aluminium bars, the stress measured by converting the strain readings in the bars would be different than the stress applied to the specimen.

3) Lengthy procedure for specimen surface preparation. The specimen surface on the sides of contact to the bars should be ground to a smooth surface, the aluminium bars should be cleaned of glue and any residues from previous tests, and then the specimen to be glued to the bars.

4) Proper alignment and specimen connection difficulties.

The using of beam specimen and attempt to analyze the tensile behavior of materials by three-point bending set up have the following disadvantages.

1) In the beam theory, it is generally assumed that plain section remains plane before and after bending. This assumption leads to a further assumption that there is a linear variation of strain-rate when applied to impact

Reproduced with permission of the copyright owner. Further reproduction prohibited without permission.

cases. The variation of strain rate across the beam depth means that it is not possible to identify a unique strain rate to any testing condition since strain rate would vary from maximum compression in one side to maximum tension in the other side as seen in Figure 3.3.

2) Another serious problem is the high inertial load to equivalent bending load ratio in concrete specimen.

After a series of study, an instrumented specimen was developed to eliminate the above shortcomings. The specimen is a closed hollow cylinder as seen in figure 3.5. It is supported at the top by a steel cylinder prepared to fit the specimen. The load is applied at the bottom of the hole by a steel column. The column is instrumented at the tip and attached to the drop hammer. The specimen is a 3 inch diameter, 4 inch height main cylinder with a transition at the top to a 4.5 inch diameter cylinder which is used as the supporting section. In order to apply the load in tension, a 1.25 inch diameter blind hole is created in the center which stops before the bottom of the cylinder. The mold was made using a 3.0 inch conventional plastic cylinder as shown in figure 3.4. The top 2 inches of the cylinders were cut and the remaining 4 inches were glued to a P.V.C. "piping bushing" at the top. In order to have the 1.25 inch diameter hole, a 1.25 inch diameter P.V.C. closed-end pipe

Reproduced with permission of the copyright owner. Further reproduction prohibited without permission.

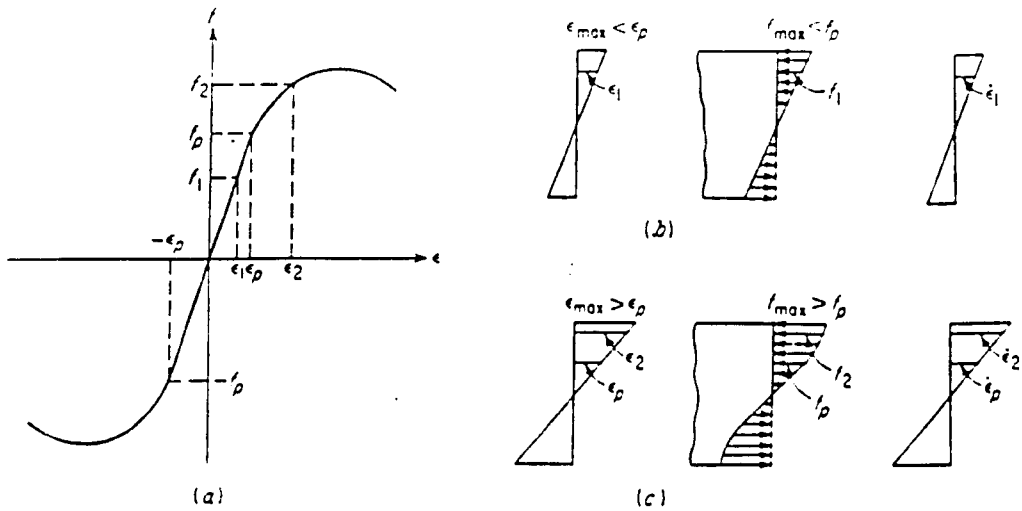

Figure 3.3 Elastic and inelastic stress distributions in homogeneous beams.

Figure 3.4 Detailed pieces of specimen mould.

Reproduced with permission of the copyright owner. Further reproduction prohibited without permission.

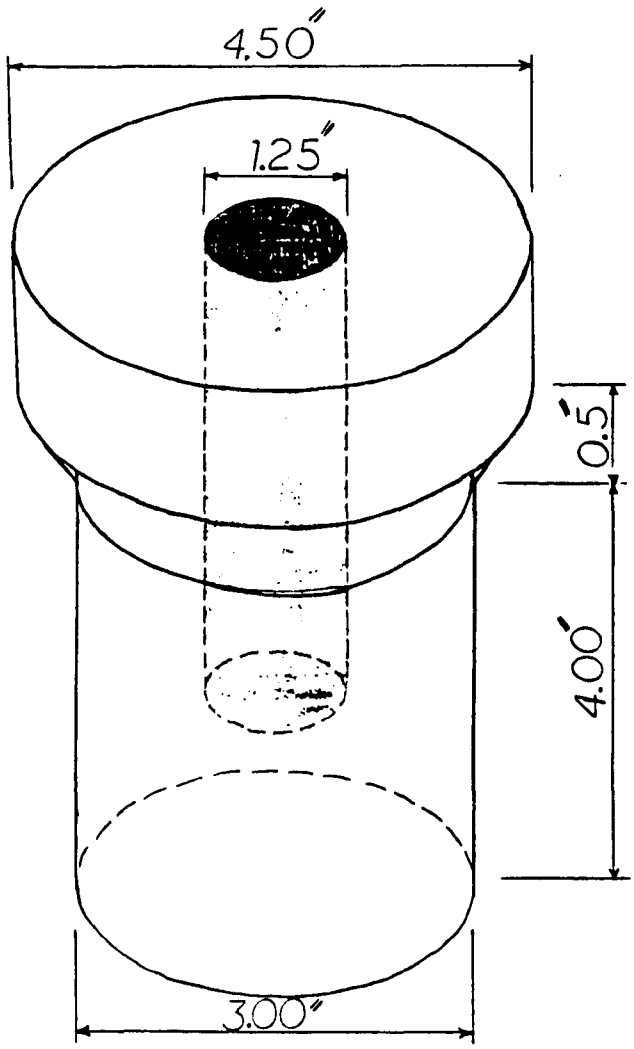

Figure 3.5 Schematic of the new hollow cylinder.

Reproduced with permission of the copyright owner. Further reproduction prohibited without permission.

was used. A cap was made for the top of the mold to keep the 1.25 inch diameter pipe in the proper position.

The strength/mass ratio between the new and the beam specimens are analyzed and compared in the Theoretical Model section. It is found that the strength/mass ratio of the new specimen is 14 times smaller than that of the beam specimen. This indicates that the inertial effect on the load readings of the present study is much smaller than the three-point-bend test.

3.3.2.2 Specimen Development

In order to develop the proper specimen configuration, the first step was to find the proper bottom thickness so that it would act as a solid plate and the specimen would fail in direct tension along the wall of the cylinder. A 0.25 inch plate thickness was first examined, but the specimen failed in shear or sometimes in a combination of shear and tension as shown in Figure 3.6. The bottom thickness was then increased gradually up to 1.25 inches. Another difficulty was encountered due to narrow stress flow path combined with a sharp corner at the interface between the main body of the specimen and the supporting section, causing a stress concentration to develop at the neck of the specimen and fail in that region as opposed to failure at somewhere below the neck

Reproduced with permission of the copyright owner. Further reproduction prohibited without permission.

as it is shown in Figure A.1 in Appendix "A". To solve this problem, the height of beveled cylindrical support was increased to 2 inches. However, this was not sufficient, as illustrated in Figure 3.7. To overcome this, rebars were installed vertically from top and extended until 1.0 inch bellow the neck of the specimen. At first two #2 rebars were installed and a trial was conducted. After examining the specimen, it was concluded that more rebars were needed. After a few more trials, the number of rebars needed to give a satisfactory results was found to be four as shown in Figure 3.8 and A.2, and A.3 in Appendix A.

3.3.2.3 Mix Detail and Specimen Fabrication

The hollow cylindrical specimens in this study were cast in P.V.C. molds. The cracking of concrete depends upon the composition of the concrete and the curing condition. To reduce the number of variables affecting the mechanical properties, the curing conditions of the specimen were kept the same. Twenty specimens were cast each time and kept under identical temperature and humidity conditions.

Impact tests were carried out on the mortar matrix using a 1:2:0:0.6 (cement:sand:aggregate:water, by weight) mix and concrete matrix using a 1:2:2:0.5 mix with compressive strength in the range of 6000-8000 psi. They

Reproduced with permission of the copyright owner. Further reproduction prohibited without permission.

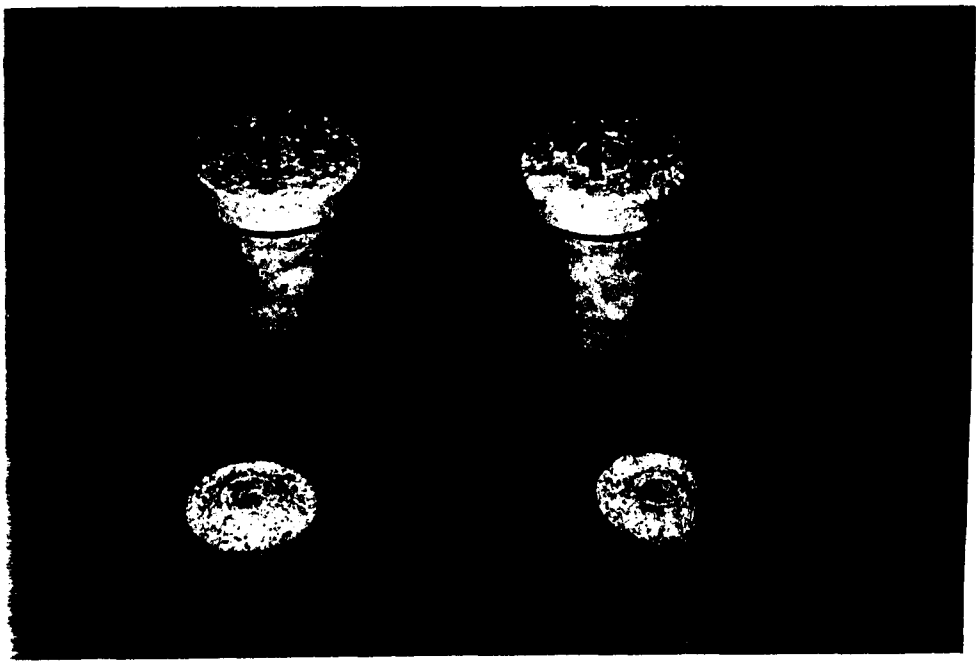

Figure 3.6 Typical specimen failure with thin bottom plate.

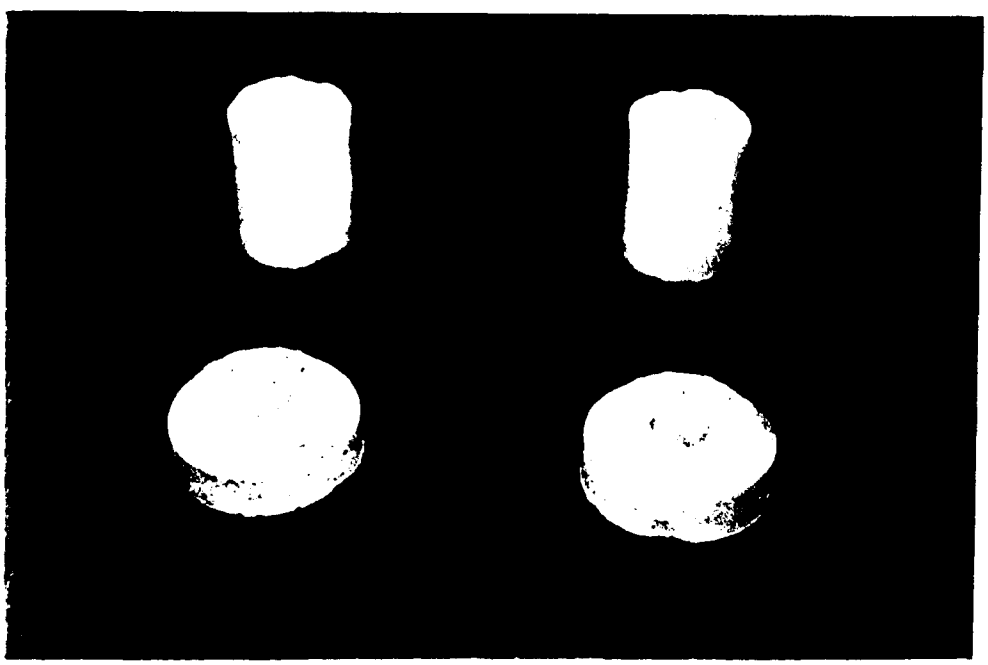

Figure 3.7 Typical specimen failure before introduction of any rebars.

Reproduced with permission of the copyright owner. Further reproduction prohibited without permission.

were made using Portland Cement Type I. In order to minimize scatter in the test results, particles of both sands and aggregate were graded strictly. Local siliceous sand passing sieve No.4, crushed limestone with maximum size of 1/4 inch were used. The mix were prepared by combining all the materials in a mechanical mixer. After they were thoroughly mixed for 5 minutes, the mixes were placed in the lubricated molds in four layers, with each layer being rodded and vibrated before the next layer was placed. Once the specimens were cast, they were covered with the cap and the four steel rebars were inserted in a fashion shown in Figure 3.9. The molds were kept under vibration for one more minute and then were allowed to cure for 24 hours before being demolded. Once removed from the molds, the specimens were submerged in lime saturated water for curing. Then the specimens were removed from the water and kept at room temperature and humidity until testing.

3.3.2.4 Specimen Set up

The new specimen configuration is supported at the top by a cylindrical steel ring mounted on a pipe. An instrumented steel column connected underneath the drop-hammer would hit the bottom end of the hole and cause tension on the wall of the specimens. The strain in

Reproduced with permission of the copyright owner. Further reproduction prohibited without permission.

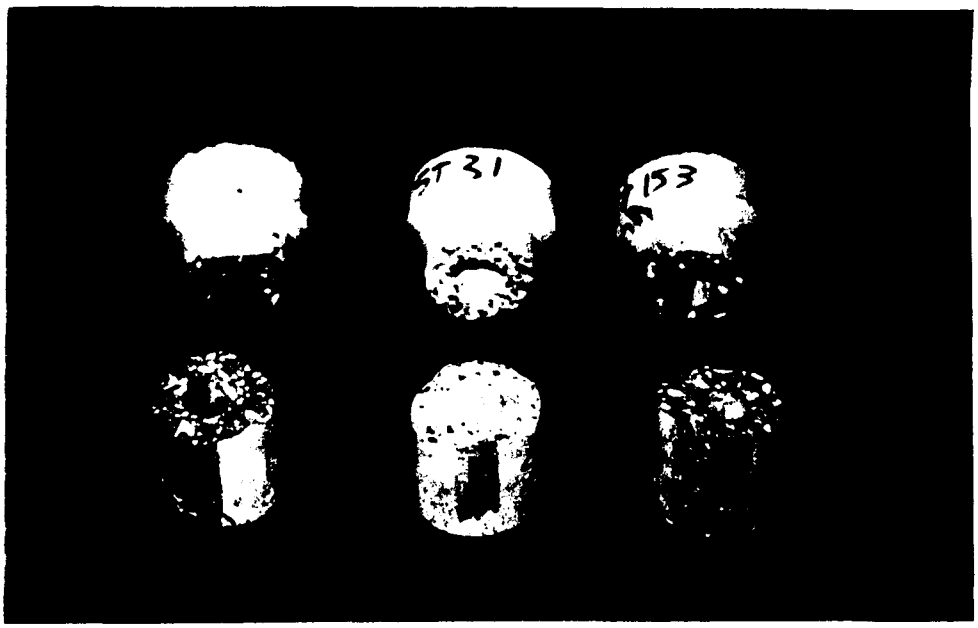

Figure 3.8 Typical specimen failure after the introduction of four rebars.

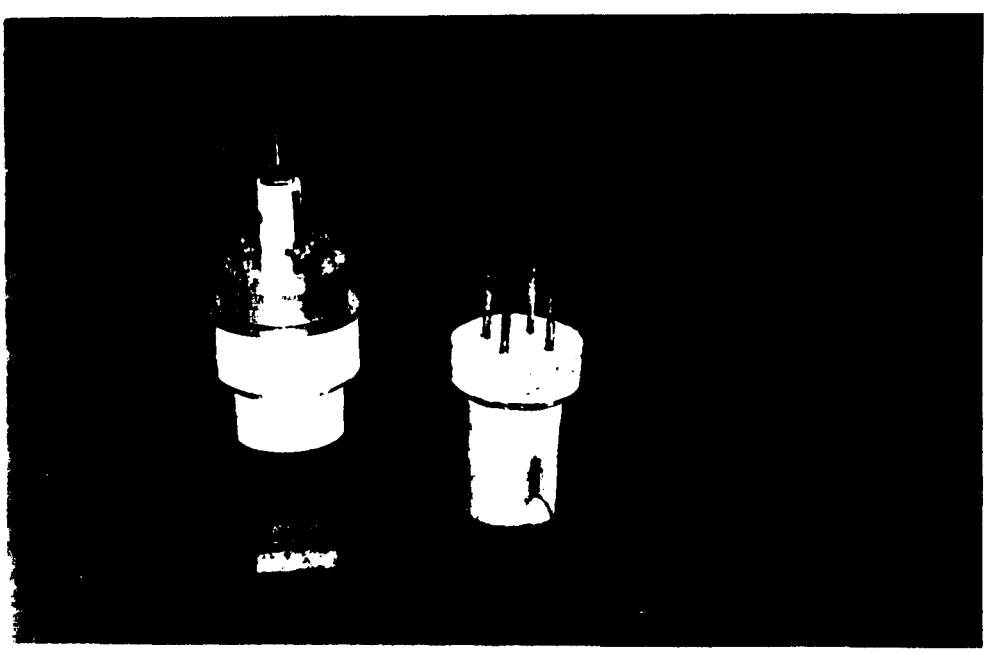

Figure 3.9 A specimen mould after the concrete is poured and a cured specimen.

Reproduced with permission of the copyright owner. Further reproduction prohibited without permission.

longitudinal direction is measured by strain gages on the specimen oriented in the direction of the applied load using a full bridge configuration as shown in Figure 3.10.

3.3.2.5 Specimen Instrumentation

After curing the specimen, (Measurements Group 500 BH-120) strain gages were bonded to cylindrical specimens using M Bound 200, as shown in Figure 3.11, for determining the strain of the specimens during impact. Due to the moisture sensitivity of M-Bond 200, the surfaces of the specimen were allowed to dry for at least two days before mounting the gage. Three strain gages are mounted on separate concrete plate and the last strain gage is cemented on the specimen to form a full Bridge configuration. The strain gage on the hollow cylinder specimen is glued on outside surface at two inches above the bottom of the cylinder oriented to measure in the direction of the applied load.

3.3.3 Rubber Padding

It has been reported[20,22,114-121] that during impact tests, the stress measured by the load-cell and that resisted by specimen are not the same. This behavior is mainly due to the inertial effect of the mass of the specimen. In high-strength ductile materials such as

Reproduced with permission of the copyright owner. Further reproduction prohibited without permission.

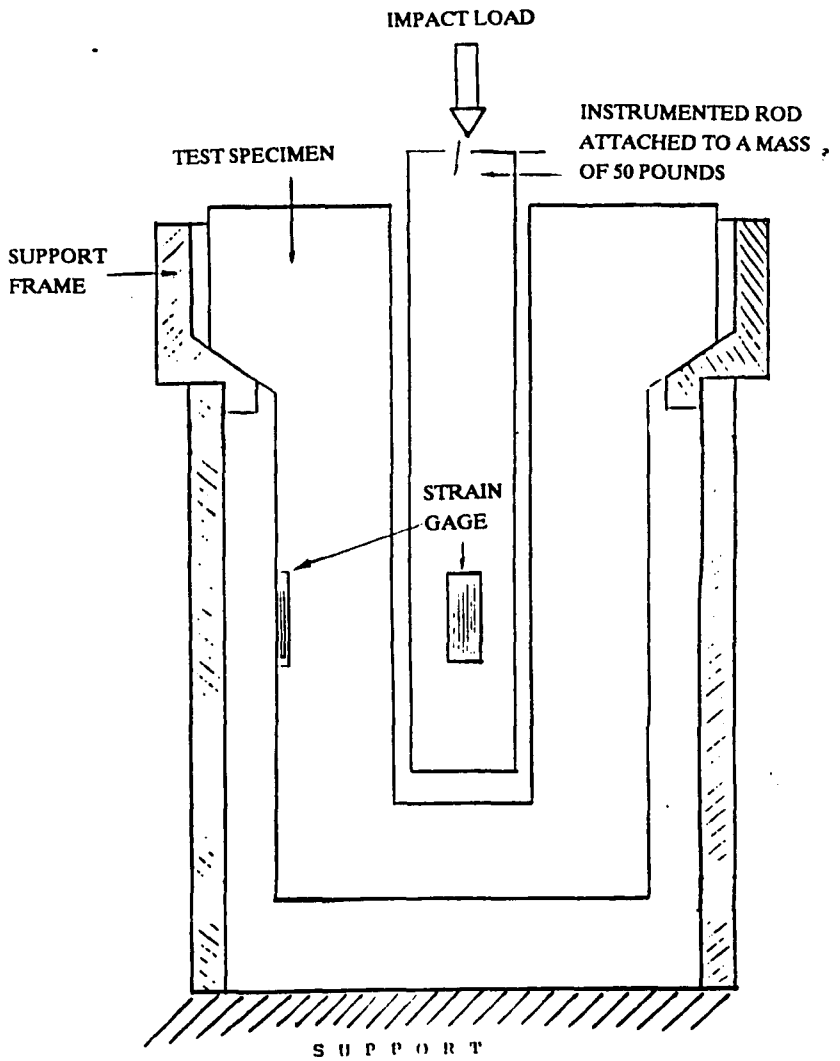

Figure 3.10 Specimen test set-up.

Reproduced with permission of the copyright owner. Further reproduction prohibited without permission.

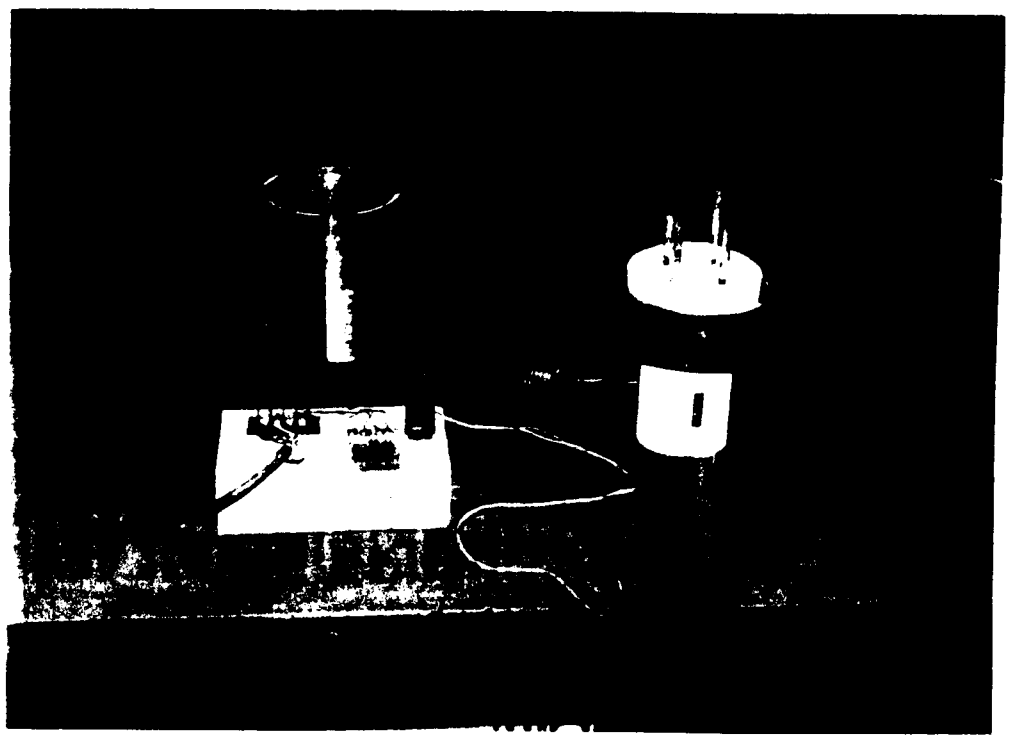

Figure 3.11 Instrumented specimen and its support.

Reproduced with permission of the copyright owner. Further reproduction prohibited without permission.

steel, the inertial oscillations are small compared to the applied load. Cotterell, B.,[114] recorded a linear relationship between inertial load and the impact velocity. He used a mean path procedure to evaluate the behavior of materials during impact test. But this approach led to large errors[107] for more brittle materials. Server, W.L., et al.,[115] then recommended that these errors can be neglected after three half periods of oscillations. Eventhough this procedure has been practiced as a standard for metal testing[114], it has been reported by Suaris and Shah[117] that such a practice is not acceptable for asbestos cement composites under impact loading. Using optical measurement of the araldite specimens, Kalthoff, J.F., et al.,[118] reported that peak loads recorded from the load cell can be overpredicted by as much as an order of magnitude. This overprediction is increased when specimens are larger and the impact velocity is higher.

In the study by Hibbert, A.P.,[119] on 100 X 100 X 500 mm plain and fiber reinforced concrete specimens, load-time and energy-time histories were recorded using an instrumented Charpy type testing set-up. He has concluded that there is a ten fold increase in impact strength over static strength of the same specimen. The same result has been reported for fracture energy of plain concrete.

Reproduced with permission of the copyright owner. Further reproduction prohibited without permission.

Kalthoff, et al.,[118] also observed the same increase in the peak load and energy absorption capacity.

In order to eliminate the inertial effect during the impact test, Winkler, et al.,[120] introduced an aluminium damping pad and noted that the pad reduced the recorded peak load. Suaris and Shah[117], studied the introduction of rubber pad at the tip of the striker and concluded that it reduced the specimen's inertial oscillations.

To eliminate the oscillation in load cell readings, the hollow cylindrical configuration is a more suitable specimen for direct tensile test on concrete based materials. Its small mass to specimen load resistance ratio, along with rubber pad application at the tip of the load cell, result in an ideal set up for studying the impact behavior of cementitious material. The effect of rubber pad on the impact properties of concrete is studied for the proposed specimen configuration.

3.3.4 Load Cell

For direct tension test, a load cell is developed to measure the applied force during impact at the point of contact. Measurement Group 250 BG semi-conductor strain gages are applied to a steel column in a full-Bridge configuration for high accuracy reading. A 2.7×10^3 V DC bridge excitation is used for the load cell. A cylindrical

Reproduced with permission of the copyright owner. Further reproduction prohibited without permission.

hole is cut at the tip of the load cell along its longitudinal axis to increase the sensitivity of the load cell. Four vertical notches are cut on the perimeter of the cylinder to concentrate the strain in the area of the strain gages and to increase the accuracy of the load cell. The notch lengths are twice as long as the length of the strain gages and have round ends to prevent the development of stress concentrations which may cause incorrect load readings. Finally, a steel disk with a diameter larger than that of the column is welded at the tip of the load cell to produce a uniform contact area with the specimen and to protect the load cell electric circuit against rubbing to the inside surface of the hole at the time of testing.

Elastic properties of steel are relatively strain-rate independent[122]. Since the load is measured by signals produced from the strain-gages for elastic strains, static and dynamic loads will produce the same strain-gage signals. Thus, the load cells are calibrated statically using a testing machine calibrated using standard traceable to NIST.

3.3.5 Trigger

The signal display component requires a command signal (external trigger) for coordination of the CRT

Reproduced with permission of the copyright owner. Further reproduction prohibited without permission.

sweep and the time when the tup makes or is about to make initial contact with the specimen. The time during which an impact event takes place could be as short as 1 millisecond. For the oscilloscope to capture the data during the impact, an automatic method to signal the start of the event must be employed. A switch was mounted on the column and set so that the drop weight would activate it when the weight reached a certain height. A positive line was connected to the oscilloscope triggering device and the other line was connected to the switch. The switch was attached to a Harison Laboratories 6204A DC voltage power supply. During the test, just before impact, the switch completed the circuit and triggered the oscilloscope. It should be mentioned that internal triggering of the sweep from the initial portion of the instrumented tup signal is not recommended since the zero load base line is not clearly defined. It is also desired to have the trigger signal constructed so that mechanical adjustments can be made for variations in specimen size or hammer velocity or both.

3.3.6 Electronic Signal Recording Devices

Since the time for completion of an impact event is very short, high speed tape recorders, transient signal recorders, computers and oscilloscope are some of signal

Reproduced with permission of the copyright owner. Further reproduction prohibited without permission.

display components. The most commonly used signal display component for instrumented impact testing is a digital oscilloscope system. It provides better signal resolution with respect to time than any other display component.

To provide the excitation voltage to the transducers and amplifier, and to filter low-level signal from strain gages before sending them to the oscilloscope for digitizing and recording, Measurement Group's 2311 amplifier conditioners were used, as illustrated on Appendix "A", Figure A.4. The input voltage can be amplified between 1 to 11,000 times. Five filters are available on the 2311 amplifier conditioners; 10 Hz, 100 Hz, 1,000 Hz, 10,000 Hz, and 100,000 Hz. A filter averages the voltage signal to smooth out spikes that are usually caused by electric noises. The 2311 amplifier can provide regulated excitation voltages up to 15 volts, in both A.C. and D.C. voltages.

To digitize and record the signal voltage from the transducers a Nicolet Model 4094 digital Oscilloscope is used as illustrated on appendix A, Figure A.5. The Nicolet 4094 records an event by converting the voltage signal into a series of 16 bit binary numbers and storing them in temporary registers. A permanent record can be made by recording the information onto a floppy disk. The 4094 digital oscilloscope with 16 K memory can track a maximum of four channels simultaneously and record up to 15,872

Reproduced with permission of the copyright owner. Further reproduction prohibited without permission.

bytes per channel at a maximum rate of 2,000,000 analog to digital conversions per second per channel. The 16 K maximum memory size can be divided into two 8 K, or four 4 K memory subgroups to save memory space. Results from twenty tests can be stored on each floppy diskette for a permanent record.

Output from strain gages, and load cells are sent to four independent channels of the oscilloscope and saved after passing through analog transducers. Then the data are transferred to a personal computer for further analysis.

Reproduced with permission of the copyright owner. Further reproduction prohibited without permission.

CHAPTER 4

EXPERIMENTAL RESULTS

Both static and dynamic tensile tests were conducted on the proposed specimens, while the compressive tests were performed on a standard three by six inch solid cylinder, as shown in Figure A.6, Appendix A. An MTS closed-loop servo controlled hydraulic system was used for quasi-static direct tension and compression tests, as illustrated in Figures A.7 and A.8 in Appendix A. The results were recorded on a personal computer for further analysis as illustrated in Appendix "B", Figures B.1 to B.4, B.35 and B.36. High strain rate direct tensile tests were conducted using a drop-weight. In order to achieve different strain rates, drop weight, drop height as well as rubber pad thickness at the tip of drop-hammer were varied. To study the effect of a specific parameter, the other parameters were kept constant.

Three different drop hammer weights 50, 83 and 110 lb were used with a constant 1/8 inch rubber pad thickness and 16 in. drop hammer height.

Rubber pad thickness were varied from zero to 3/16 inch by 1/16 inch increment to reduce the inertia effect on the load cell reading and study their effect on strain rate. Drop hammer weight and height were kept at 50 lb and 16 inches, respectively, during these tests.

Reproduced with permission of the copyright owner. Further reproduction prohibited without permission.

To study the effect of heights in drop hammer weight, four different drop heights 2, 4, 8, 16 inches were selected with a constant 50 lb drop-hammer weight and 1/8 in. rubber pad thickness.

4.1 Stress History

The stress versus time relation was generated from the voltage produced from the load cell. By using the calibrated conversion factor, load history is found. After converting the load to stress, ultimate strength of the material is recorded as described in Figures 4.1 to 4.3 and Figures B.5 to B.14 in Appendix B.

It can be seen that the ultimate stress increases by increasing the height of the drop-hammer and decreasing the rubber-pad thickness. When there is no rubber-pad at the tip of the drop-hammer the increase in the ultimate stress is more noticeable. This observation is also reported by Gopalaratnam, V.S., and Shah, S.P.[20]. It was found that there was no significant effect in ultimate stress due to variation of the drop-hammer weight.

4.2 Strain History

Strain history in voltage was recorded from the strain gage mounted on the specimen which makes a full

Reproduced with permission of the copyright owner. Further reproduction prohibited without permission.

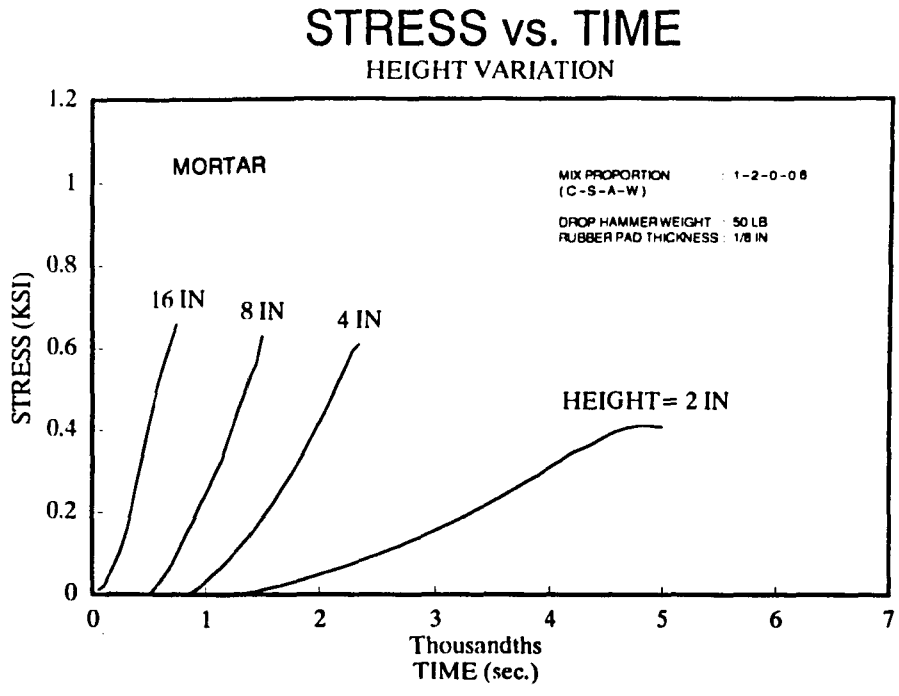

Figure 4.1 Tensile stress history of mortar specimens due to different drop-hammer heights.

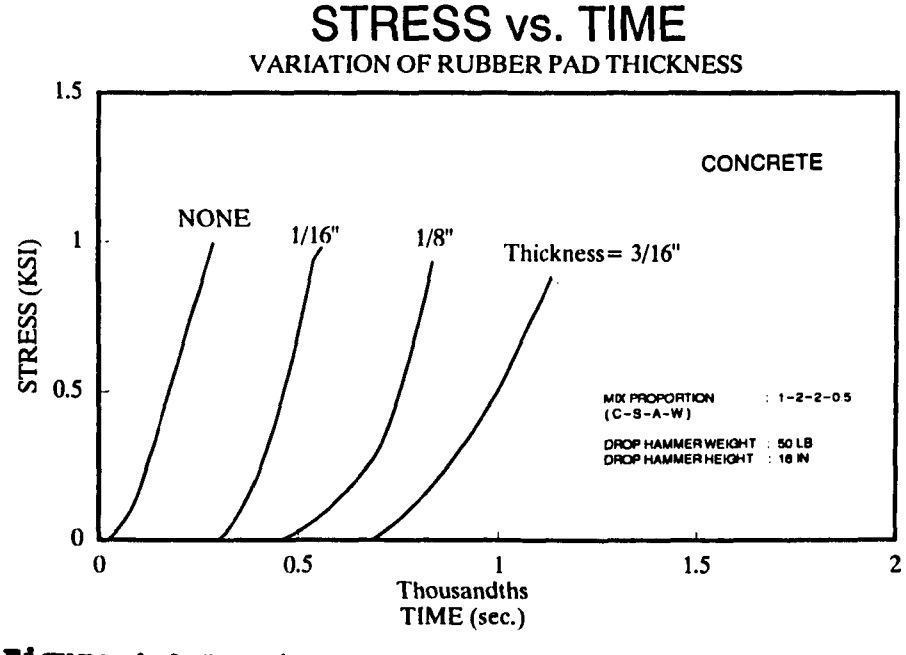

Figure 4.2 Tensile stress history of concrete specimens due to different rubber pad thicknesses.

Reproduced with permission of the copyright owner. Further reproduction prohibited without permission.

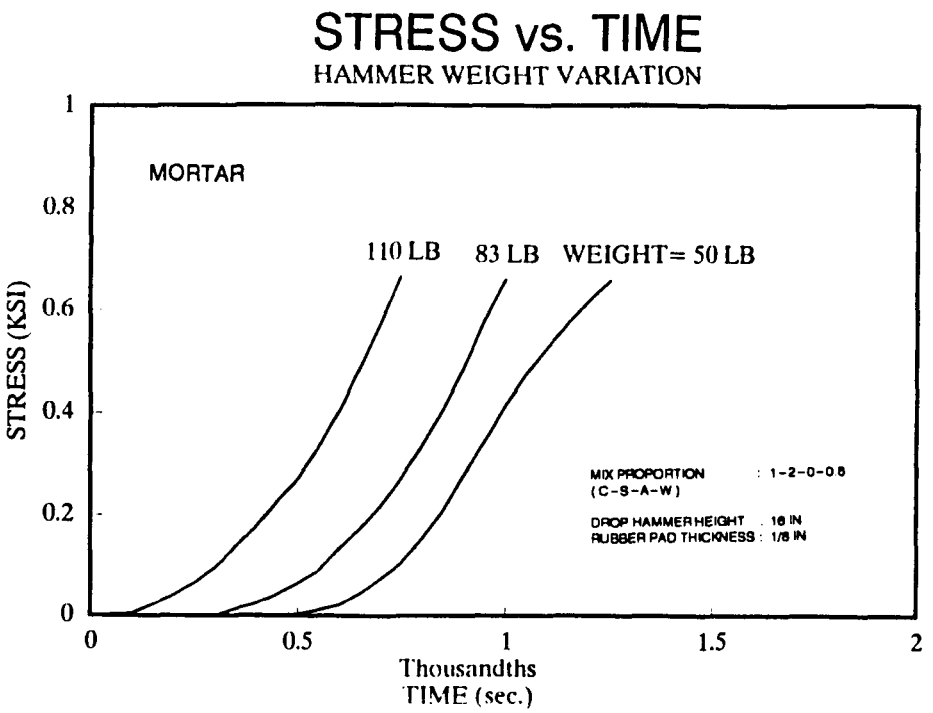

Figure 4.3 Tensile stress history of mortar specimens due to different drop-hammer weights.

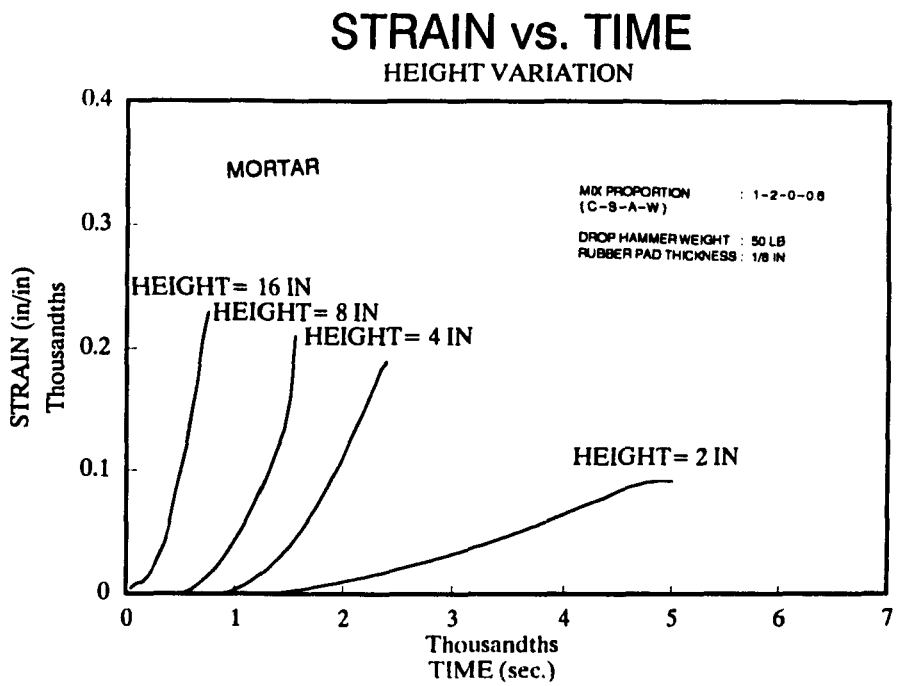

Figure 4.4 Strain history of mortar specimens due to different drop-hammer heights.

Reproduced with permission of the copyright owner. Further reproduction prohibited without permission.

bridge with three other gages that were glued to another concrete plate. After applying the conversion factor, strain history is achieved as it is shown in Figures 4.4 to 4.6.

From the strain history, it can be seen that the maximum strain increases noticeably by increasing the drop hammer height, while the reduction in rubber pad thickness causes a slight increase in the maximum strain. The drop hammer weight does not seem to have any effect on the ultimate strain, as shown in Figures B.15 to B.24 of Appendix "B".

4.3 Stress-Strain Relation

Stress versus strain is constructed by plotting each point of the stress history with corresponding point on the strain as illustrated in Figures 4.7 to 4.9 and Figures B.25 to B.34 in Appendix B. Figure 4.10 compares the dynamic and static stress-strain curves. As it can be seen the dynamic ultimate stress and strain are larger than static ones. However, the increase in the maximum stress is greater than the increase in the maximum strain. This fact is more visible by normalizing the stress-strain curve, illustrated in Figure 4.11. It is also evident that the dynamic stress-strain behavior is more linear than the static behavior.

Reproduced with permission of the copyright owner. Further reproduction prohibited without permission.

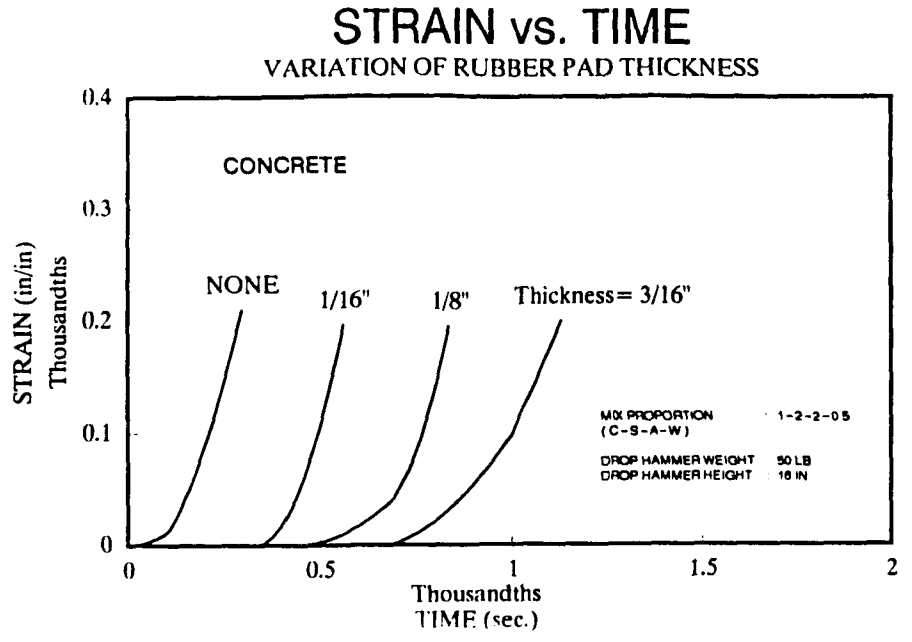

Figure 4.5 Strain history of concrete specimens due to different rubber pad thicknesses.

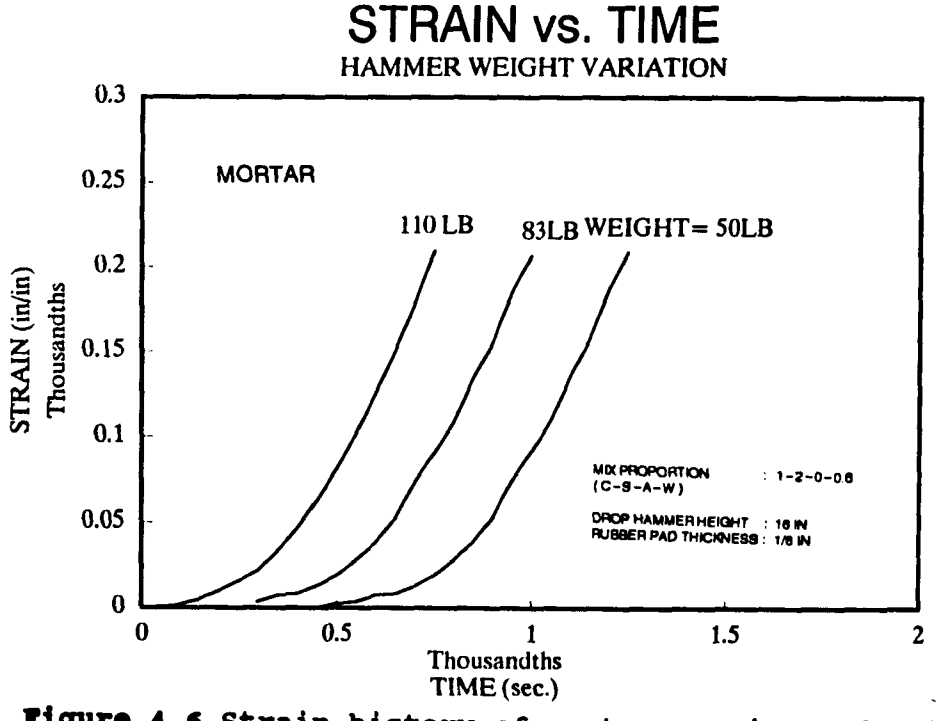

Figure 4.6 Strain history of mortar specimens due to different drop-hammer weights.

Reproduced with permission of the copyright owner. Further reproduction prohibited without permission.

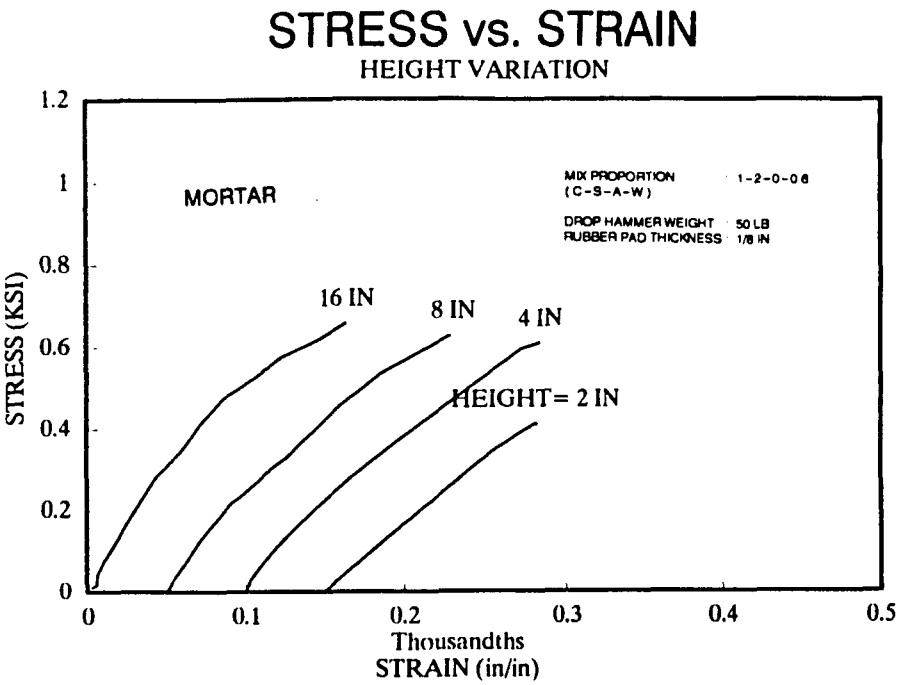

Figure 4.7 Stress vs. strain of mortar specimens due to different drop-hammer heights.

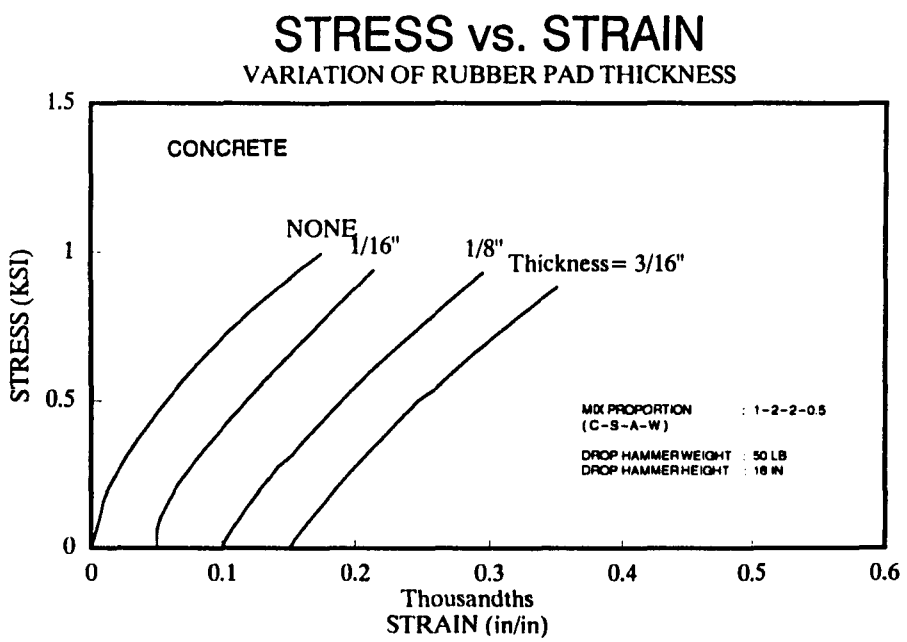

Figure 4.8 Stress vs. strain of concrete specimens due to different rubber pad thicknesses.

Reproduced with permission of the copyright owner. Further reproduction prohibited without permission.

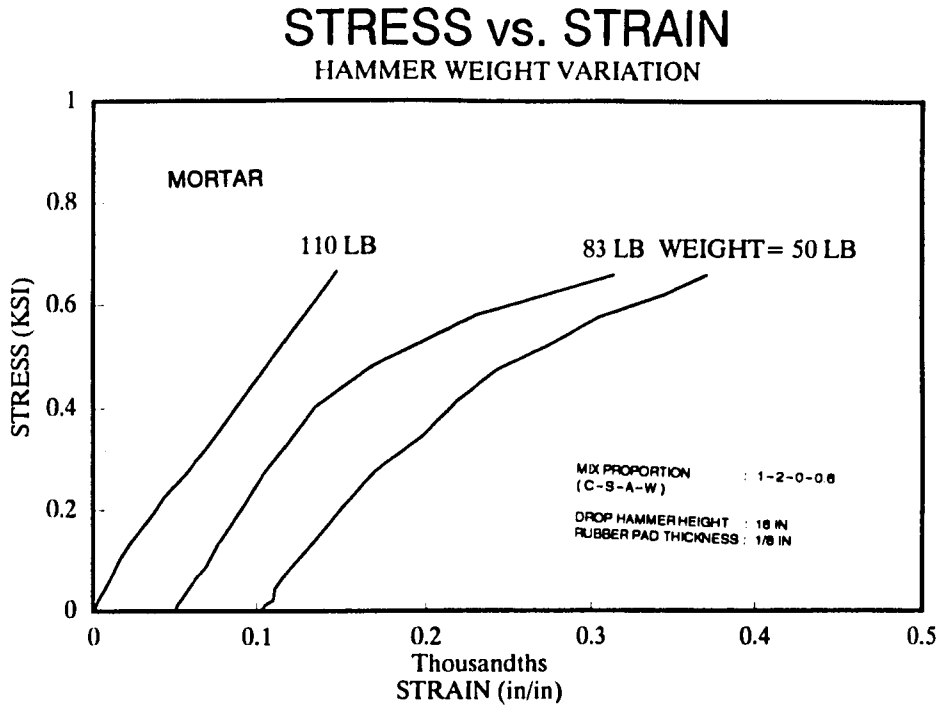

Figure 4.9 Stress vs. strain of mortar specimens due to different drop-hammer weights.

Reproduced with permission of the copyright owner. Further reproduction prohibited without permission.

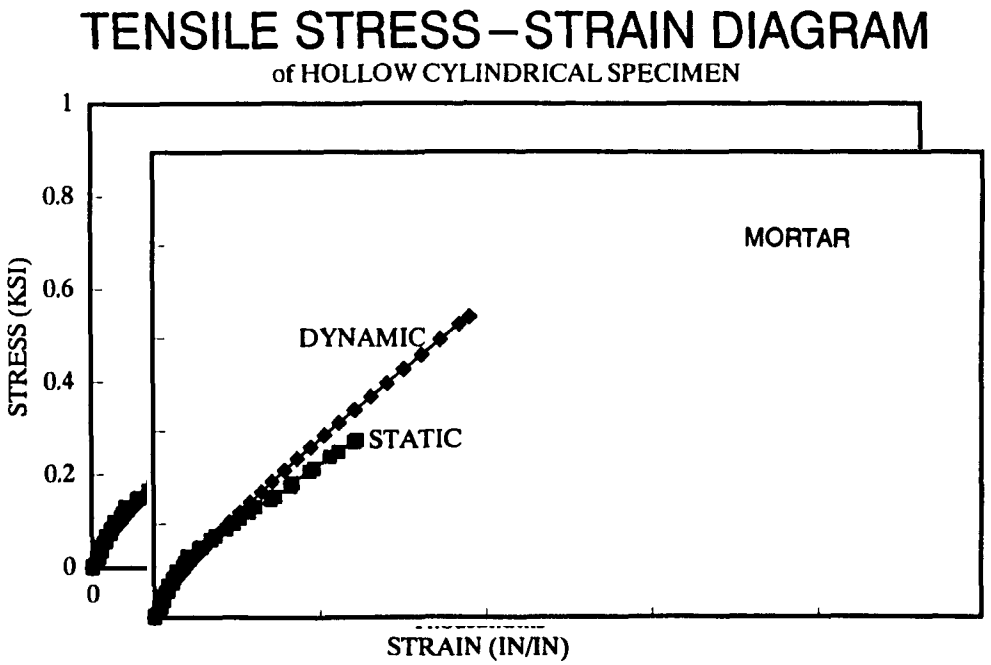

Figure 4.10 Static and impact stress-strain curves for mortar.

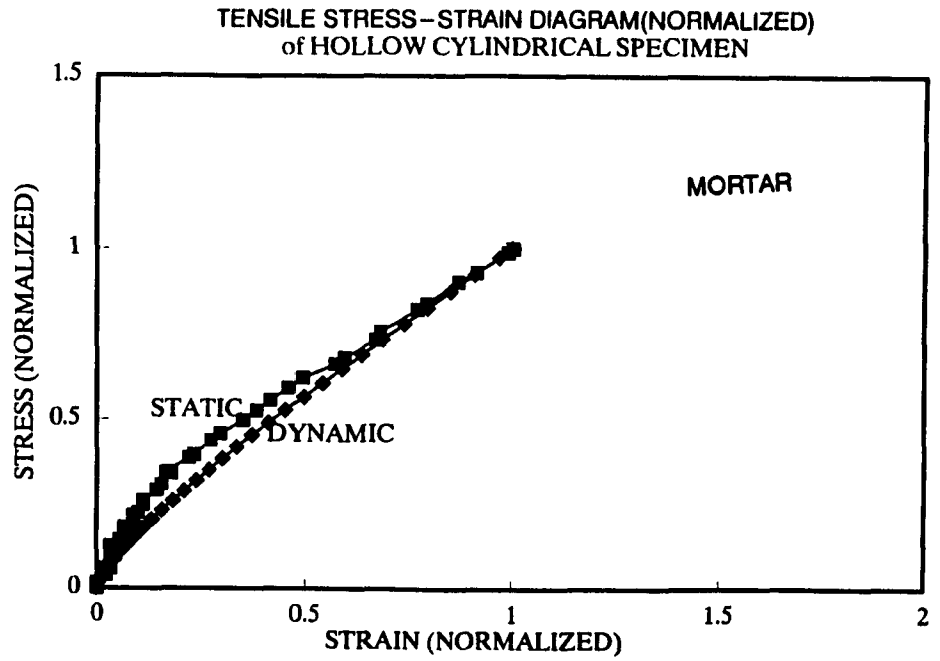

Figure 4.11 Normalized static and impact stress-strain lines for mortar.

Reproduced with permission of the copyright owner. Further reproduction prohibited without permission.

4.4 Stress Rate

The slope of the stress history is considered as the stress-rate, as illustrated in Figures 4.12 to 4.14. It can be seen that the slope of stress history curves increases from 537 Ksi/sec to 1400 Ksi/sec by increasing the drop-hammer height from 4 inches to 16 inches. The stress rate increases from 1172 Ksi/sec to 1984 Ksi/sec by decreasing the rubber pad thickness from 3/16 inch to no pad, with the most significant increase observed when no rubber pad is used. However, the stress rate did not change noticeably by changing the drop-hammer weight.

4.5 Strain Rate

The slope of the strain history is recorded as the strain rate, as shown in Figures 4.15 to 4.17. It can be observed from the strain history that by increasing the drop-hammer height from 4 inches to 16 inches, the strain rate increases from 0.03 1/sec to 0.75 1/sec and by decreasing the rubber pad thickness at the load cell from 3/16 inch to no pad, the strain rate increases from 0.51 1/sec to 0.97 1/sec. However, no change in strain rate was noticed by increasing the drop-hammer weight.

Reproduced with permission of the copyright owner. Further reproduction prohibited without permission.

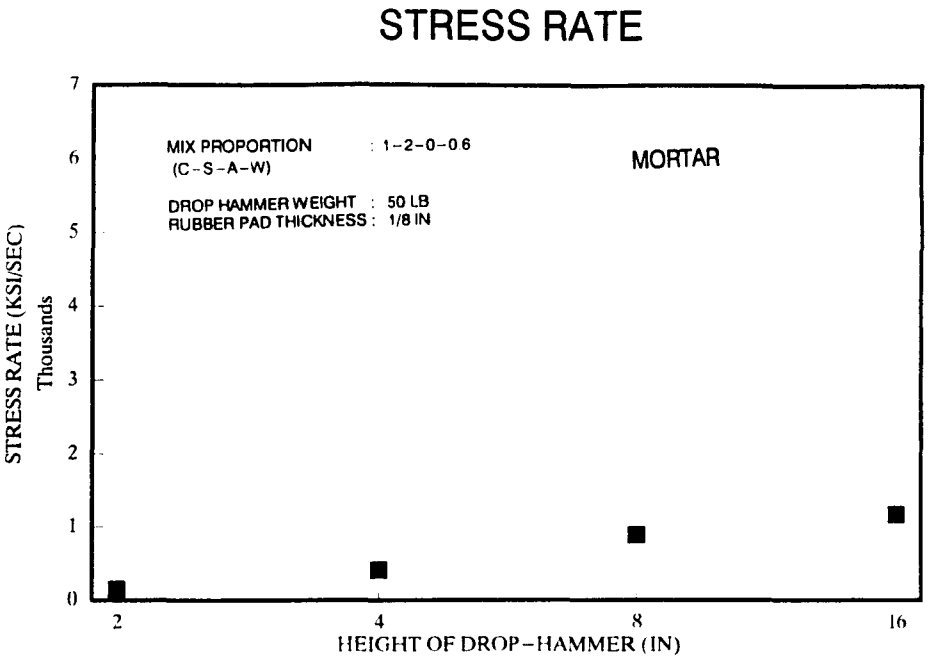

Figure 4.12 Stress rate in mortar specimens due to different heights of drop-hammer.

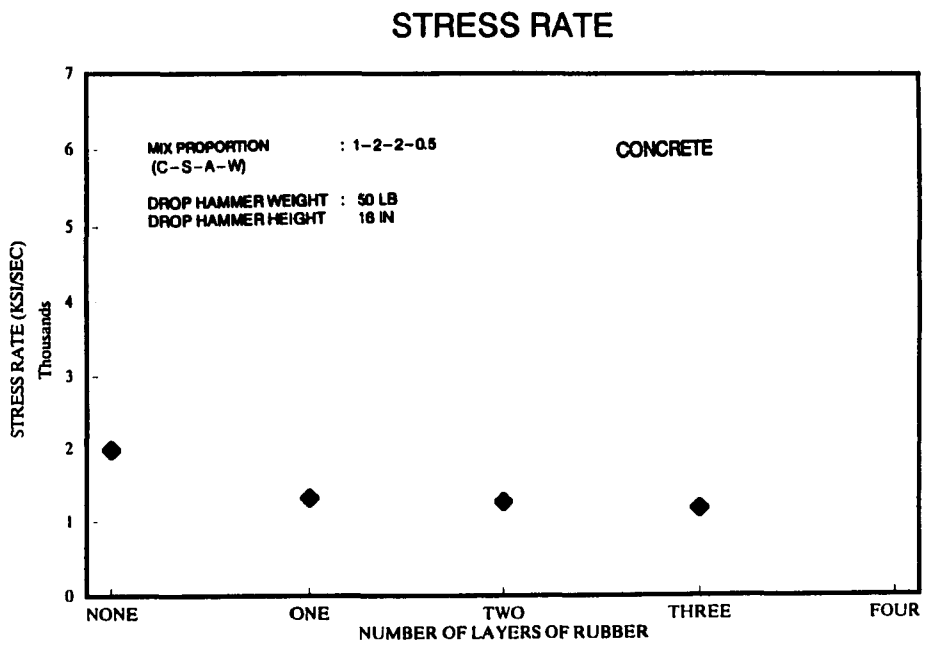

Figure 4.13 Stress rate in concrete specimens due to different number of rubber-pad layers.

Reproduced with permission of the copyright owner. Further reproduction prohibited without permission.

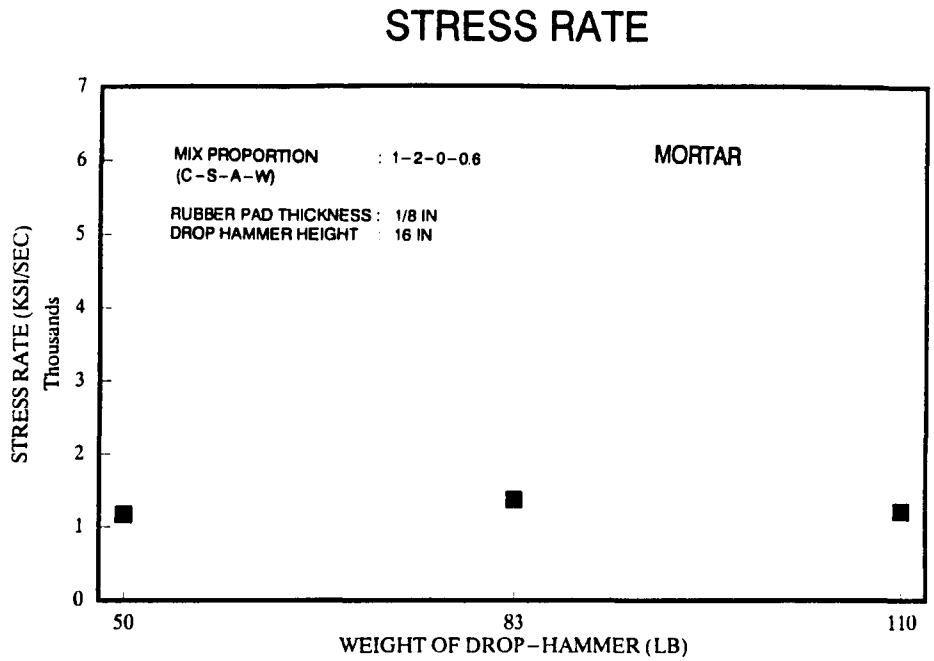

Figure 4.14 Stress rate in mortar specimens due to different weights of drop-hammer.

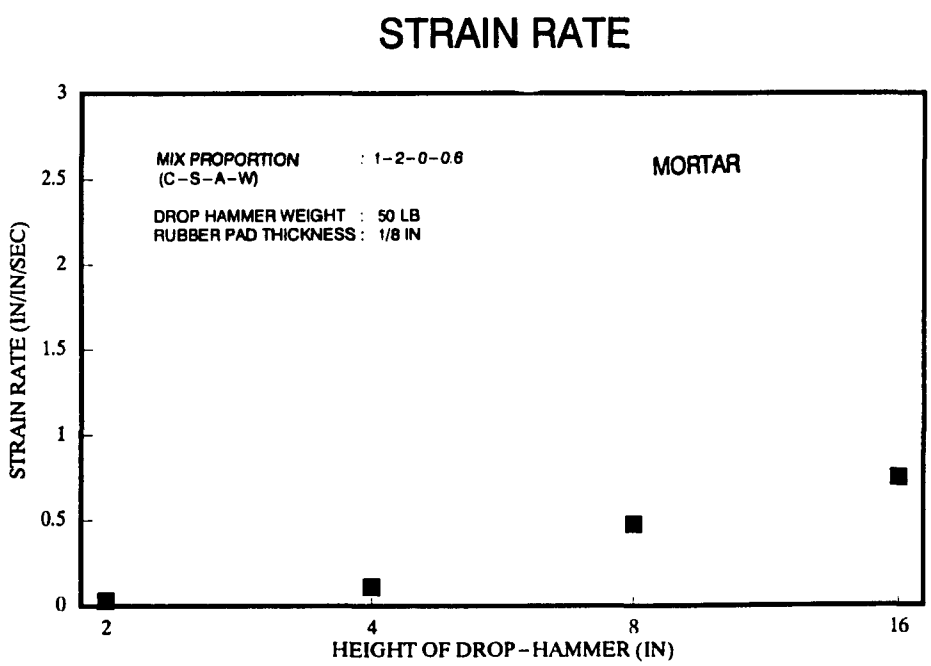

Figure 4.15 Strain rate in mortar specimens due to different heights of drop-hammer.

Reproduced with permission of the copyright owner. Further reproduction prohibited without permission.

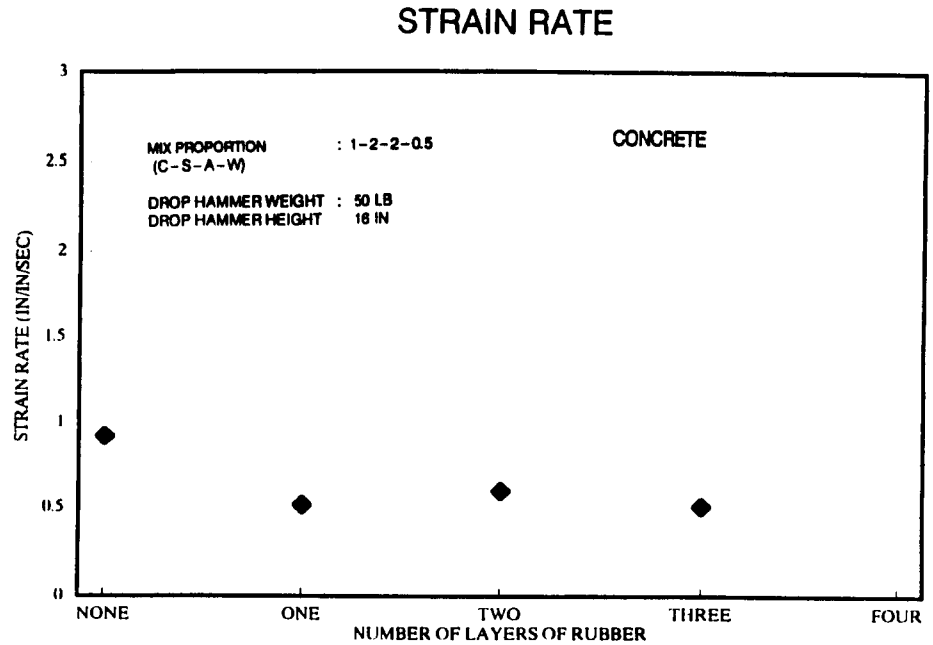

Figure 4.16 Strain rate in concrete specimens due to different number of rubber-pad layers.

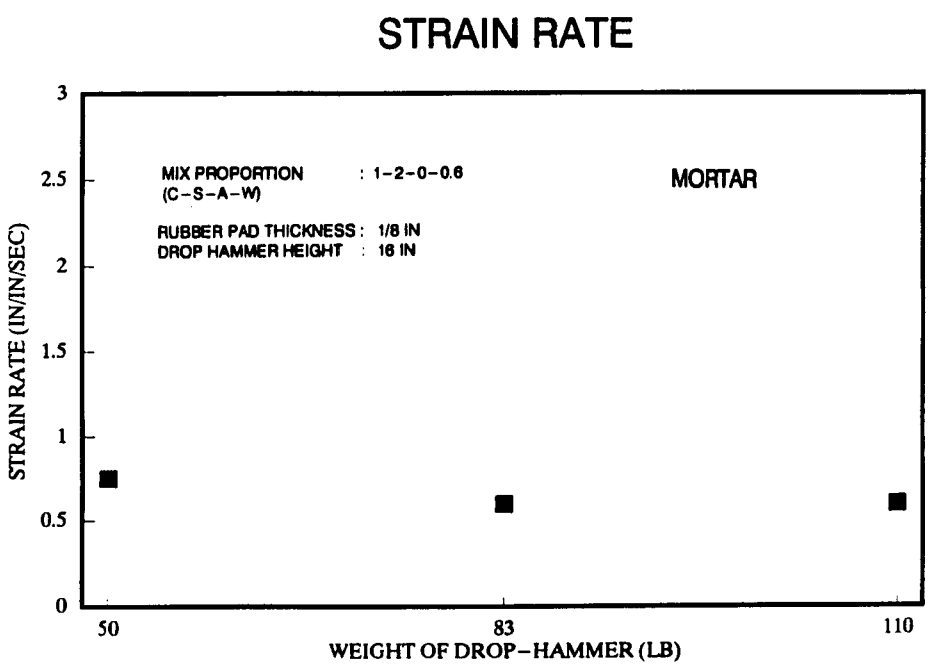

Figure 4.17 Strain rate in mortar specimens due to different weights of drop-hammer.

Reproduced with permission of the copyright owner. Further reproduction prohibited without permission.

4.6 Modulus of Elasticity

Modulus of elasticity was obtained from the slope of stress-strain relationship. The chord modulus from 40% of ultimate strength reading to that of ultimate strength was calculated and considered as the modulus of elasticity of the specimen, as illustrated in Figures 4.18 to 4.20. From the test result, it was evident that variations of the drop hammer height, rubber pad thickness and the drop hammer weight have minimal effect on the modulus of elasticity. By increasing the strain rate, the modulus of elasticity increases slightly.

4.7 Energy Absorption

Since total energy absorption to failure is a special characteristic for any material, it should be calculated for further analysis of the material behavior. Total energy is obtained by multiplying the magnitude of each point of the stress to the corresponding strain increment from stress-strain curve. By summing the increments of the energy history from the beginning of the test to time(t), the total energy absorption to that specific time can be obtained as shown in Figures 4.21 to 4.23. From the test result, it is evident that the energy absorption increases from 164% to 216% by increasing the drop hammer height from 4 inches to 16 inches and, energy absorption

Reproduced with permission of the copyright owner. Further reproduction prohibited without permission.

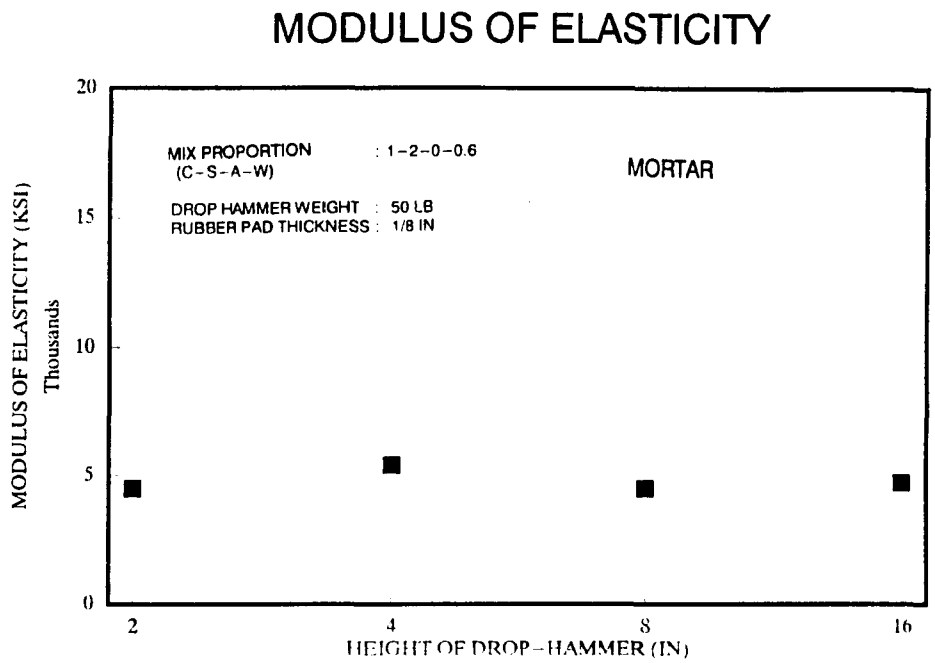

Figure 4.18 Tensile modulus of elasticity for mortar specimens due to different heights of drop-hammer.

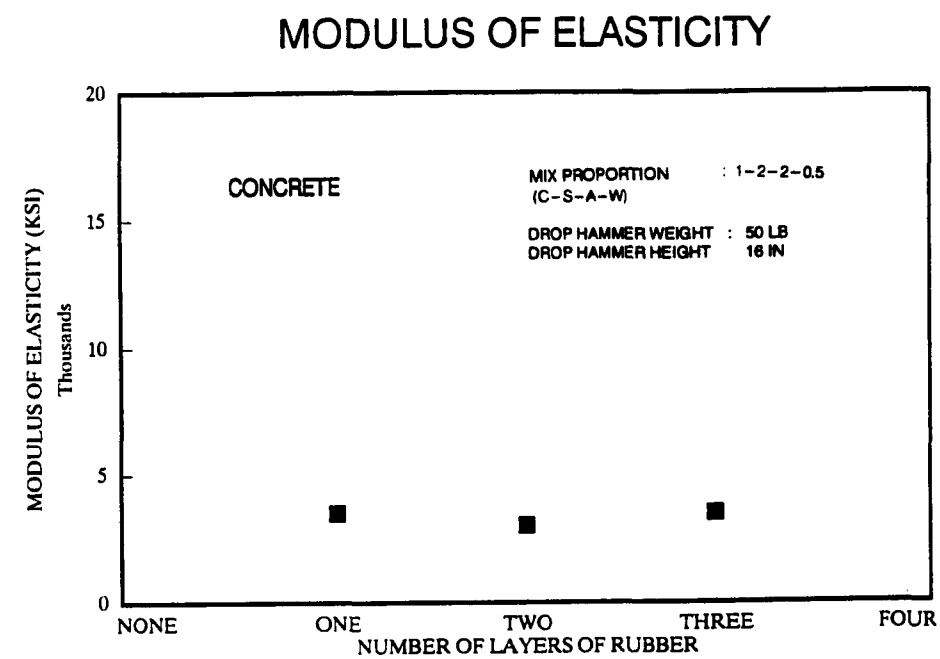

Figure 4.19 Tensile modulus of elasticity for mortar specimens due to different rubber pad thickness.

Reproduced with permission of the copyright owner. Further reproduction prohibited without permission.

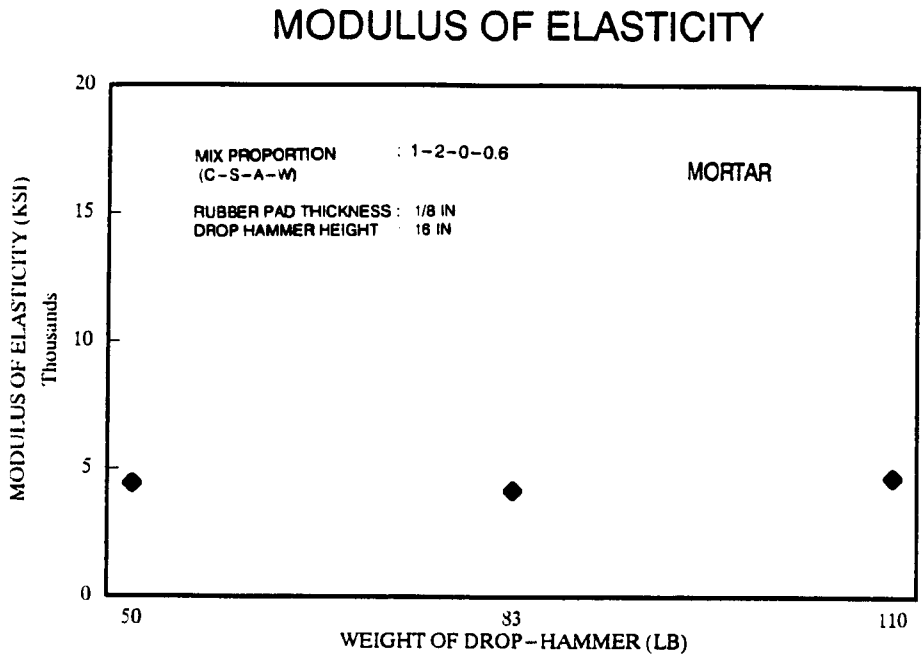

Figure 4.20 Tensile modulus of elasticity for concrete specimens due to different weights of drop-hammer.

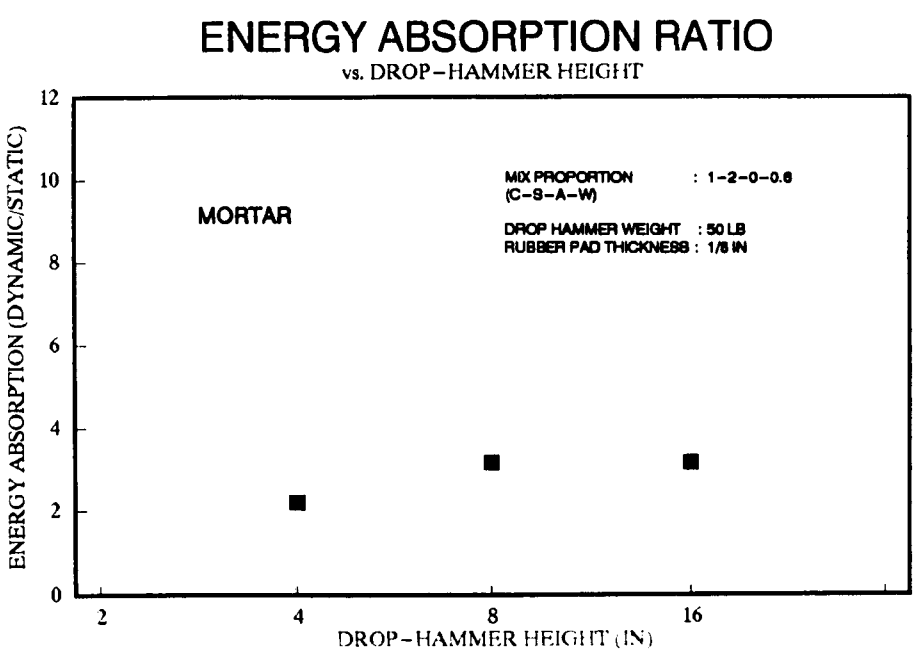

Figure 4.21 Energy absorption in mortar due to different height of drop hammer.

Reproduced with permission of the copyright owner. Further reproduction prohibited without permission.

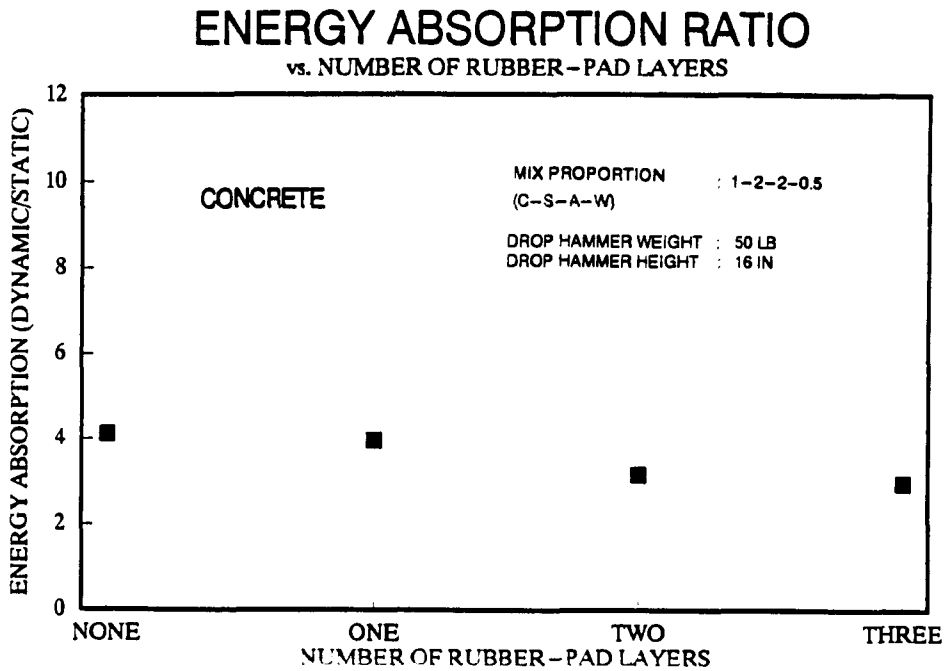

Figure 4.22 Energy absorption in concrete due to different rubber pad thickness.

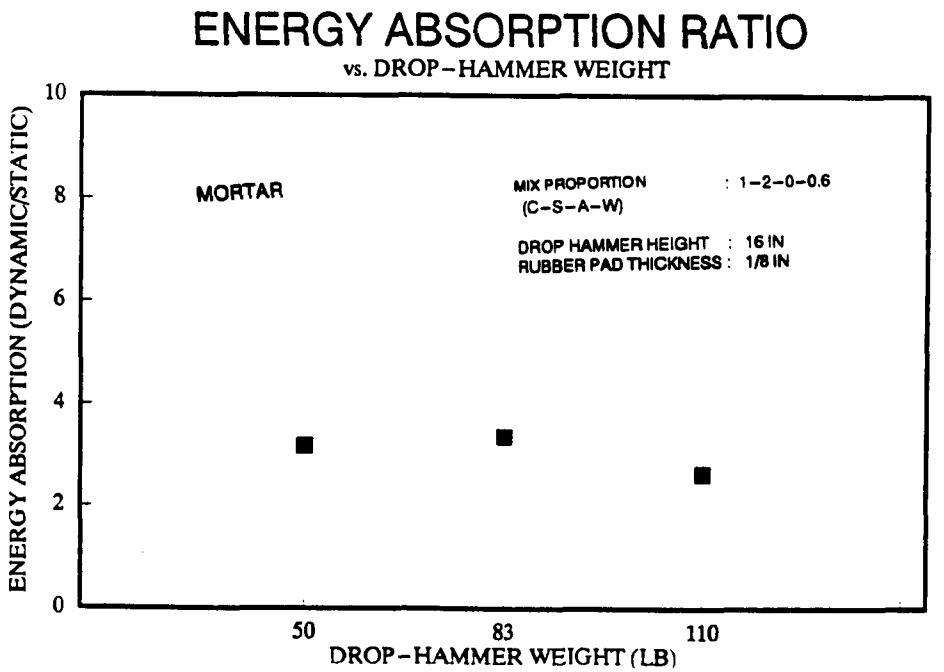

Figure 4.23 Energy absorption in mortar due to different weight of drop hammer.

Reproduced with permission of the copyright owner. Further reproduction prohibited without permission.

increases from 164% to 291% by reducing the rubber pad thickness from 3/16 inch to no pad. On the other hand, the drop hammer weight has a minimal effect on the energy absorption. As it can be seen in Figures 4.24 and 4.25 concrete is more strain rate sensitive in direct tension when considering energy absorption than mortar. This result has also been reported by Suaris, and Shah[67] in flexural behavior of cement based materials under impact load.

Reproduced with permission of the copyright owner. Further reproduction prohibited without permission.

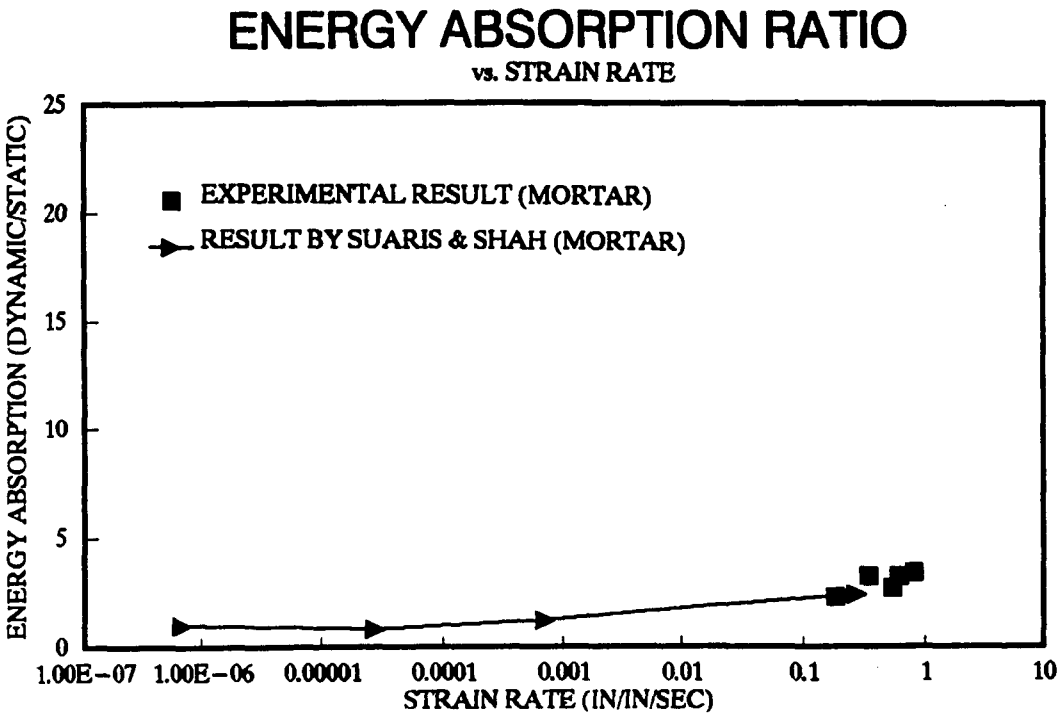

Figure 4.24 Energy absorption of mortar.

Reproduced with permission of the copyright owner. Further reproduction prohibited without permission.

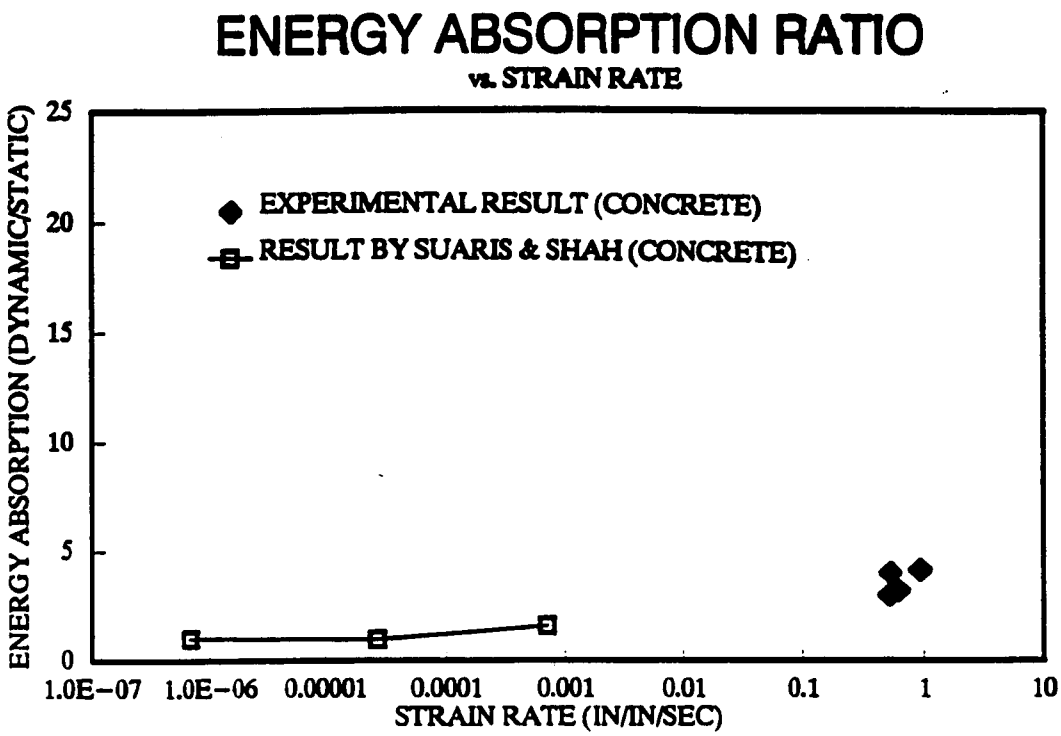

Figure 4.25 Energy absorption of concrete.

Reproduced with permission of the copyright owner. Further reproduction prohibited without permission.

CHAPTER 5

Theoretical Modeling

5.1 Inertia Comparison Between the Proposed and Beam Specimens

To demonstrate that the inertial effect is small in the new specimen, let us compare the ratio of inertial load versus the equivalent inertial resistance for the new hollow cylindrical specimen to a typical beam specimen.

For the case of hollow cylindrical specimen, assuming that a linear displacement field is as shown in Figure 5.1

$$U(X,t) = \frac{U_0(t)\ X}{L-1.25} \quad for \quad X < L-1.25 \tag{5.1}$$

$$U(X,t) = U_0(t) \quad for \quad X > L-1.25 \tag{5.2}$$

Where:

- $U(X,t)$ = Displacement along the specimen below the supporting elevation.
- $U_0(t)$ = Displacement at the base of the specimen.
- L = Length of the specimen wall.

If the distributed inertial load along the length of the cylinder is replaced by the inertial load, $P_i(t)$, then the virtual work done by all of the distributed inertial loads

Reproduced with permission of the copyright owner. Further reproduction prohibited without permission.

is equal to the virtual work done by $P_i(t)$ alone. This leads to:

$$P_i(t)\ \delta U_0 = \int_{L-2}^{L-1.25} \rho A_1 \left[\frac{\dot{U}_0(t)\ X}{L-1.25}\right]\left[\frac{\delta U_0\ X}{L-1.25}\right] dX$$

$$+ \int_{L-1.25}^{L} \rho A_2\ \dot{U}_0(t)\ \delta U_0\ dX \qquad (5.3)$$

Where:

ρ = Mass density of the specimen material.
$P_i(t)$ = Generalized inertial load.
δU_o = Virtual displacement at the bottom plate.
$\ddot{U}_o(t)$ = Acceleration of bottom plate.
A_1, A_2 = Cross-sectional area of the specimen at the wall and the base respectively.

Equation 5.3 can be further simplified, assuming a prismatic condition and homogeneous material, to:

$$P_i(t) = \rho\ A_1\ \frac{\dot{U}_0(t)}{(L-1.25)^2}\frac{X^3}{3}\Bigg|_{L-2}^{L-1.25}$$

$$+ \rho\ A_2\ \dot{U}_0(t)\ X\Big|_{L-1.25}^{L} \qquad (5.4)$$

To evaluate the effect of inertia on three-point impact bending test specimen, the following assumptions are made:

Reproduced with permission of the copyright owner. Further reproduction prohibited without permission.

- the damage in the compression region is negligible,
- the strain distribution across the depth is linear,
- the effect of shear stress is small,
- the displacement is linear along the beam(Fig. 5.2).

It can be shown that:

$$U(X,t) = \frac{2\ U_0(t)\ X}{L} \tag{5.5}$$

$$U(Y,t) = \frac{-2\ U_0(t)\ Y}{L} \tag{5.6}$$

Where:

U(X,t) = Displacement of the beam between the support portion.
U(Y,t) = Displacement of the beam at the overhang portion.
$U_0(t)$ = Midspan displacement.
L = Length of the beam span

If the distributed inertial load along the length of the beam is replaced by the inertial load, $P_i(t)$ as similar to the case of the cylindrical specimen, then the virtual work done by all of the distributed inertial load is equal to the virtual work done by $P_i(t)$ alone.

Thus,

Reproduced with permission of the copyright owner. Further reproduction prohibited without permission.

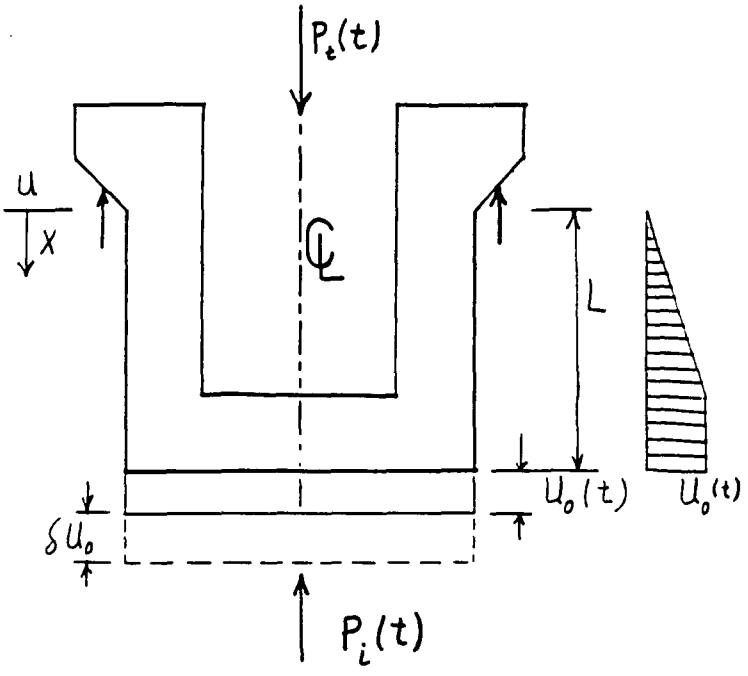

Figure 5.1 Displacement along the hollow cylinder.

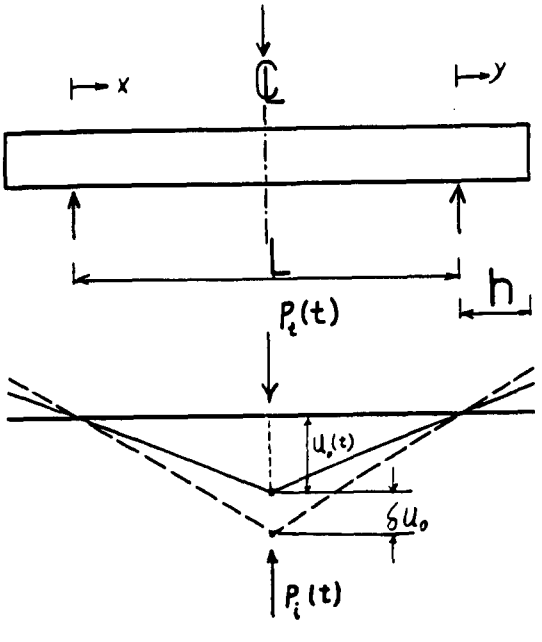

Figure 5.2 Displacement diagram along the beam.

Reproduced with permission of the copyright owner. Further reproduction prohibited without permission.

$$P_i(t)\ \delta U_0 = 2\int_0^{L/2}\rho A\left[\frac{2\ddot{U}_0(t)\ X}{L}\right]\left[\frac{2\delta U_0\ X}{L}\right]dX$$

$$+2\int_0^{h}\rho A\left[\frac{-2\ddot{U}_0(t)\ Y}{L}\right]\left[\frac{-2\delta U_0\ Y}{L}\right]dY \qquad (5.7)$$

Where:

ρ	=	Mass density of the specimen material
$P_i(t)$	=	Generalized inertial load
δU_o	=	Virtual displacement at the bottom plate
$\ddot{U}_o(t)$	=	Acceleration of beam at midspan
A	=	Cross-sectional area of the specimen
h	=	Length of the overhang

Assuming a prismatic, homogeneous material, equation (5.7) can be simplified to:

$$P_i = \rho A\ddot{U}_0(t)\left[\frac{L}{3}+\frac{8}{3}\frac{h^3}{L^2}\right] \qquad (5.8)$$

If the specimen is modeled as a single degree of freedom system, the equivalent load can be obtained from the dynamic equilibrium condition that [96]:

$$P_r(t) = P_t(t) - P_i(t) \qquad (5.9)$$

Where;

P_r (t)	=	Equivalent material resistance load.
P_t (t)	=	Observed tup load.
P_i (t)	=	Generalized inertial load.

Reproduced with permission of the copyright owner. Further reproduction prohibited without permission.

In order to compare the inertial effect on the three-point-bend specimen with the proposed cylindrical specimen, the following specimen dimensions are used:

Cylindrical Specimen		Beam Specimen	
$L = 4$	in	$A = 4 \times 4$	in
$D_1 = 1.25$	in	$L = 15$	in
$D_2 = 3.0$	in	$h = 0.5$	in

The ratio of the inertial versus the resistance load of the beam and cylindrical specimens becomes:

$$R = \frac{(P_i / P_r)\ [\text{beam}]}{(P_i / P_r)\ [\text{cylinder}]} = \underline{14} \qquad (5.10)$$

It can be concluded that the new specimen configuration has a much smaller inertial effect than the beam specimen.

5.2 Theoretical Analysis of the Proposed Specimen

To study the effect of wave propagation on the proposed specimen, a numerical analysis was performed on the specimen by employing ANSYS[112] finite element programs. The procedures are outlined as shown in figure 5.3. Wave propagation analysis was performed using a three-dimensional axisymmetric solution with the elastic material model. The results are shown in Figure 5.4 and 5.5.

Reproduced with permission of the copyright owner. Further reproduction prohibited without permission.

Reproduced with permission of the copyright owner. Further reproduction prohibited without permission.

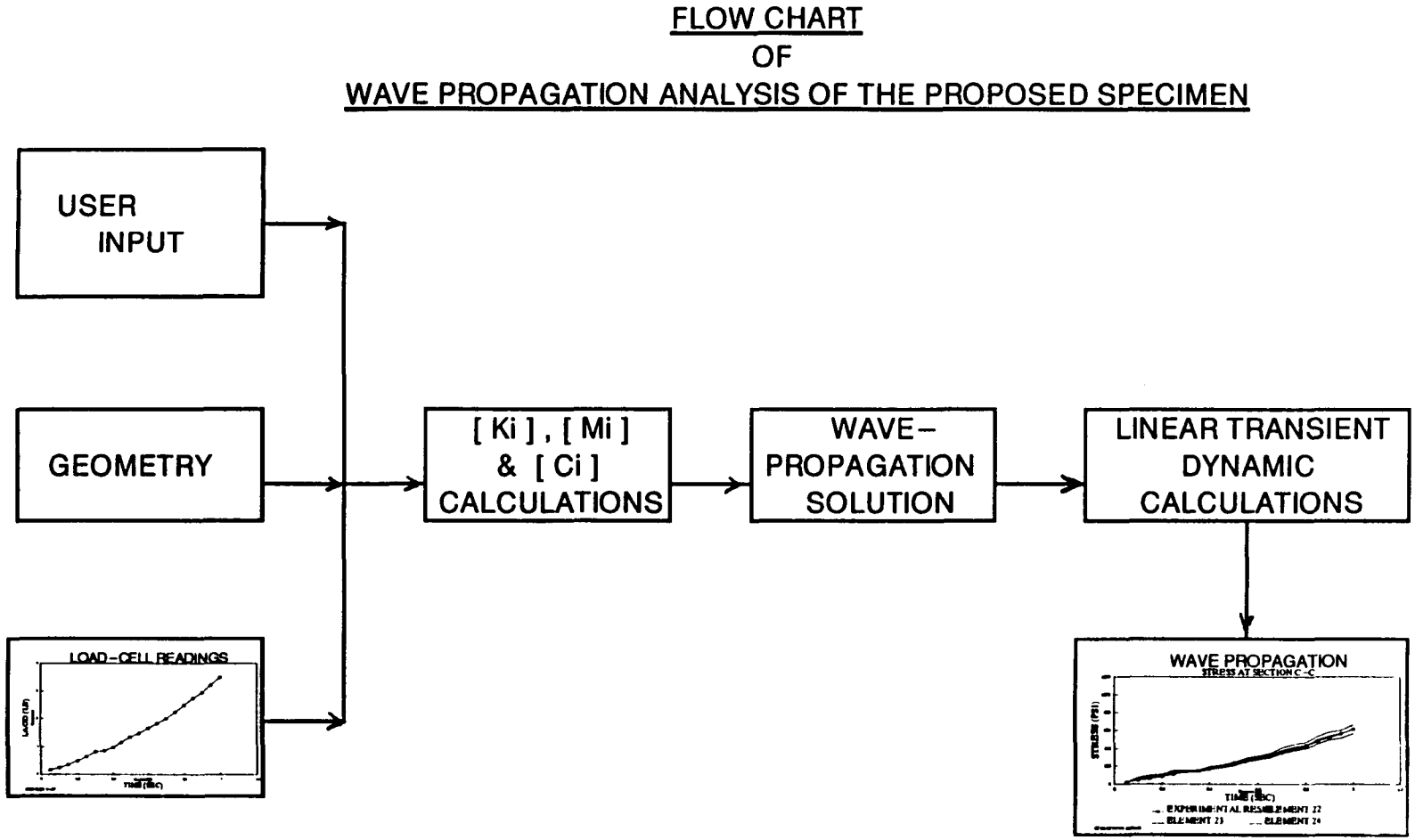

Figure 5.3 Flow chart of wave propagation analysis of the proposed specimen using ANSYS computer software.

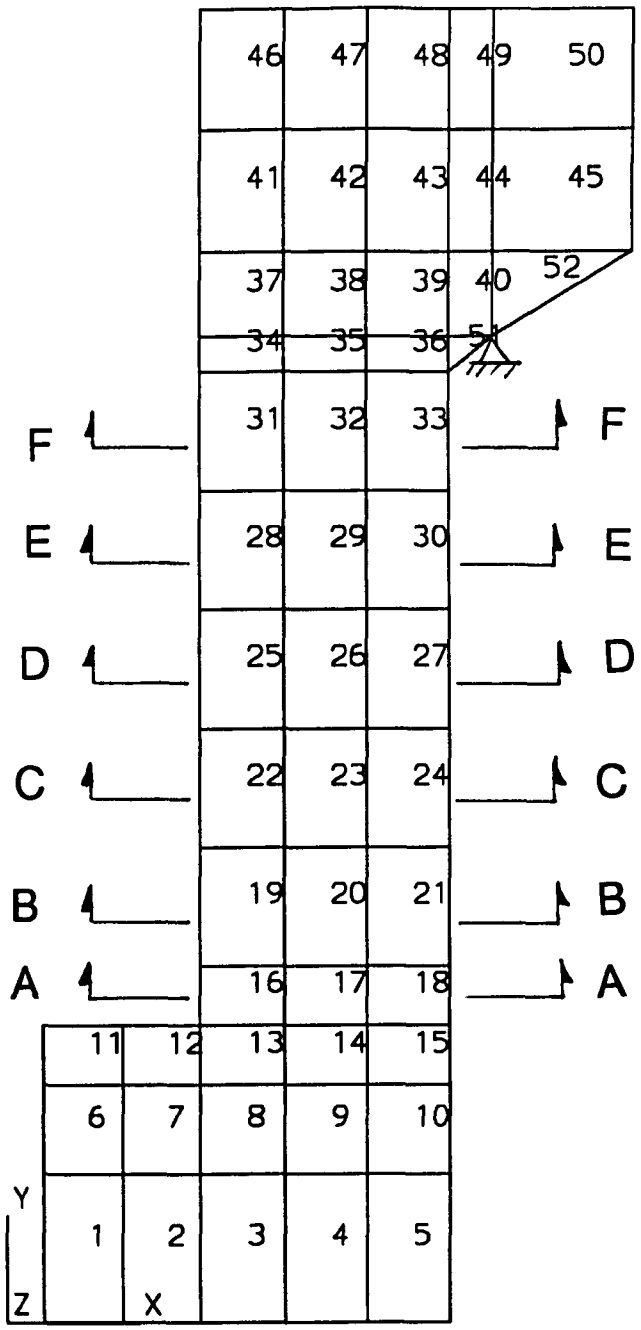

Figure 5.4 Elevation view of finite element model of specimen with element number.

Reproduced with permission of the copyright owner. Further reproduction prohibited without permission.

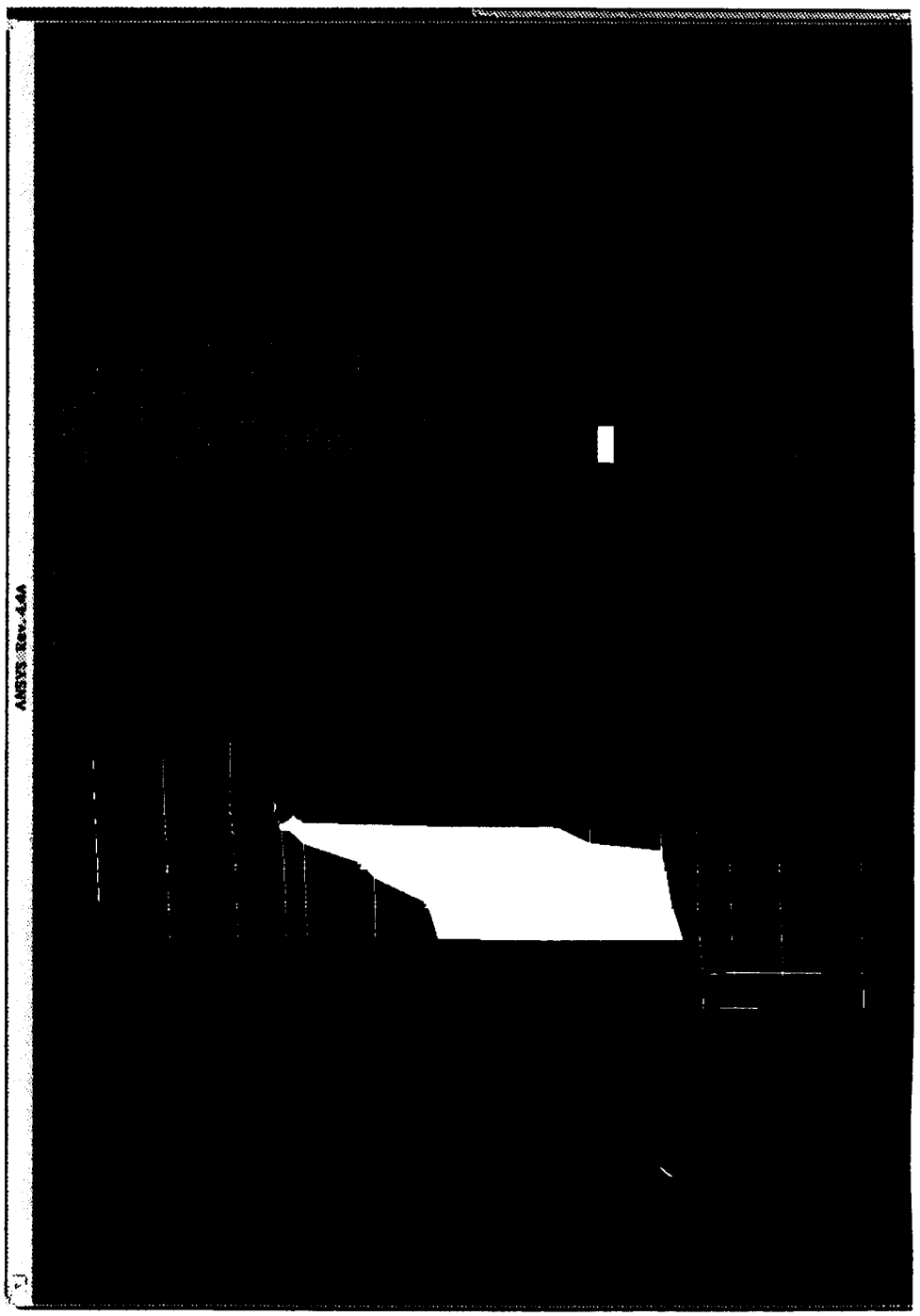

Figure 5.5 Contour of longitudinal tensile stress along the specimen.

Reproduced with permission of the copyright owner. Further reproduction prohibited without permission.

Because of the decrease in pre-peak nonlinearity at high strain rates, a linear-elastic analysis approach is justified. This approach has also been employed by Reji and Shah[113] where they analyzed a concrete specimen using linear elastic fracture mechanics. The analysis on the specimen without rebars at the neck indicates a build up of stress at the vicinity of the support as illustrated on Figure 5.6. The prediction was verified by the experimental result since the specimen failed at the neck as illustrated on Figure 3.7. Applying the four rebars vertically from the top to 1.0 inch below the support, reduced the stress build up and stopped the specimen failure at the neck during impact test as illustrated on Figure 5.7. Furthermore, with four rebars the longitudinal stress along the wall was more evenly distributed as shown on Figures 5.8 and 5.9. The prediction was verified by experimental observation. When the specimen was tested, it failed at the central region of the wall at sections B-B, C-C or D-D, as illustrated on Figure 3.8. The computer results given on Figures 5.10, 5.11, and 5.12 suggest that stress variation at these sections along the wall of the specimen are less than 7%. This indicates that the specimen is failing in direct tension with uniform stress distribution across the thickness. This approach is a simple means to find the stress in the test specimen during an impact test.

Reproduced with permission of the copyright owner. Further reproduction prohibited without permission.

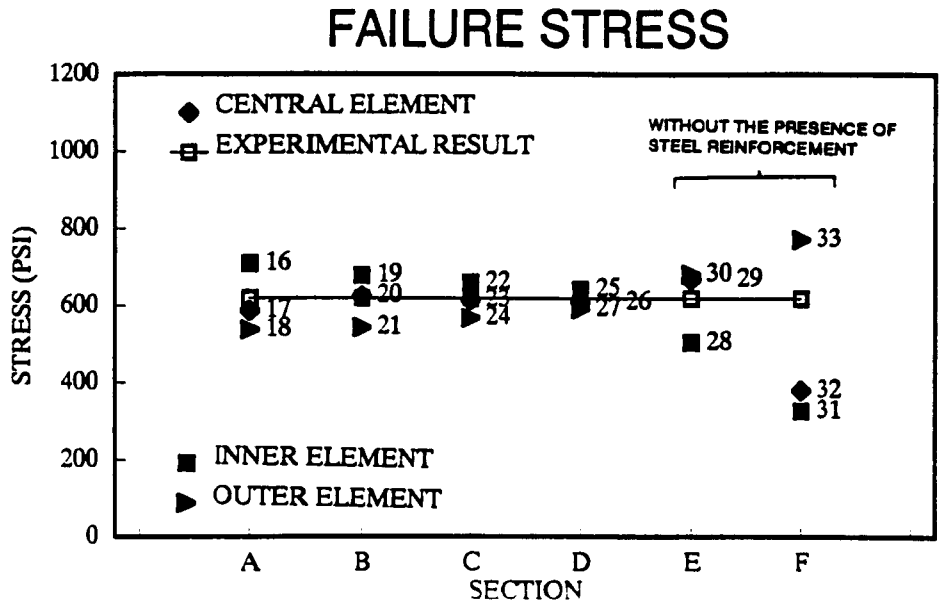

Figure 5.6 Stress at different locations of specimen wall without rebars, based on computer analysis.

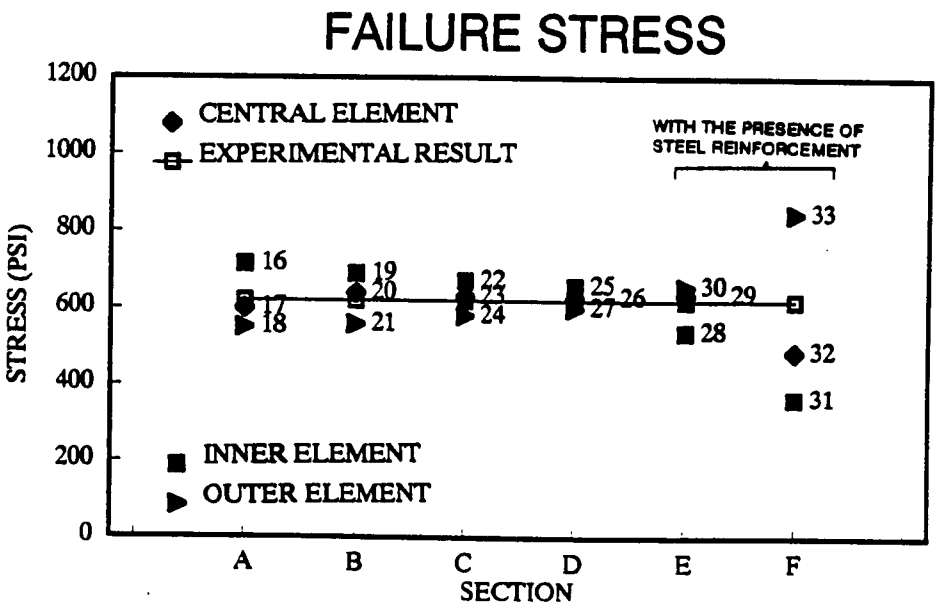

Figure 5.7 Stress at different locations of specimen wall with rebars at sections E-E and F-F, based on computer analysis.

Reproduced with permission of the copyright owner. Further reproduction prohibited without permission.

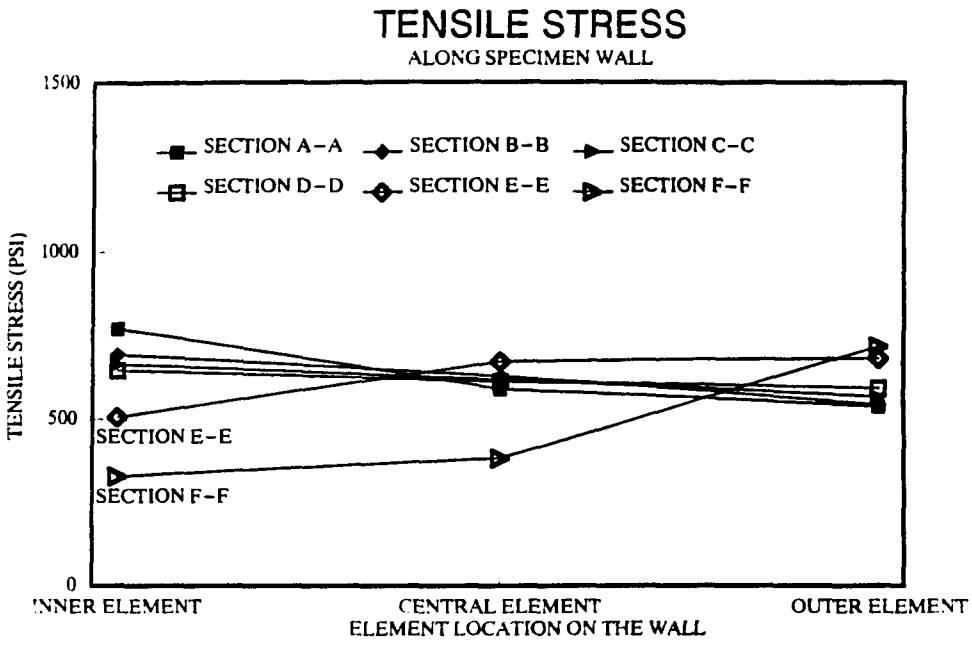

Figure 5.8 Tensile stress on the sections of the specimen wall without presence of rebars, based on computer analysis.

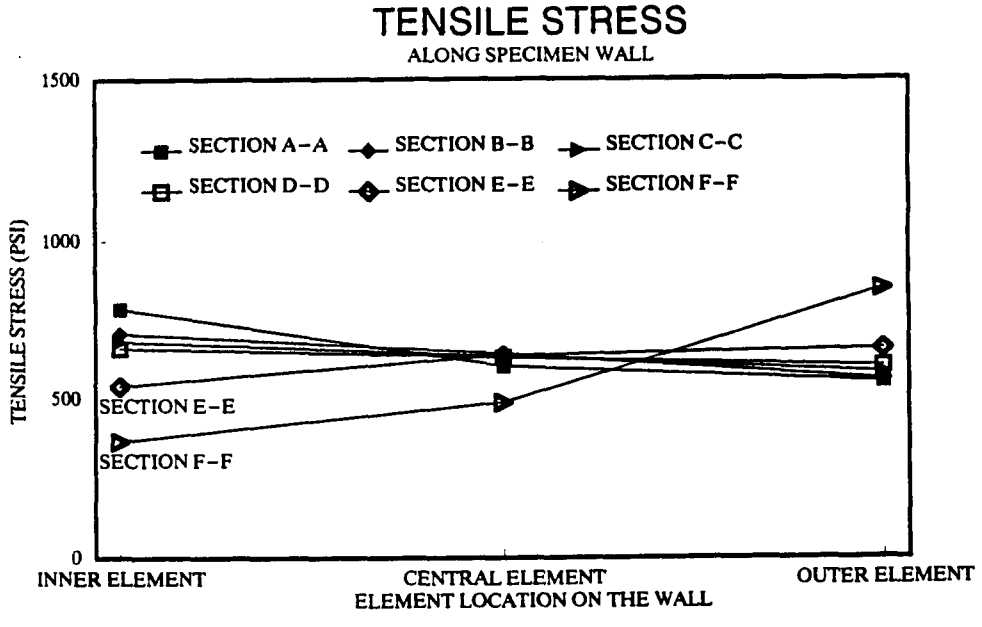

Figure 5.9 Tensile stress on the sections of the specimen wall with presence of rebars, based on computer analysis.

Reproduced with permission of the copyright owner. Further reproduction prohibited without permission.

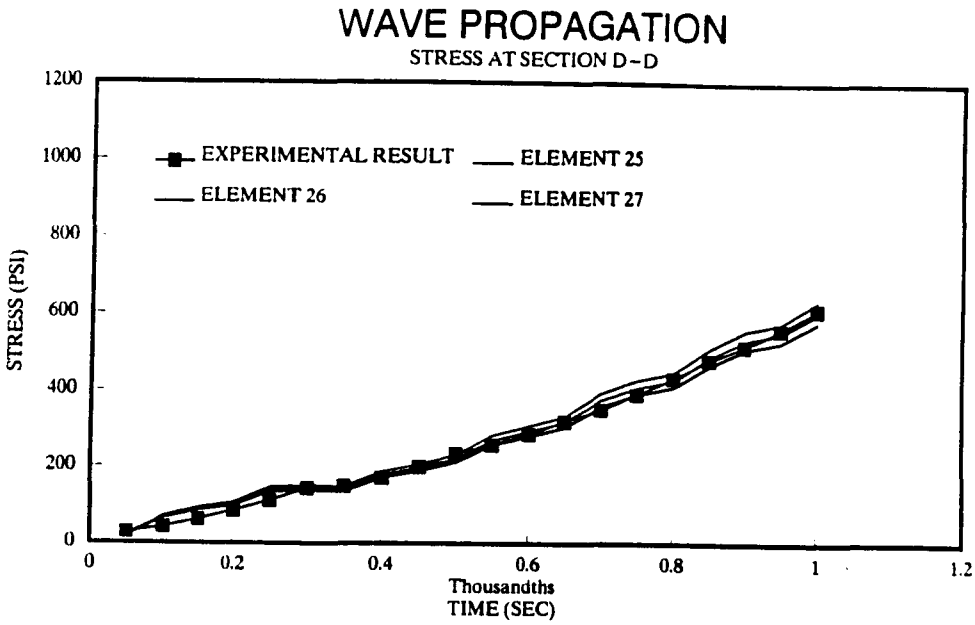

Figure 5.10 Stress history at section D-D. Note the correlation of the experimental with analytical results.

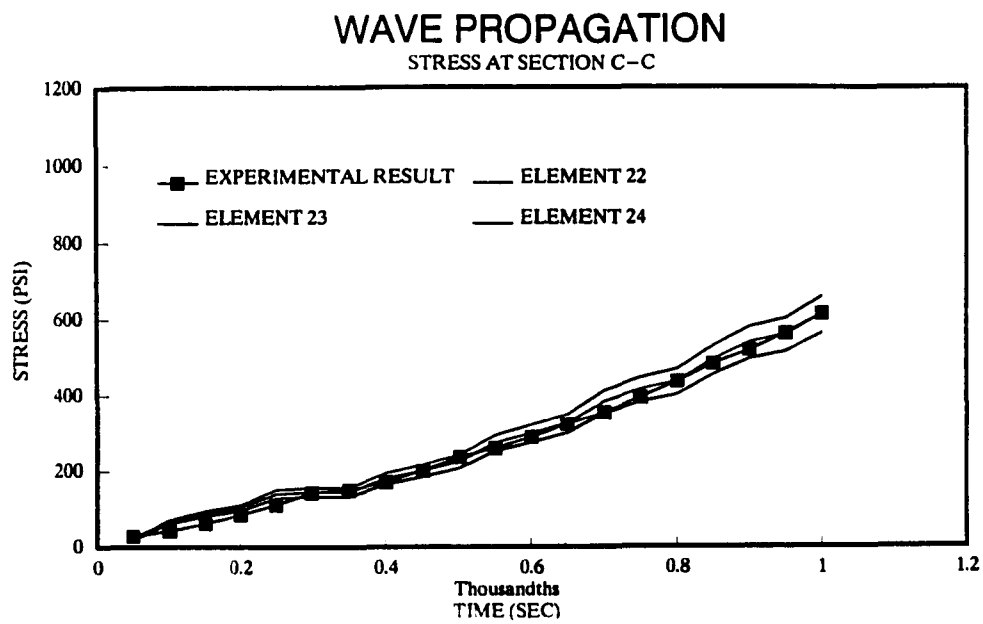

Figure 5.11 Stress history at section C-C. Note the correlation of the experimental with analytical results.

Reproduced with permission of the copyright owner. Further reproduction prohibited without permission.

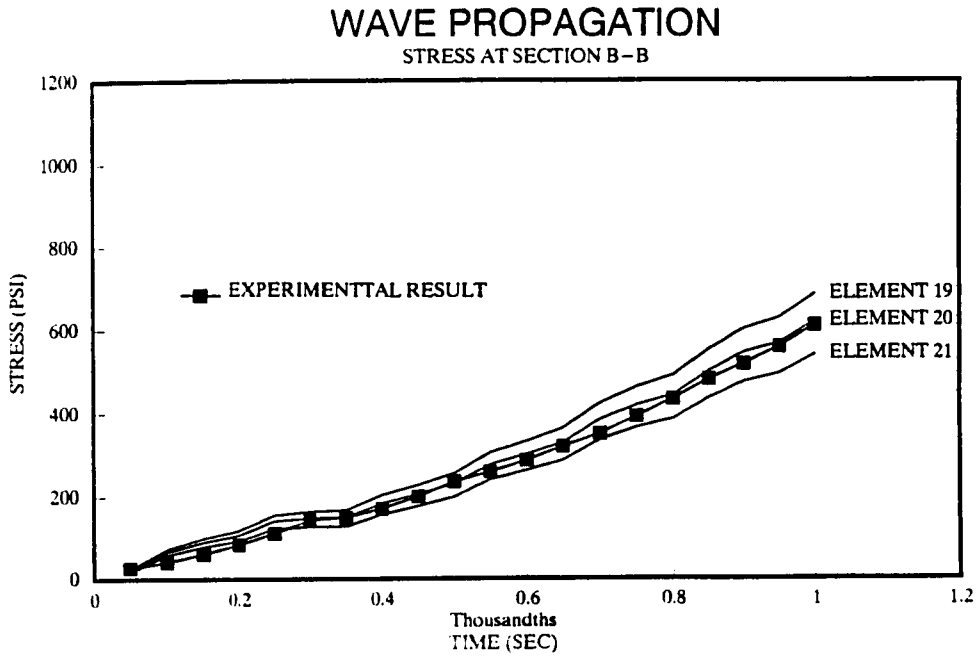

Figure 5.12 Stress history at section B-B. Note the correlation of the experimental with analytical results.

Reproduced with permission of the copyright owner. Further reproduction prohibited without permission.

5.3 Theoretical Model

Concrete composite is one of the materials which is widely used in the construction industry. Concrete is a strain rate sensitive material. Its behavior under direct impact tensile load changes relative to its static condition. To consider the effect of strain rate on the design of concrete materials, a model would be necessary to predict the ultimate tensile stress under an expected strain rate. Following is a systematic approach to develop such a model.

Considering concrete as an inelastic material, Perzyna[129] has assumed that strain rate can be divided into elastic and inelastic parts:

$$\dot{\varepsilon}_{ij} = \dot{\varepsilon}^{p}_{ij} + \dot{\varepsilon}^{e}_{ij} \qquad (5.3)$$

where $\dot{\varepsilon}^{p}_{ij}$ is the inelastic part of the strain rate which represents the combined viscous and plastic effects. The one dimensional constitutive equations for rate sensitive and inelastic materials are given as follow by Prager[130,131]:

$$2\eta \dot{\varepsilon}^{p}_{ij} = 2K \langle F \rangle \frac{\partial F}{\partial \sigma_{ij}} \qquad (5.4)$$

Reproduced with permission of the copyright owner. Further reproduction prohibited without permission.

where

$$F = \frac{J_2^{1/2}}{\kappa} - 1 \tag{5.5}$$

or

$$F = \frac{[\, S_{ij}S_{ij}/2 \,]^{1/2}}{\kappa} - 1 \tag{5.6}$$

and

$$\langle F \rangle = \begin{cases} 0 & for \quad F \leq 0 \\ F & for \quad F > 0 \end{cases} \tag{5.7}$$

Introducing the elastic portion into equation (5.4), the strain deviation can be written as[132]:

$$\dot{e}_{ij} = \frac{1}{2\mu}\dot{S}_{ij} + \frac{1-\kappa J^{-1/2}}{2\eta} S_{ij} \quad if \quad J_2^{1/2} \leq \kappa$$

$$\dot{e}_{ij} = \frac{1}{2\mu}\dot{S}_{ij} \quad if \quad J_2^{1/2} \leq \kappa \tag{5.8}$$

$$\dot{\varepsilon}_{ii} = \frac{1}{3\kappa}\dot{\sigma}_{ii}$$

By replacing the 2k < F > by $\overset{0}{\gamma}\Phi(F)$ where F is given by equation (5.5) will result in:

Reproduced with permission of the copyright owner. Further reproduction prohibited without permission.

$$\Phi(F) = 0 \quad if \quad F \leq 0$$

$$\Phi(F) \neq 0 \quad if \quad F > 0 \tag{5.9}$$

Introducing the elastic strain into equation (5.4), the following constitutive relationship can be concluded:

$$\dot{e}_{ij} = \frac{1}{2\mu}\dot{S}_{ij} + \overset{0}{\gamma}\Phi(F)\frac{\partial F}{\partial \sigma_{ij}} \quad for \quad F > 0$$

$$\dot{e}_{ij} = \frac{1}{2\mu}\dot{S}_{ij} \qquad for \quad F \leq 0 \tag{5.10}$$

$$\dot{\varepsilon}_{ii} = \frac{1}{3K}\dot{\sigma}_{ii}$$

Assuming $\gamma = \overset{0}{\gamma}/2\kappa$ one can write:

$$\dot{e}_{ij} = \frac{1}{2\mu}\dot{S}_{ij} + \gamma\Phi(F)\frac{S_{ij}}{J_2^{1/2}} \quad for \quad J_2^{1/2} > \kappa$$

$$\dot{e}_{ij} = \frac{1}{2\mu}\dot{S}_{ij} \qquad for \quad J_2^{1/2} \leq \kappa \tag{5.11}$$

$$\dot{\varepsilon}_{ii} = \frac{1}{3K}\dot{\sigma}_{ii}$$

Reproduced with permission of the copyright owner. Further reproduction prohibited without permission.

where $\Phi(F)$ can be chosen to represent the results of tests on the behavior of materials under dynamic loading. To develop equation (5.11), the following assumptions were made:

- The rate of increase in the plastic components of the strain tensor is a function of the excess stresses above the static yield condition.
- The elastic components of the strain tensor are considered to be independent of the strain rate.

Applying equation (5.5) into the constitutive equation (5.11):

$$\dot{e}_{ij} = \frac{1}{2\mu}\dot{S}_{ij} + \gamma\Phi\left(\frac{J_2^{1/2}}{\kappa} - 1\right)\frac{S_{ij}}{J_2^{1/2}} \quad for \quad J_2^{1/2} > \kappa$$

$$\dot{e}_{ij} = \frac{1}{2\mu}\dot{S}_{ij} \quad for \quad J_2^{1/2} \leq \kappa \qquad (5.12)$$

$$\dot{\varepsilon}_{ii} = \frac{1}{3K}\dot{\sigma}_{ii}$$

Also, equation (5.5) can be written in the following form:

$$J_2^{1/2} = \kappa(F+1) \qquad (5.13)$$

Considering the inelastic part of the equation (5.11):

Reproduced with permission of the copyright owner. Further reproduction prohibited without permission.

$$\dot{\varepsilon}_{ij}^{p} = \gamma\Phi(F)\,\frac{S_{ij}}{J_2^{1/2}} \qquad (5.14)$$

By squaring both sides of equation (5.14), one obtains:

$$\dot{\varepsilon}_{ij}^{p}\,\dot{\varepsilon}_{ij}^{p} = (\gamma\Phi(F))^2\,\frac{S_{ij}S_{ij}}{J_2} \qquad (5.15)$$

The second invariant inelastic strain rate tensor is given as follows:

$$I_2^{p} = \frac{1}{2}\,\dot{\varepsilon}_{ij}^{p}\,\dot{\varepsilon}_{ij}^{p} \qquad (5.16))$$

Applying this equation into equation (5.15), one obtains:

$$2\,I_2^{p} = (\gamma\Phi(F))^2\,\frac{S_{ij}S_{ij}}{J_2} \qquad (5.17)$$

Considering that $J_2 = 1/2\ S_{ij}\ S_{ij}$, the above equation becomes:

$$I_2^{p} = (\gamma\Phi(F))^2 \qquad (5.18)$$

or

$$(I_2^{p})^{1/2} = \gamma\Phi(F) \qquad (5.19)$$

Reproduced with permission of the copyright owner. Further reproduction prohibited without permission.

Combining equations (5.13) and (5.19) gives:

$$J_2^{1/2} = \kappa(1+\Phi^{-1}([I_2^p]^{1/2}/\gamma)) \tag{5.20}$$

For one dimensional state of stress, substituting equation (5.19) into equation (5.11) leads to:

$$\dot{\varepsilon} = \frac{\dot{\sigma}}{E} + \gamma\left\langle \Phi\left(\frac{\sigma}{\sigma_0}-1\right)\right\rangle \tag{5.21}$$

It has been observed that tensile strength of cement composites increases significantly as the rate of loading or straining increases. Also, if a logarithmic scale is adapted to account for the effect of strain rate, equal successive increments on this scale tend to produce progressively greater increases in the ratio of dynamic to static tensile strength[93, 103,125-128]. Let us assume that the shape function $\Phi(F)$ has the following form:

$$\Phi(F) = \left[\exp(pF) - Q\right]^{\beta} \tag{5.22}$$

Applying equation (5.22) to equation (5.21), one obtains:

Reproduced with permission of the copyright owner. Further reproduction prohibited without permission.

$$\dot{\varepsilon} = \frac{\dot{\sigma}}{E} + \gamma \left\{ \exp\left[p\left(\frac{\sigma}{\sigma_0} - 1 \right) \right] - Q \right\}^{\beta} \qquad (5.23)$$

Assuming the elastic deformations are negligible in comparison with the plastic deformations, we conclude that:

$$\frac{\sigma}{\sigma_0} = 1 + \frac{1}{p} \log \left[\left(\frac{\dot{\varepsilon}}{\gamma} \right)^{1/\beta} + Q \right] \qquad (5.24)$$

where γ, p, Q, β are material constants:

Assuming:

$$\alpha = \gamma^{-1/\beta} \qquad P = \frac{1}{p} \qquad \lambda = \frac{1}{\beta}$$

equation (5.24) can be written as follow:

$$\frac{\sigma}{\sigma_0} = 1 + P \log[\alpha \dot{\varepsilon}^{\lambda} + Q] \qquad (5.25)$$

For static condition, $\frac{\sigma}{\sigma_0} = 1$ and $\dot{\varepsilon} = 0$. Applying these two conditions to equation (5.25) gives Q = 1 and equation (5.25) becomes:

$$\frac{\sigma}{\sigma_0} = 1 + P \log[\alpha \dot{\varepsilon}^{\lambda} + 1] \qquad (5.26)$$

Reproduced with permission of the copyright owner. Further reproduction prohibited without permission.

By applying the experimental results into equation (5.26), as illustrated on Figure 5.13, the following values were obtained for the material constants:

$P=1.2$ $\alpha=3.2$ $\lambda=0.45$ for concrete

$P=1.2$ $\alpha=4.1$ $\lambda=0.46$ for mortar

Applying the above values of these three variables into equation(5.26) gives the following models for predicting the direct impact tensile strength of concrete and mortar respectively as a function of strain rate:

$$\frac{\sigma}{\sigma_0} = 1+1.2\log(3.2\dot{\varepsilon}^{0.45}+1)$$

$$\frac{\sigma}{\sigma_0} = 1+1.2\log(4.1\dot{\varepsilon}^{0.46}+1) \qquad (5.27)$$

It can be seen in Figure 5.13 that the model is in good agreement with the experimental results.

Reproduced with permission of the copyright owner. Further reproduction prohibited without permission.

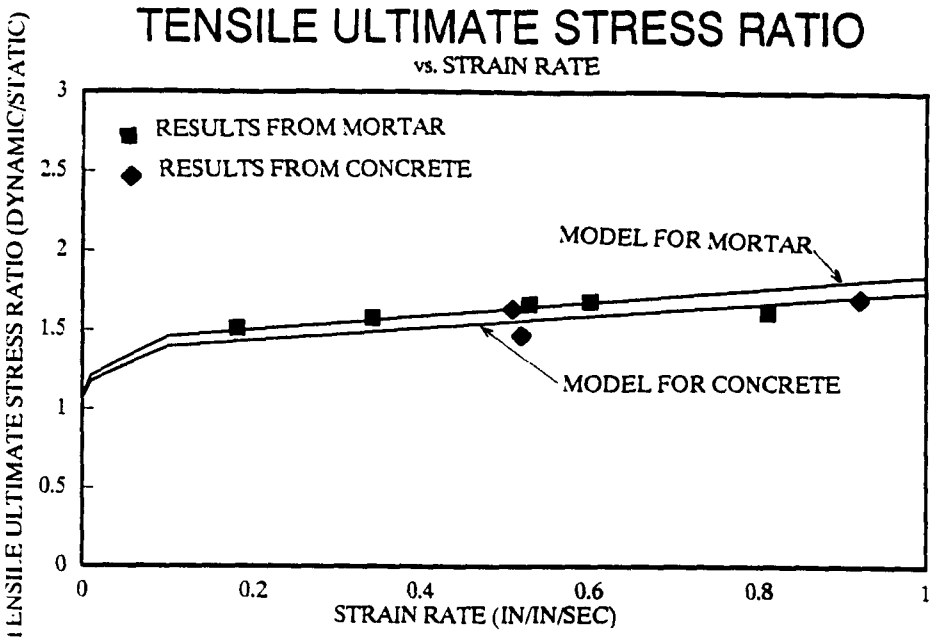

Figure 5.13 A comparison of the analytical model with experimental results. Normalized direct tensile stress is plotted versus strain rate.

Reproduced with permission of the copyright owner. Further reproduction prohibited without permission.

CHAPTER 6

Results and Discussion

In studying the impact behavior of concrete materials, the proper instrumentation is essential. This can even be more critical in investigating the behavior of cement based composites under direct tensile load because when measuring small loads, small errors in measurement can be a significant portion of the total result. Due to shortcomings which were discussed earlier at section 3.3.2.1, an instrumented drop-weight test was chosen. Additionally, a new hollow cylindrical specimen was developed. It has been reported that the strain rate is a control factor determining the material behavior in impact tests of cementitious composites[82,124]. A drop hammer testing set-up depends on three physical parameters, the drop hammer height, the drop hammer weight, and the rubber pad thickness at the contact zone between the striker and specimen. In order to achieve different strain rates, the effect of these parameters were studied.

6.1 Effect of Drop Hammer Height on Impact Test

The first parameter in drop hammer apparatus is the initial height difference between the drop hammer and the specimen. To study the effect of drop hammer height on the tensile impact test height variations of 16 in., 8 in., 4

Reproduced with permission of the copyright owner. Further reproduction prohibited without permission.

in. and 2 inches were chosen while the other parameters such as drop hammer weight and rubber pad thickness were kept at constant values of 50 lb and 1/8 inch respectively. By comparing the results from the above drop hammer heights, several observations were made.

1. The general patterns of stress versus time and strain versus time are similar with each other.

2. Increasing the drop hammer heights from 4 inches to 16 inches results in increase of ultimate tensile strength from 51% to 68% relative to the static test as shown in figure 6.1. It was also observed that the specimen did not fail at a drop hammer height of 2 inches.

3. Fracture time for the specimen were reduced from 1.6 milliseconds to 0.72 millisecond by increasing the drop hammer height from 4 to 16 inches.

4. The slopes of stress versus time and strain versus time curves which are representative of stress and strain rates increase with increasing drop hammer height.

5. The total energy absorption to failure of the specimen was increased from 164% to 216% by increasing the drop hammer height from 4 to 16 inches, relative to the static test.

From the above observation it can be concluded that by changing the drop hammer height, different strain rates can be achieved. Therefore, the drop hammer height is one

Reproduced with permission of the copyright owner. Further reproduction prohibited without permission.

of the controlling parameters in the direct impact tensile test which contributes to the variation of strain rate and can be an effective variable in the impact testing.

6.2 Effect of Rubber Pad on Impact Test

In order to reduce the stiffness at the contact zone and minimize possible inertial oscillations, a rubber pad was used. The presence of the pad was studied for possible effect on strain rates in direct impact tests. Tests were performed on three different rubber pads with shore hardness of about 70, and thicknesses of 3/16 inch, 1/8 inch and 1/16 inch as well as with no rubber pad. Other test parameters such as drop hammer height and weight were kept at constant values (50 lb and 16 inches respectively) to eliminate possible interference with the test results. By reducing the rubber pad thickness the following general observations were made:

1. The results of the four cases follow a similar pattern.
2. The ultimate tensile stresses using 3/16 inch and no pad exhibit increases in magnitude from 63% to 85% with respect to the static test as shown in figure 6.2.
3. The specimen fracture time is observed to decrease from 1.42 milliseconds to 0.58 millisecond.

Reproduced with permission of the copyright owner. Further reproduction prohibited without permission.

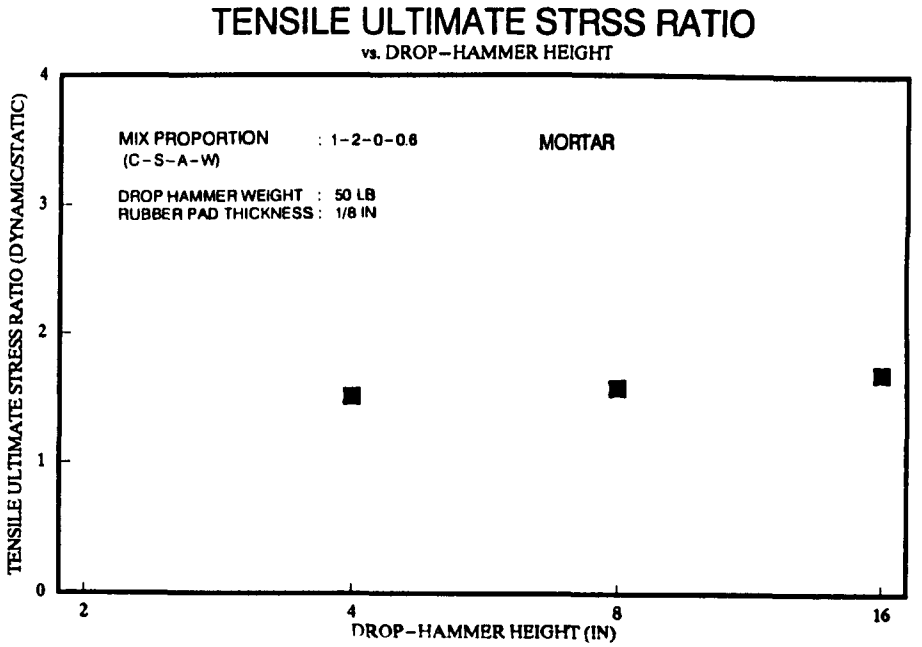

Figure 6.1 Effect of drop-hammer height on tensile ultimate stress (Dynamic/Static).

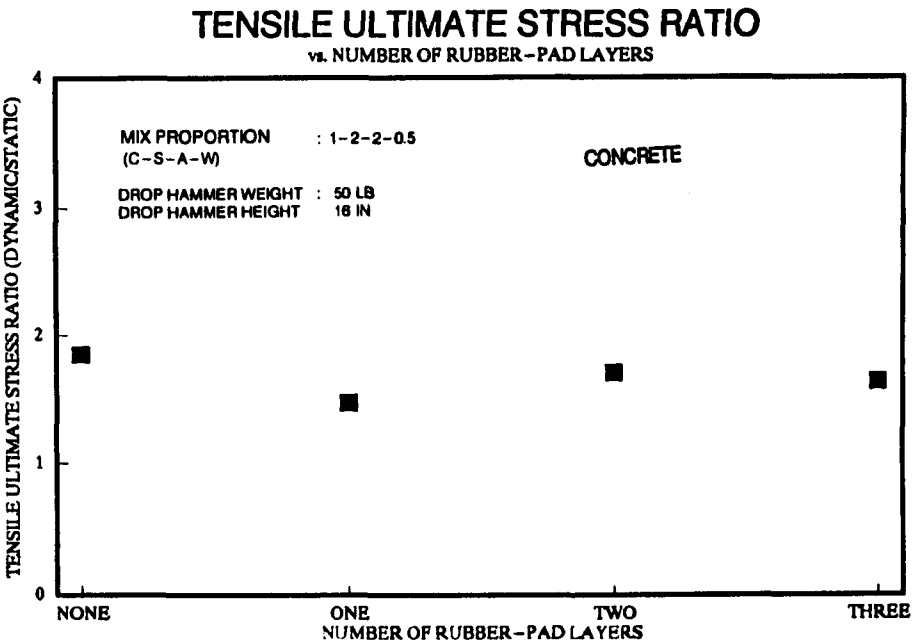

Figure 6.2 Effect of number of rubber-pad layers on tensile ultimate stress (Dynamic/Static).

Reproduced with permission of the copyright owner. Further reproduction prohibited without permission.

4. The strain rate increases from 0.51 1/sec to 0.97 1/sec.

5. Total energy absorption to specimen failure increases by 164 % to 291% with respect to the static test.

Based on the above observations, it can be concluded that the rubber pad thickness is another controlling parameter in direct impact tensile tests.

6.3 Effect of Drop Hammer Weight on Impact Test

Another variable in a drop hammer weight test is the weight of the striker. In order to study its effect on the impact test, three different weights, 50 Lb, 83 Lb, and 110 Lb were selected while the other parameters such as drop hammer height and rubber pad thickness were kept constant at the value of 16 inches and 1/8 inch respectively. From the results it was observed that the stress versus time and strain versus time curves have similar patterns, which indicated the consistency of the test set up. However, the drop hammer height did not contribute any noticeable effect on the testing results as shown in figure 6.3. This can be due to the fact that velocity of a falling object is not related to the mass of the object.

It is found that the drop hammer height and rubber pad thickness are two variables which control the direct

Reproduced with permission of the copyright owner. Further reproduction prohibited without permission.

tensile impact test. But drop hammer weight does not contribute a noticeable effect on the impact test result.

The strain rates are increased from 0.03 1/sec to 0.75 1/sec by increasing the drop hammer height from 4 inches to 16 inches. And they are increased from 0.51 1/sec to 0.97 1/sec by reducing the rubber pad thickness from 3/16 inch to none(dry impact).

To evaluate a relationship between stress and strain rates, regression analysis is employed and the following equation is found:

$$\dot{\sigma} = 200 + 1925\,\dot{\varepsilon} \qquad (6.1)$$

As it can be seen from Figure 6.4 and equation (6.1), a linear relationship exists between the stress and strain rates.

6.4 Effect of Strain Rate on the Tensile Strength

It was found that increasing the drop hammer height and reducing the rubber pad thickness resulted in larger strain rate in drop hammer weight test. The result of the experiments indicate that direct tensile strength obtained in the present study were increased by increasing strain rate. Concrete is an inhomogeneous material consisting of sand and aggregate particles, cement paste and the interfacial bond zone. It may be cracked due to different

Reproduced with permission of the copyright owner. Further reproduction prohibited without permission.

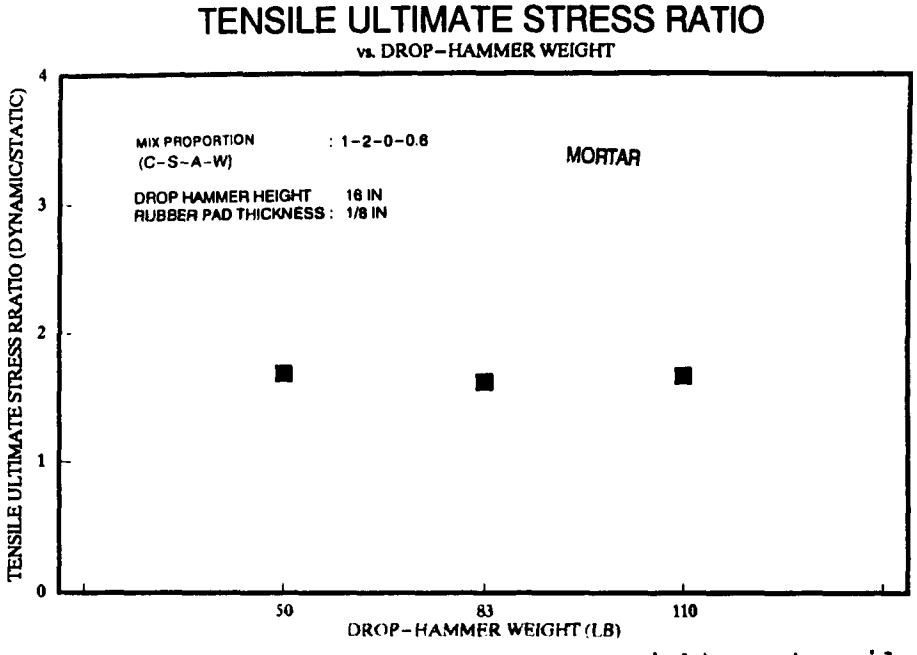

Figure 6.3 Effect of drop-hammer weight on tensile ultimate stress (Dynamic/Static).

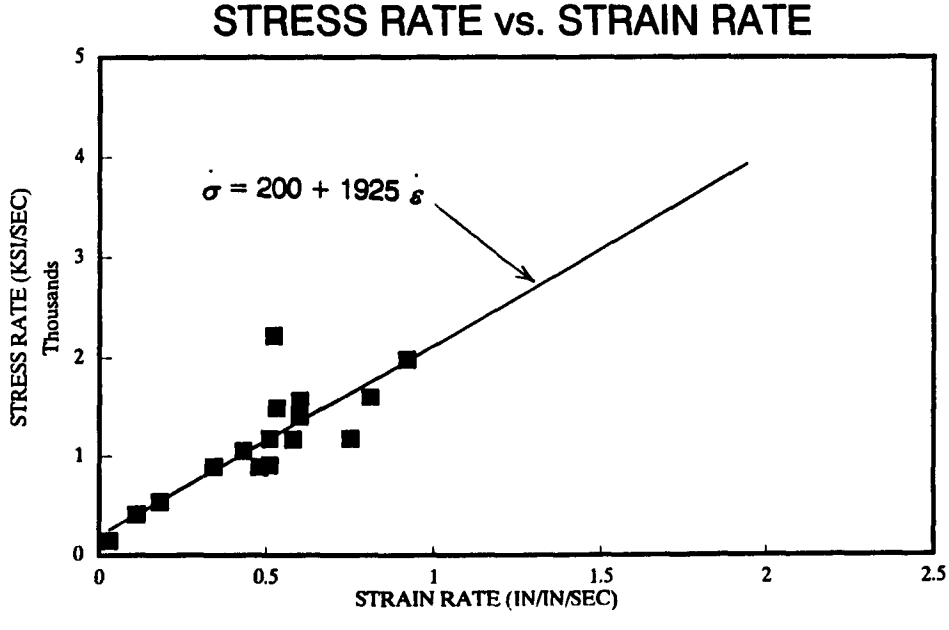

Figure 6.4 Relationship between Stress-Rate and Strain-Rate.

Reproduced with permission of the copyright owner. Further reproduction prohibited without permission.

thermal movement and shrinkage during hydration and drying. Sand and aggregate are mostly produced from crushed rock. Rock generally is stronger than cement paste, therefore, the interfacial bond zone usually is the weakest link in cement based matrix. It can be seen in Figure 6.5 that during direct tensile test, fracture planes exhibit fewer interfacial bond failure and more fracture aggregate particles as compared with the static fracture planes. Tensile strength of concrete increased from 655 psi to 1120 psi when the strain rate was changed from $1x10^{-5}$ 1/sec to 0.97 1/sec, and for mortar, the tensile strength increased from 440 psi to 740 psi when the strain rate increased from $1x10^{-5}$ 1/sec to 0.756 1/sec. This larger sensitivity of strain rate in mortar than concrete is a reason that micro cracking has been a major process responsible for the strain rate sensitivity of cementitious composites.

The present result of concrete can be compared with the results by Suaris and Shah[67] using an instrumented drop hammer test on three point bending test set up, and results from Gopalaratnam, Shah, and Reji[20] using instrumented charpy test on three point bending test. The ultimate dynamic to static tensile stress ratio versus strain rate of present result from direct tensile tests along with their results are plotted as illustrated in Figure 6.6. It can be noted that the present result is

Reproduced with permission of the copyright owner. Further reproduction prohibited without permission.

satisfactory since the general trend is similar to that of the other investigators, despite the fact that the testing apparatus, specimen configuration and size were different. The decrease in magnitude of the present results with respect to the others could be due to, a) inertial effect, b) difference between modulus of rupture in bending test versus direct tension, or c) differences in the static strength of the mixes. It has been recorded by Suaris and Shah[67], and Gopalaratnam and Naaman[22] as well as present results that weaker mixes of concrete exhibit greater strain rate sensitivity. The static tensile strength of present study is 655 psi while modulus of rupture reported by Suaris, et al. and Gopalaratnam, et al. are 1400 and 1430 psi which suggest that in the present study, the concrete mix should be more strain rate sensitive. Also it is reported by Brooks and Samaraie[74] and Suaris and Shah[67] that direct tensile strength is more strain rate sensitive than modulus of rupture, therefore, the reason that the magnitude of result from the present study is lower than the others is probably the presence of inertia in the three point bending test. Thus, the present result shows that the cementitious composites are strain rate sensitive in the direct tensile impact test, but it is smaller than the results reported by Suaris and Shah[67] and Gopalaratnam and Naaman[22] which were inflated due to inertia.

Reproduced with permission of the copyright owner. Further reproduction prohibited without permission.

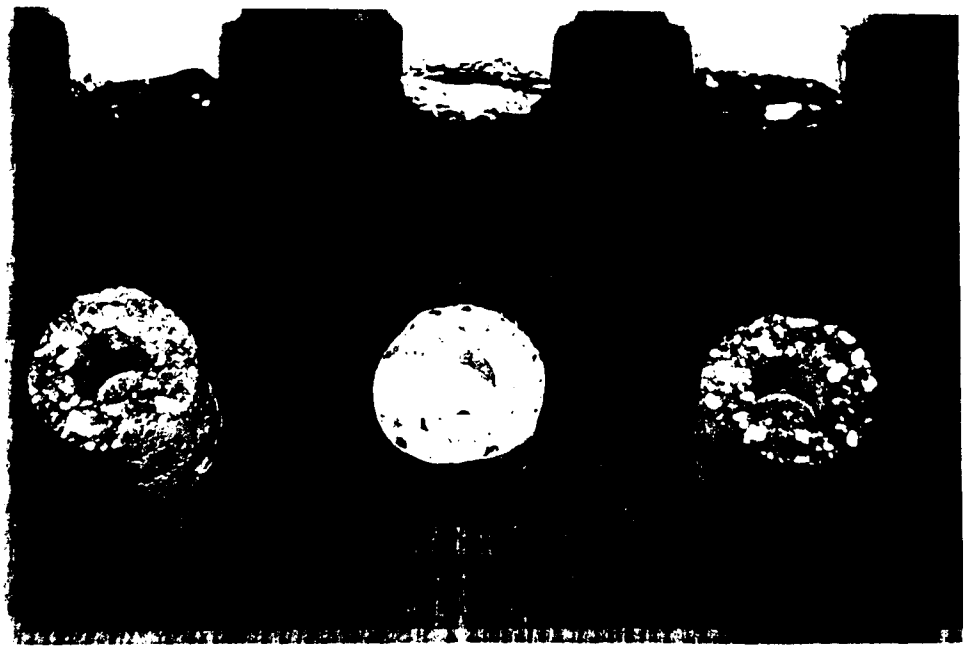

Figure 6.5 Fracture plane of specimens made with maximum aggregate size of 1/4 inch under direct impact tensile load.

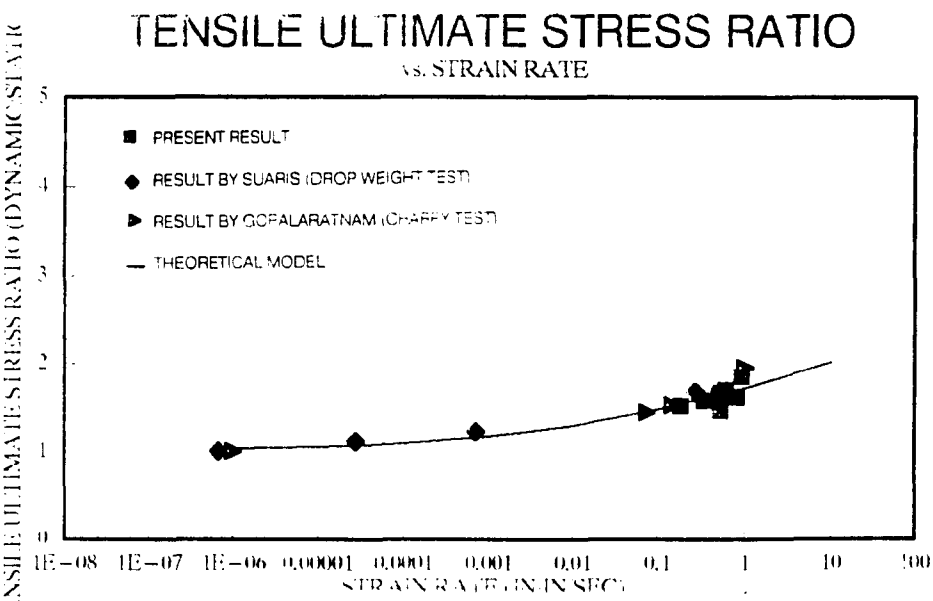

Figure 6.6 Comparison of the Strain Rate sensitivity in MOR of surveyed results with direct tensile strength of present study.

Reproduced with permission of the copyright owner. Further reproduction prohibited without permission.

6.5 Effect of Strain Rate on Energy Absorption

Fracture of concrete matrix is the major component of energy absorption in tensile failure of cement composites. The magnitude of energy absorption to tensile failure of concrete increased by 291% when the strain rate increased from $1x10^{-5}$ 1/sec to 0.97 1/sec and that of mortar increased by 216% during the strain rate from $1x10^{-5}$ 1/sec to 0.75 1/sec. Comparing the present results with that of Suaris and Shah[67] indicates that the energy absorption (static to dynamic ratio) from present direct tensile impact test has similar pattern to that of their results on three point bending test, as shown in Figure 6.7. The energy absorption during fracturing of the material is mainly associated with crack extension in the matrix, aggregate and interfacial bond zones. And normalized energy absorption increases by increasing the strain rate. Also concrete exhibits more sensitivity at higher strain rate than mortar. This is perhaps due to the fact that during impact test, fracture tends to pass through the shortest distance, while in the static case fracture seeks for the path with the least energy.

Reproduced with permission of the copyright owner. Further reproduction prohibited without permission.

6.6 Effect of Strain Rate on Modulus of Elasticity

The stress versus strain curves in direct tensile impact tests exhibit a slight increase in slope than that of static curve as illustrated in Figure 6.8. Using regression analysis, the following relationship between the modulus of elasticity and strain rate in direct tensile impact test is found:

$$E = 4340 + 19\ \dot{\varepsilon} \qquad (6.2)$$

The increase in modulus of elasticity due to increase in strain rate is perhaps caused by reduced micro cracking at the higher strain rate. From the test results, it is evident that by increasing strain rate the increase in ultimate tensile stress is larger than the increase in failure strain. Also the stress versus strain curve becomes less nonlinear.

Reproduced with permission of the copyright owner. Further reproduction prohibited without permission.

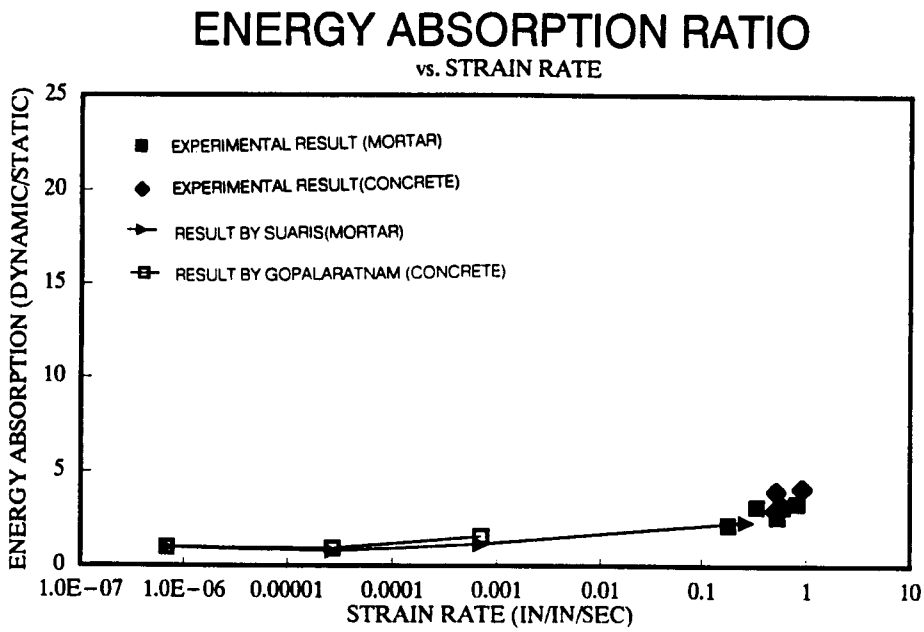

Figure 6.7 Comparison of the strain sensitivity of surveyed results with present result.

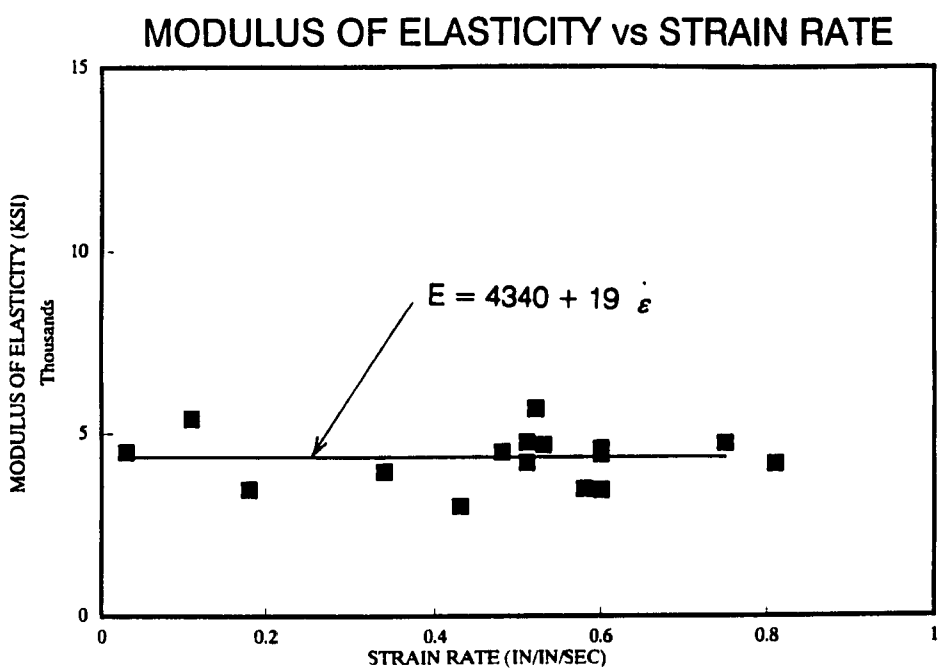

Figure 6.8 Strain rate sensitivity of modulus of elasticity in present study.

Reproduced with permission of the copyright owner. Further reproduction prohibited without permission.

CHAPTER 7

Conclusions

Based on the results obtained in this investigation, the following conclusions can be drawn:

1) The instrumented drop weight test along with the new specimen configuration described here are a useful combination for the study of the direct tensile behavior of cement based materials under impact loading. The test method yields true material properties, which are less sensitive to inertial effects. The direct tensile failure makes the proposed test specimen a more suitable configuration for studying the direct tensile properties of concrete under impact load. It produces more accurate results for direct tensile behavior of low tensile strength brittle cement based materials.

2) The hollow cylindrical specimen which is developed for this study produces the real direct tensile behavior of material rather than a surrogate parameter like modulus of rupture, independent of the specimen shape, the impact mass and the set-up stiffness.

3) The drop hammer height and rubber pad thickness are two key variables controlling the results of the impact tensile testing while the drop hammer weight does

Reproduced with permission of the copyright owner. Further reproduction prohibited without permission.

not contribute any noticeable effect on the impact tensile test.

4) The peak tensile loads obtained under direct impact loading with the strain rate of 0.92 1/sec are 71% higher than those obtained under the static loading.

5) An increase in the strain rate from the quasi-static condition to the impact range of 0.92 1/sec results in 235% increase in the fracture energy.

6) An increase in the strain rate results in an increase in the strain at the failure of the material.

7) The modulus of elasticity exhibits a slight increase due to higher strain rate.

8) Mortar and concrete exhibit increased tensile strength at the higher strain rates. The increase is more pronounced for mortar which is a weaker material than concrete.

9) It appears that in direct tensile test, as the strain rate increases there is a tendency to minimize the size of the crack plane. At low strain rates the cracks spread through the interfacial zone causing bond failures. Whereas at high strain rates there is a pronounced increase in aggregate splitting. In other words, the crack follows the shortest path to the failure. This is perhaps due to the fact that the failure will follow the path of least resistance. Normal concrete, tested under static conditions, generally fails due to bond failures. But, for

Reproduced with permission of the copyright owner. Further reproduction prohibited without permission.

the direct tensile impact case the excessive magnitude of applied energy at the crack tip forces the crack through a zone of higher resistance.

10) The model developed, based on the constitutive law, represents the inelastic material behavior of cement based composites. It predicts the ultimate direct tensile stress for cementitious materials for a given strain rate.

11) The advantages of the proposed test specimen configuration are the fact that it has a smaller inertia effect on the load readings and the specimen provides a direct uniform tensile failure across the section. This ensures a uniform strain rate across the failure plane. The disadvantage of this proposed test specimen is the limitation of maximum aggregate size in concrete which is controlled by the wall thickness. However, this shortcoming can be overcome if a larger specimen is employed.

Reproduced with permission of the copyright owner. Further reproduction prohibited without permission.

BIBLIOGRAPHY

1) Zielinski, A. J.,and Reinhardt H. W. "Stress-strain behavior of concrete and mortar at high rates of tensile loading" Cement and Concrete Research, Vol. 12, 1982, pp. 309-319.

2) Mainstone, R.J., and Kavyrchine M. "Introduction to Impact Loading" Materiaux Et Constructions, Vol. 8 No. 44, 1975, pp.79-80.

3) Berthelsen, G. "Caltrans Engineering Refine Design for Earthquake" Roads and Bridge, August 1987, pp. 42-44.

4) Knab L. I., and Clifton J. R. "Cumulative damage of reinforced concrete subjected to repeated impact" Cement and Concrete Research, Vol. 12, 1982, pp. 359-370.

5) Lindholm, U.S. "Some Experiments in Dynamic Plasticity Under Combined Stress. Symposium on Mechanical Behavior Under Dynamic Loads" Springer, New York, 1968, PP. 77-95.

6) Anderson, W.F., Watson, A. J., and Armstrong, P. J. "High Velocity Projectile Impact on Fiber-Reinforced Concrete" Ibid, PP. 368-379.

7) Gueraud, R., and Sokolovsky, A. "Study of the Perforation of Reinforced Concrete Slabs by Rigid Missiles" Nuclear Engineering and Design, Vol. 41, 1977, pp. 91-102.

8) Mayhofer, C., and Thor, H.J. "Dynamic Response of Fiber and Reinforced Concrete Plates Under Simulated Blast Load" Proceedings of the RILEM-CEB-IABSE-IASS Symposium on Concrete Structures under Impulsive Loading, West Berlin.

9) Hulsewig, M., and Stilp, A. "Behavior of Fiber Reinforced Concrete Slabs Under Impact Loading" Ibid, pp. 322-329.

10) Schrader, E. K. "Impact Resistance and Test Procedure for Concrete" ACI Journal, Vol. 78, No. 2, Mar-Apr. 1981, PP. 141-146.

Reproduced with permission of the copyright owner. Further reproduction prohibited without permission.

11) Kormeling, H.A., Zielinski, A.J., and Reinhardt, H.W. "Experiments on Concrete under Single and Repeated Impact Loading" Report No. 5-80-3, Delft University of Technology, Stevin Laboratory, May 1980.

12) Takeda, J. I., Tachikawa H., and Fujimoto K. "Mechanical behavior of concrete under higher rate loading than in static test" Proceedings of the 1974 Symposium on Mechanical Behavior of Materials (Kyoto,Japan), Vol. II, Kyoto, August 21-24, 1974, pp. 479-486.

13) Hibbert A. P., and Hannant D. J. "Impact resistance of fibre concrete" Construction Materials Research Group, Dept. of Civil Eng. University of Surrey, 1981.

14) Suaris, W., and Shah, S.P. "Test Methods for Impact Resistance of Fiber Reinforced Concrete" SP 81-12, pp. 247-265.

15) Ross, C.A., Kuennen, S.T., and Tedesco, J.W. "Experimental and Numerical Analysis of High Strain-Rate Concrete Tensile Tests" pp. 353-364.

16) Nicholas, T. Materials Behavior at High Strain Rates Impact Dynamics, John Willey and Sons, New York, 1982, PP. 277-332.

17) Ross, C.A. "Split-Hopkinson Pressure Bar Tests" Report ESL-TR-88-82, Engineering and Services Laboratory, HQ Air Force Engineering and Services Center, Tyndall AFB, FL, March 1989, PP. 80.

18) Orner, G.M., and Hartbower, C.E. "Sheet Fracture Toughness Evaluated by Charpy Impact and Slow Bend" The Welding Journal, Vol. 40, Oct. 1961, pp. 405s-416s.

19) Perry, E.S., Burns, N.H., and Thompson, J.N. "Behavior of Concrete beams Reinforced with Steel Plates Subjected to Dynamic Loads" J. Amer. Concr. Inst., Vol. 64, 1967, pp. 662-668.

20) Gopalaratnam, V. S., Shah, S.P., and Reji, J. "A modified instrumented charpy test for cemented based composites" Experimental Mechanics, Vol. 24, No. 2, June 1984, pp. 102-111.

Reproduced with permission of the copyright owner. Further reproduction prohibited without permission.

21) Suaris, W., and Shah, S.P. "Strain-rate effects in fibre-reinforced concrete subjected to impact and impulsive loading" Int. J. Cement Composites, Vol. 13, No. 2, April 1982, pp. 153-159.

22) Gopalaratnam, V.S., and Naaman, A. E. "Impact Resistance in Flexure of Steel Fiber Reinforced Concrete" 3rd Progress Report for U. S. Army Research Office, DAAG 29-79-C-0162, University of Illinois at Chicago, May 1982.

23) Mindess, S., and Nadeau, J.S. "Effect of Loading Rate on the Flexural Strength of Cement and Mortar" Bulletin of the American Cement Society, Vol. 56, No. 44, April 1977, pp. 429-430.

24) Zielinski, A.J., Reinhardt, H.W., and Kormeling, H.A. "Experiments on concrete under uniaxial impact tensile loading" Materiaux et constructions, vol.14, 1980, PP. 103-112.

25) Popp, C. "Investigations on the Impact of Vehicles on Reinforced Concrete Columns" Heft 14, Stahlbauverlag Koln, 1965.

26) Riera, J.D. "On the Stress Analysis of Structures Subjected to Aircraft Impact Forces" Nuclear Engin. and Design, Vol. 8, 1968, pp. 415-426.

27) Mainstone, R.J. "Structural Tests on an Experimental Helicopter Platform" Inst. Civil Eng. Proc., Vol. 33, 1966, pp. 65-91.

28) American Association of State Highway and Transportation Officials. Subcommittee on Bridge and Structures, 1990, Sect. 3.8.2.1.

29) Sliter, G.E. "Assessment of Empirical Concrete Impact Formulas" Journal of the Structural Division, ASCE, May 1980, pp. 1023-1045.

30) Struk, W., Limberger, E., and Eifler, H. "Problems and Gaps of Knowledge in the Assessment of the Response of Reinforced Concrete Structures Under Impact Loading" 2nd International Conference on Structural Mechanics in Reactor Technology, Berlin, 1973, CID-publ., Luxembourg Vol. 4, Part J 3/4, S. 1-13.

Reproduced with permission of the copyright owner. Further reproduction prohibited without permission.

31) Baker, T.C. "The Designed of Framed Buildings Against High Explosive Bombs" Tall Building Criteria and Loading, Conceal on Tall Building and Urban Habitat, Vol. CL, 1980, pp. 393-438.

32) Griffiths, A.A., et al. "Report on the Inquiry into the Collapse of Flat at Ronan Point" Tall Building Criteria and Loading, Conceal on Tall Building and Urban Habitat, Vol. CL, 1980, pp. 393-438.

33) Granstorm, and Carlsson "Terrorist Explosion in the German Embassy" Tall Building Criteria and Loading, Conceal on Tall Building and Urban Habitat, Vol. CL, 1980, pp. 393-438.

34) Mainstone, R.J. "The Hazard of Internal Blast in Buildings" Building Research Establishment Current, Paper CP 11/73, April 1973.

35) Newberry ,C.W., Eaton, K.J., and Mayne, J.R. "The Nature of Gust Loading on Tall Buildings" Proceedings of the International Research Seminar on 'Wind Effects on Buildings and Structures', Ottawa, Vol. I, 1967, pp. 399-428, University of Toronto Press.

36) Newberry , C.W., Eaton, K.J., and Mayne, J.R. "Wind Loading on Tall Buildings" Further Results from Royex House, Building Research Establishment, Current Paper CP 29/73, November 1973.

37) Mainstone, R.J. "The Effects of Explosions on Buildings. Building and the Hazard of Explosion" Proceedings of a Symposium at BRE, 1972, pp. 7-18.

38) Nadai, A. "Theory of Flow and Fracture of Solids" Engineering Societies Nomographs, Vol. I, 2nd Ed. Mcgraw-Hill Book Co. Inc., New York, 1950.

39) Feldman, A., Keenan, W. A., and Seiss, C.P. "Investigation of Resistance and Behavior of Reinforced Concrete Members Subjected to Dynamic Loading" Part III, Civil Engineering Studies, No. 243, University of Illinois, Urbana, I11., Feb. 1962.

40) Flathau, W.J. "Dynamic Tests of Large Reinforcing Bar Splices" Technical Report N-71-2, U.S.Army Engineer Division, Euntsville, Ala., April 1971.

41) Campbell, J.D., and Ferguson, W.G. "The Temperature and Strain Rate Dependence of the Shear Strength of Mild Steel" Phil. Mag., Vol. 21, 1970, PP. 63-82.

Reproduced with permission of the copyright owner. Further reproduction prohibited without permission.

42) Steidel, R.F., and Makerov, C.E. "The Tensile Properties of Some Engineering Materials at Moderate rated of Strain" American Society Testing Materials Bulletin, No. 247, 1960,PP. 57-64.

43) Smith, J.E. "Tension Tests of Materials at Strain Rates Up to 200s" Mater. Res. and Standard., Vol. 3, 1963, pp. 713-718.

44) Lindholm, U.S. "Some Experiments with the Split Hopkinson Pressure Bar" J. Mech. Phys. Solids, Vol. 12, 1964, PP. 317-335.

45) Lengyel, B., and Mohitpur, M. "Dynamic Stress/Strain Data to Large Strains" J. Inst. Metals, Vol. 100. 1972, PP. 1-5.

46) Bailey, J.A., and Singer, A. R. E. "Effects of Strain Rate and Temperature on the Resistance and Deformation of Aluminium Alloys, and Lead" J. Inst. Metals, Vol. 92, 1963-1964, PP. 404-408.

47) Baker, T.C., and Pretson, F. W. "Fatigue of Glass under Static Loads" J. Appl. Mech., Vol. 17, 1946, PP. 170-178.

48) Mould, R.E., and Southwick, R. D. "Strength and Static Fatigue of Glass Under Controlled Ambient Conditions: Part I and II" J. Amer. Ceram. Soc., Vol. 42, 1959, PP. 542-547 and 582-592.

49) Proctor, B.A., Whitney, I., and Johnson, J. W. "The Strength of Fused Silica" Proc. Roy. Soc., Series A, Vol. 297, 1967, PP. 534-557.

50) Thompson, N.J., and Cousins, E. W. "Explosion Tests on Glass Windows, Effect on Glass Breakage of Varying the Rate of Pressure Application" J. Amer. Ceram. Soc., Vol. 32, 1949, PP. 313-315.

51) Ogorkiewicz, R.M. Engineering Properties of Thermoplastics Wiley-Interscience, London, 1970.

52) Kolsky, H. "An Investigation of Mechanical Properties of Materials at Very High Rates of Loading" Proc. Phys. Soc., Section B, Vol. 62, 1949, PP. 676-700.

53) Dietz, A.G.H., and McGarry, E. J. "Effect of Speed in Plastics Testing Materials" Symposium on Speed of Testing, Amer. Soc. Testing Materials, STP 185, 1956.

Reproduced with permission of the copyright owner. Further reproduction prohibited without permission.

54) Dietz, A.G.H., Galius, W.J., and Yurenka, S. "Effect of Speed of Test upon Strength Properties of Plastics" Proc Amer. Soc. Testing Materials, Vol. 48, 1948, PP. 1160-1186.

55) Markwardt, L.J., and Liska, J. A. "Speed of Testing of Wood: Factors in its Control and its Effect on Strength" Proc. Amer. Soc., Testing Materials. Vol. 48, 1948, PP. 1139-1159.

56) Markwardt, L.J., and Liska, J.A. "The Influence of Rate of Loading on the Strength of Wood and Wood-base Materials" Symposium of Speed of Testing, Amer. Soc. Testing Materials, STP 185, 1956.

57) Sugiyama, H. "On the Effect of Loading Time on the Strength Properties of Wood" Wood Soc. Tech., Vol. 1, 1967, PP. 289-303.

58) Liska, J.A. "Effect of Rapid Loading on the Compressive and Flexural Strength of Wood" Report No. 1767, US Forest Products Laboratory, 1950.

59) Harding, J.R., Laird, R. T., and Beech, D. G. "Effect of Rate of Loading and Type of Packing on measured Strength of Bricks" Proc. British Ceram. Soc., Vol. 21, 1973, PP. 7-23.

60) ACI Committee 318 "Building Code Requirements for Reinforced Concrete" (ACI 318-89), American Concrete Institute, Detroit, Mich, 1989.

61) Canadian Standards Assoc. "Design of Concrete Structures for Building" CAN3-A23.3-M84, Rexdale, Ontario, Canada, 1984.

62) Fu, H.C., Erki, M.A., and Seckin, M. "Review of Effects of Loading Rate on Reinforced Concrete" Journal of Structural Engineering, Vol. 117, No. 12, 12, December, 1991, pp. 3660-3679.

63) Campbell, J.D., and Cooper, R.H. "Yield and Flow of Low-Carbon Steel at Medium Strain Rates" Conference on the Physical Basis of Yield and Fracture, Inst. Phys. and Phys. Soc., London, 1966, pp. 77-87.

64) Lueth, R.C. "An Analysis of Charpy Impact Testing as Applied to Cemented Carbide" Instrumented Impact Testing, ASTM STP 563, American Society for Testing and Materials, 1974, pp. 166-179.

Reproduced with permission of the copyright owner. Further reproduction prohibited without permission.

65) Tardif, H.P., and Marquis, H., Canadian Metals Quarterly, Vol. 2, 1963, pp. 373.

66) ACI Committee 544 "Measurement of Properties of Fiber Reinforced Concrete" ACI Journal, Vol. 75, No. 7, July 1978, pp. 283-289.

67) Suaris, W., and Shah, S.P. "Properties of Concrete Subjected to Impact" Journal of Structural Division, ASCE, Vol. 109, No. 7, July 1983, PP. 1727-1741.

68) Hughes, B.P., and Gregory, R. "The Impact Strength of Concrete Using Green's Ballistic Pendulum" Proc. Inst. Civil. Eng., Vol. 41, 1968, PP. 731-750.

69) Mihashi, H., and Wittmann, F.H. "Stochastic Approach to Study the Influence of Rate of Loading on Strength of Concrete" Heron Vol. 25, No. 3, 1980, Delft University of Technology.

70) Cowell, W. "Dynamic Properties of Plain Portland Cement Concrete" Technical Report, No. R 447, U.S. Naval Engineering Laboratory, Port Hueneme, California, June 1966.

71) Tedesco, J.W., Ross, C.A., and Brunair, R.M. "Numerical Analysis of Dynamic Split Cylinder Test" Computers and Structures, Vol. 32, No. 3/4, 1989, pp. 609-624.

72) Neville, A.M. Properties of Concrete John Wiley & Sons, New York, 1973, pp. 480-483.

73) Ross, C.A., and Kuennen, S.T. "Fracture of concrete at high strain rates" International Conference on Recent Developments in the Fracture of Concrete and Rock, School of Eng., Univ. of Wales, UK. 20-22 Sept. 1989, pp. 152-161.

74) Brooks, J.J., and Samaraie, N.H. "Influence of Rate of Stressing on Tensile Stress-Straining Behavior of Concrete" International Conference of Recent Development in the Fracture of Concrete and Rock, Univ. of Wales College of Cardiff, UK, 20-22 Sept. 1989, pp. 397-408.

75) Takeda, J., and Tachikawa, H. "Deformation and Fracture of Concrete Subjected to Dynamic Load" Proceedings of the International Conference on Mechanical Behavior of Materials, Vol. IV, Concrete and Cement Paste, Glass and Ceramics, Kyoto, August 15-20, 1971, PP. 267-277.

Reproduced with permission of the copyright owner. Further reproduction prohibited without permission.

76) Melinger, F.M., and Birkimer, D.L. "Measurements of Stress and Strain on Cylindrical Test Specimens of Rock and Concrete Under Impact Loading" Technical Report No. 4-46, Department of the Army, Ohio River Division, Laboratories, April 1966.

77) Grady, E.E. and Lipkin, J. "Criteria for Impulsive Rock Fracture" Geophysical Research Letters, Vol. 7, No. 4, April 1980, pp. 255-258.

78) Grady, D.E. "The Mechanics of Fracture Under High-Rate Stress Loading" Sandia National Laboratories Report, SAND-82-1148C, 1983.

79) Grady, D.E., and Lipkin, J. "Mechanisms of Dynamic Fragmentation: Factors Governing Fragment Size" Sandia National Laboratories Report, SAND-84-230c, 1984.

80) Wakabayashi, M., et al. "Dynamic Loading Effects on the Structural Performance of Concrete and Steel Materials and Beams" Proc. 7th. World Conference on Earthquake Engineering, Istanbul, Turkey, 6(3), 1980, PP. 271-278.

81) Komlos, K. "Factors Affecting the Stress-Strain Relation of Concrete in Uniaxial Tension" ACI J., 66(2), 1969, pp. 111-114.

82) Suaris, W., and Shah, S.P. "Mechanical Properties of Materials Subjected to Impact" An Introductory Report, Proceedings of the RILEM-CEB-IABSE Symposium on 'Concrete Structures Under Impact and Impulsive Loading' Bundesanstadt fur Materialprufung (BAM), Berlin, June 1982, pp. 33-62.

83) Weerheijm, J., and Reinhardt, H.W. "Modelling of Concrete Fracture Under Dynamic Tensile Loading" Int. Conf. on Recent Development in the Fracture of Concrete and Rock, Univ. of Wales Uk, 20-22 September 1989, pp. 721-728.

84) Bennett, E.W., and Raju, N.K. "Cumulative Fatigue Damage of Plain Concrete in Compression" Proc. Conference: Civil Engineering Materials, Southampton, 1969, pp. 1089-1102.

85) Tepfers, R. "Tensile Fatigue Strength of Plain Concrete" Journal of ACI, August 1979, pp. 919-933.

Reproduced with permission of the copyright owner. Further reproduction prohibited without permission.

86) Cornelissen, H.A.W., and Timmers, G. "Fatigue of Plain Concrete in Uniaxial Tension and Alternating Tension-Compression" Stevin Report 5-81-7, Delft 1981.

87) Heilmann, A., Hilsdorf, H., and Finsterwalder, K. "Festigkeit und Verformung von Beton unter Zugspannungen" Deutscher Ausschuss fur Stahlbeton, Heft 203, 1977.

88) Charles, R.J. "Dynamic Fatigue of Glass" J. of Applied Physics, Vol. 29, No. 12, Dec. 1958, PP. 1657-1662.

89) Charles, R.J. "Static Fatigue of Glass" J. of Applied Physics, Vol. 29, No. 11, 1958.

90) Nadeau, J.S., Mindess, S., and Hay, J.M. "Slow Crack Growth in Cement Paste" J. of the American Society, Vol. 57, No. 2, Feb. 1974, pp. 51-54.

91) Evans, A.G. "Slow Crack Growth in Brittle Materials Under Dynamic Loading" International Journal of Fracture, Vol. 10, No. 2, June 1974, PP. 251-259.

92) Mihashi, H., Izumi, M. "A Stochastic Theory for Concrete Fracture" Cement and Concrete Research, Vol. 7, 1977, pp. 411-422.

93) Komlos, K. "Investigation of Rheological Properties of Concrete in Uniaxial Tension" Material prufung, No. 9, pp. 300-304.

94) Kvirikadze, O.P., et al. "Determination of the Ultimate Strength and Modulus of Deformation of Concrete at Different Rates of Loading" Int. Symposium: Testing Insitu of Concrete Structures, Budapest, 1977, pp. 109-117.

95) Zielinski, A.J. Fracture of Concrete and Mortar under Uniaxial Tensile Loading Delft University Press, 1982.

96) Banthia, N.P., Mindess, S., and Bentur, A. "Energy Balance in Instrumented Impact Tests on Plain Concrete Beams" SEM/RILEM International Conference on Fracture of Concrete and Rock, Houston, Texas, 1987, PP. 26-36.

Reproduced with permission of the copyright owner. Further reproduction prohibited without permission.

97) Mindess, S. "Rate of Loading Effects on the Fracture of Cementitious materials" Application of Fracture Mechanics to Cementitious Composites, NATO-ARW - Sept. 4-7, Northwestern University, 1984, pp. 617-636.

98) Birkimer, D.L., and Lindeman, R. "Dynamic Tensile Strength of Concrete Materials" ACI Journal, Jan. 1971, PP. 47-49.

99) Birkimer, D.L. "A Possible Fracture Criterion for the Dynamic Tensile Strength of Rock" Proceedings of the 12th. Symposium on Rock Mechanics, 1971, PP. 573-589.

100) Rinehardt, J. "Dynamic Fracture Strengths of Rock" Proceedings of the 7th. Symposium on Rock Mechanics, 1965, PP. 205-207.

101) Rinehardt, J. "Some Quantitative Data Bearing on the Scabbing of Metals Under Explosive Attack" J. Appl. Phys., V. 22, 1951, PP. 555.

102) Rusch, H. "Researches Toward a General Flexural Theory for Structural Concrete" Journal of the American Concrete Institute, 57, 1960, pp. 1-28.

103) Wright, P.J.F. "The Effect of Method of Test on the Flexure Strength of Concrete" Magazine of Concrete Research, Vol. 4, No. 7, Oct. 1952, pp. 67-76.

104) Petersson, P.E. "Fracture Energy of Concrete: Practical Performance and Experimental Results" Cement and Concrete Res., 10, 1980, pp. 91-101.

105) Reinhardt, H.W. "Tensile Fracture of Concrete at High Rate of Loading" Application of Fracture Mechanics to Cementitious Composites, NATO-ARW, Sept. 4-7, 1984, pp. 559-590, Northwestern University.

106) Sexton, H.J., Ireland, D. R., and Server, W. L., A Symposium Presented at the Seventy-Sixth Annual Meeting ASTM, Philadelphia, Pa., 24-29 June 1973, pp. 50-73.

107) Venzi, S., Priest, A. H., and May, M. J "Influence of Inertial Load in Instrumented Impact Tests" ,'Impact Testing of Metals' ASTM STP 466, American Society for Testing and Materials, 1970, PP. 165-180.

Reproduced with permission of the copyright owner. Further reproduction prohibited without permission.

108) Turner, C.E. "Impact Testing of Metals" ASTM STP 466, American Society for Testing and Materials, 1970, pp. 93.

109) Turner, C.E., Kennish, P., Culver, L. E., and Radon, J. C. "A Study of the Mechanics of Notched-Bar Impact Tests" Imperial College Department of Mechanical Engineering, Final Report of Navy Department, Advisory Committee on Structural Steels, June 1970.

110) Buys, E.C.J., and Cowan, A. "Interpretation of the Instrumented Impact Test" Document X-458-68, International Institute of Welding, July 1968.

111) Instrumented Impact Testing, ASTM 563, American Society for Testing and Materials, 1974, PP. 92-117.

112) ANSYS "Engineering Analysis System" Swanson Analysis, Inc. P.O.Box 65, Houston, PA. 14342.

113) Reji, J, and Shah, S.P. "Fracture of Concrete Subjected to Impact Loading" Cement, Concrete, and Aggregates by ASTM, Volume 8, No. 1, Summer 1986 pp. 24-32.

114) Cotterell, B. "Fracture Toughness and the Charpy V-Notch Test" British Welding Journal, Vol. 9, No. 2, Feb. 1962, PP. 83-90.

115) Server, W.L., Wullaert, R. A., and Sheckhard, J. W. "Evaluation of Current Procedures for Dynamic Fracture Toughness Testing" Flaw Growth and Fracture, ASTM STP 631, 1977, PP. 446-461.

116) Electeric Power Research Institute "Instrumented Precracked Charpy Testing" Proceedings of the C.S.N.I. Specialist Meeting, Edited by R.A. Wullaert, California, November 1981.

117) Suaris, W., and Shah, S.P. "Inertial Effects in the Instrumented Impact Testing of Cementitious Composites" ASTM Journal of Cement, Concrete and Aggregates, Vol. 3, No. 2, Winter 1981, PP. 77-83.

118) Kalthoff, J.F., Winkler, S., Klemm, W., and Bienert, J. "On the Validity of K1d-measurements in Instrumented Impact Tests" Proceedings, 5th International Conference on Structural Mechanics in Reactor Technology, Berlin, 1979, PP. G4/6, 1-11.

Reproduced with permission of the copyright owner. Further reproduction prohibited without permission.

119) Hibber, A.P. "Impact Resistance of Fibre Concrete" Ph.D. Thesis, University of Surrey, 1977.

120) Winkler, S., Kalthoff, J. F., and Gerscha, A. "The Response of Pressure Vessel Steel Specimens on Drop Weight Loading" Proceedings 5th International Conference on Structural Mechanics in Reactor Technology, Berlin, 1979, PP. G4/6, 1-9.

121) Gonczy, S.T. "The Effects of Various Densifying Agents Upon the High Temperature Impact Strength of Hot Pressed Silicon Nitrite" Ph.D. Thesis, Northwestern University, August 1978.

122) Ireland, D.R. "Procedures and Problems Associated with Reliable Control of the Instrumented Impact Test" A Symposium Presented at the Seventy-Sixth Annual Meeting ASTM, Philadelphia, Pa., 24-29 June 1973, pp. 3-29.

123) Hibbert, A.P., and Hannant, D.J. "The Design of an Instrumented Impact Test Machine for Fiber Concrete" RILEM, Symposium, Testing and Test Methods of Fiber Cement Composites, Apr. 1978, The Construction Press Ltd. (U.K.), pp. 107-120.

124) Mainstone, R. J. "Properties of materials at high rates of straining or loading" Materiaux Et Constructions. Vol. 8 (44), 1975, pp. 102-116.

125) McNeely, D.J., and Lush, S.O. "Tensile Strength of Concrete" ACI Journal, Vol. 60, June 1963, pp. 751-761.

126) Soroushian, P., Choi, K., and Fu, G. "Tensile Strength of Concrete at Different Strain Rate" Material Research Society Symposia Proceedings, Edited by Mendess and S.T. Shah, Boston, Mass., USA, Vol. 64, 1986, pp. 87-92.

127) Oh, B.H. "Behaviour of Concrete under Dynamic Tensile Loads" ACI Materials Journal, Jan./Feb., 1987, pp. 8-13.

128) Zech, B., and Wittman, F.H. "Variability and Mean Value of Strength of Concrete as a Function of Load" ACI Journal, Sept./Oct. 1980, pp. 358-362.

129) Perzyna, P. Advanced in Applied Mechanics Academic Press Inc., Vol. 9, 1966.

Reproduced with permission of the copyright owner. Further reproduction prohibited without permission.

130) Prager, W. "Linearization in Visco-Plasticity" Oesterreichisches Ing.-Arch. 15, 1961, pp. 152-157.

131) Prager, W. Introduction to Mechanics of Continua Ginn and Company, Boston, 1961.

132) Freudenthal, A.M. "The Mathematical Theories of the Inelastic Continuum" Handbuch der Physik VI, Springer-Verlag, Berlin, 1958.

133) Gopalaratnam, V. S. Shah S.P. "Properties of steel fiber reinforced concrete subjected to impact loading" ACI Journal, Proceeding, V. 83, No. 1, 1984.

Reproduced with permission of the copyright owner. Further reproduction prohibited without permission.

APPENDIX "A"

Reproduced with permission of the copyright owner. Further reproduction prohibited without permission.

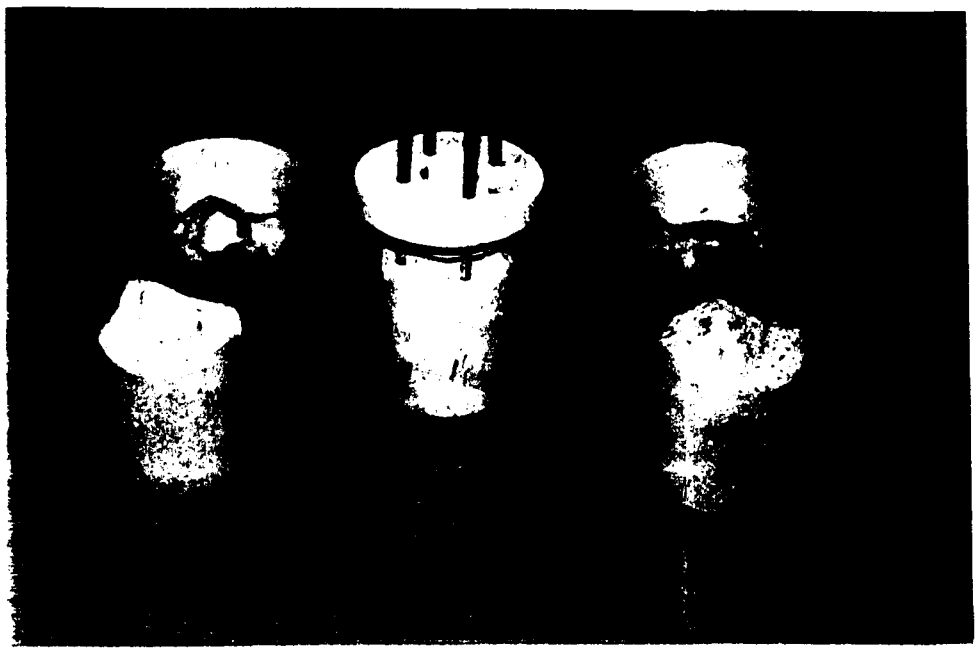

Figure A.1 Typical specimen failure with thin top ring support.

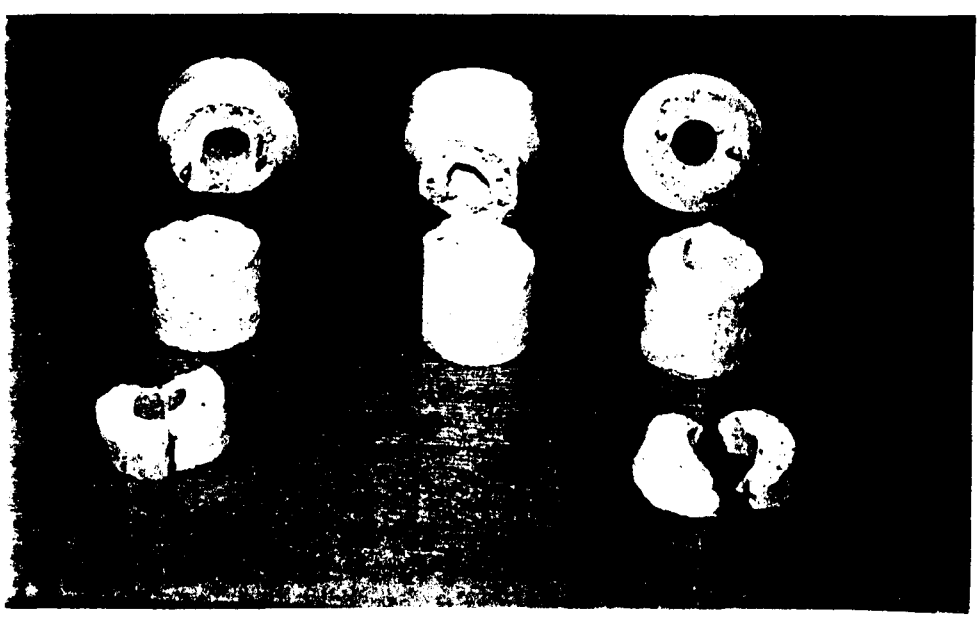

Figure A.2 Typical specimen failure when two rebars are used.

Reproduced with permission of the copyright owner. Further reproduction prohibited without permission.

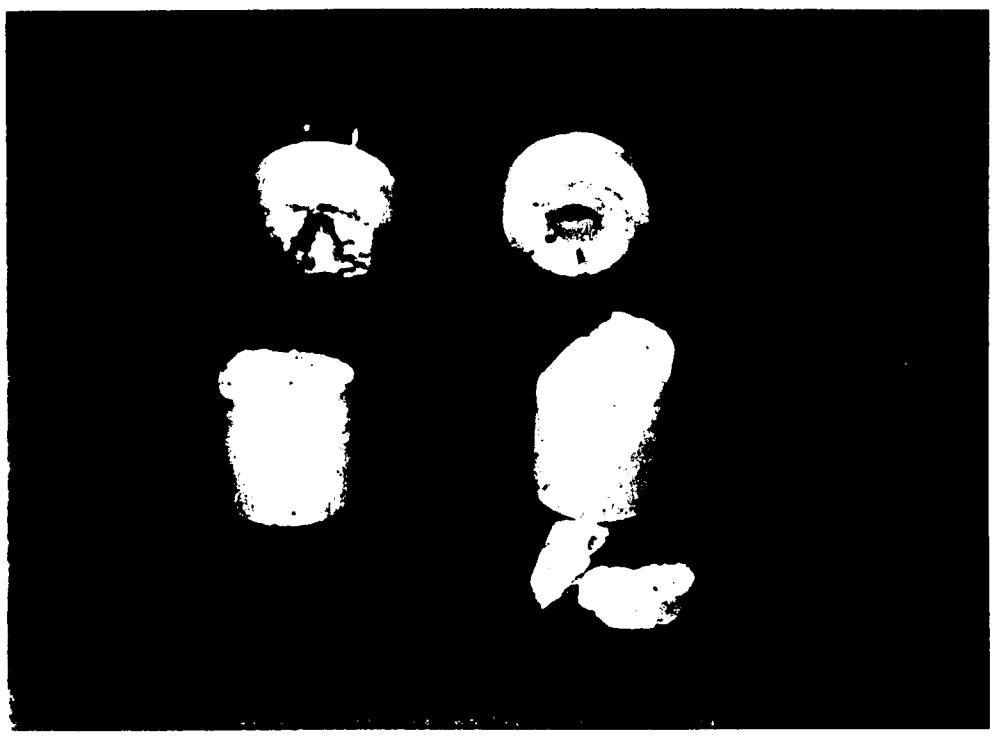

Figure A.3 Typical specimen failure when three rebars are used.

Reproduced with permission of the copyright owner. Further reproduction prohibited without permission.

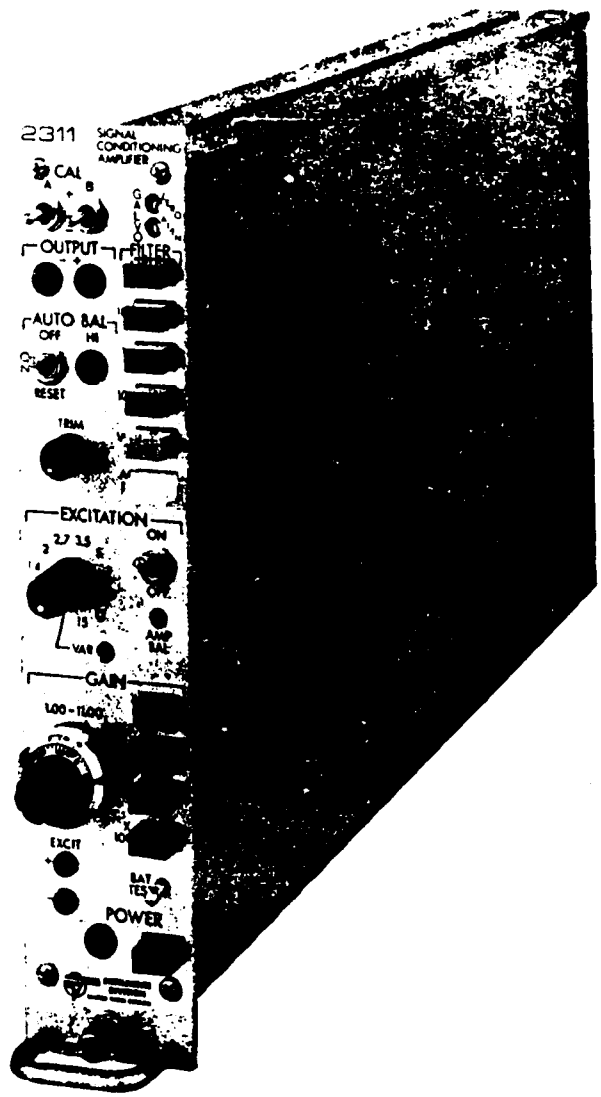

Figure A.4 "2311" Signal conditioning amplifier.

Reproduced with permission of the copyright owner. Further reproduction prohibited without permission.

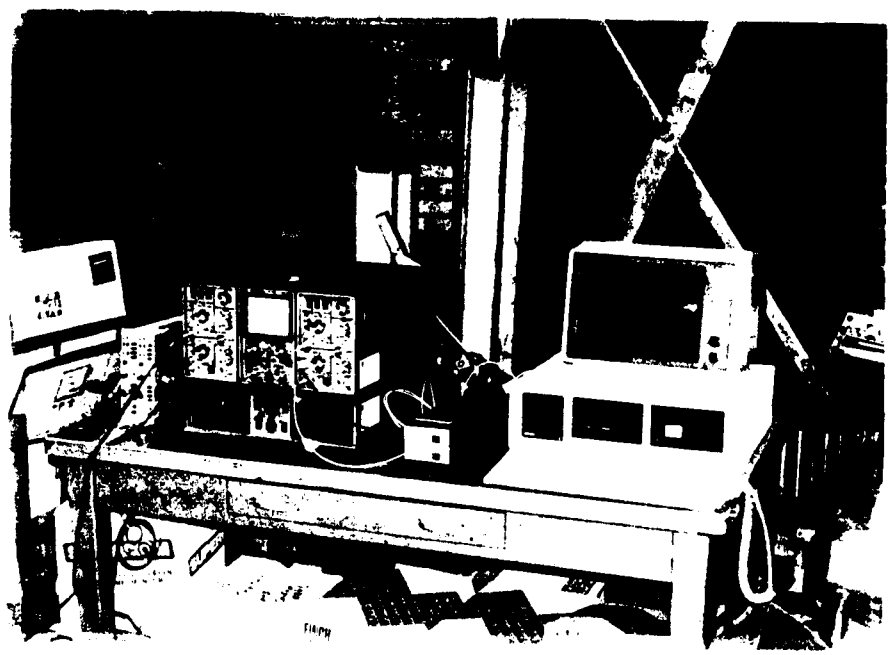

Figure A.5 View of impact test recording devices.

Reproduced with permission of the copyright owner. Further reproduction prohibited without permission.

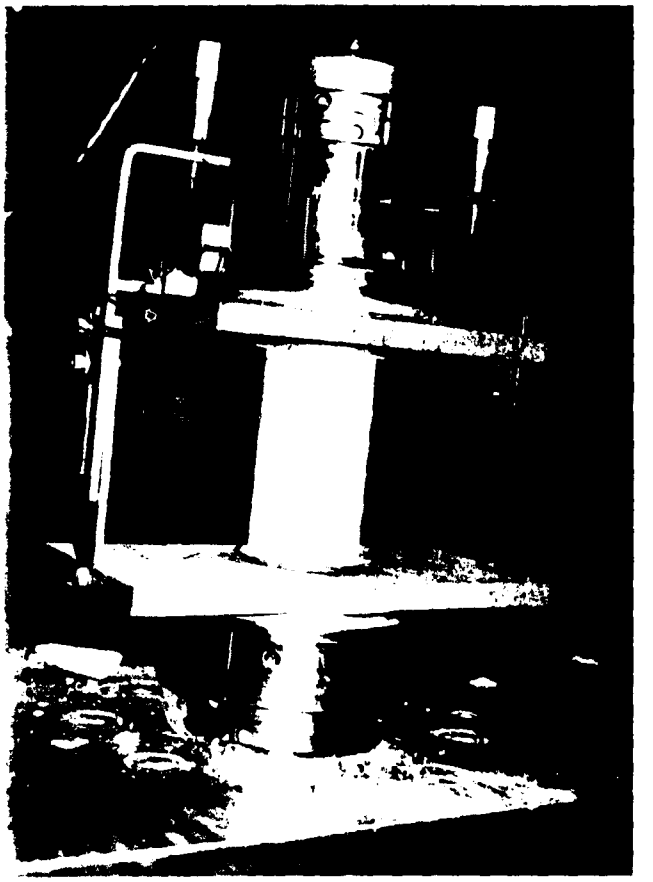

Figure A.6 "Strain controlled" specimen set-up for static compressive test.

Reproduced with permission of the copyright owner. Further reproduction prohibited without permission.

Figure A.7 M.T.S. static testing system.

Reproduced with permission of the copyright owner. Further reproduction prohibited without permission.

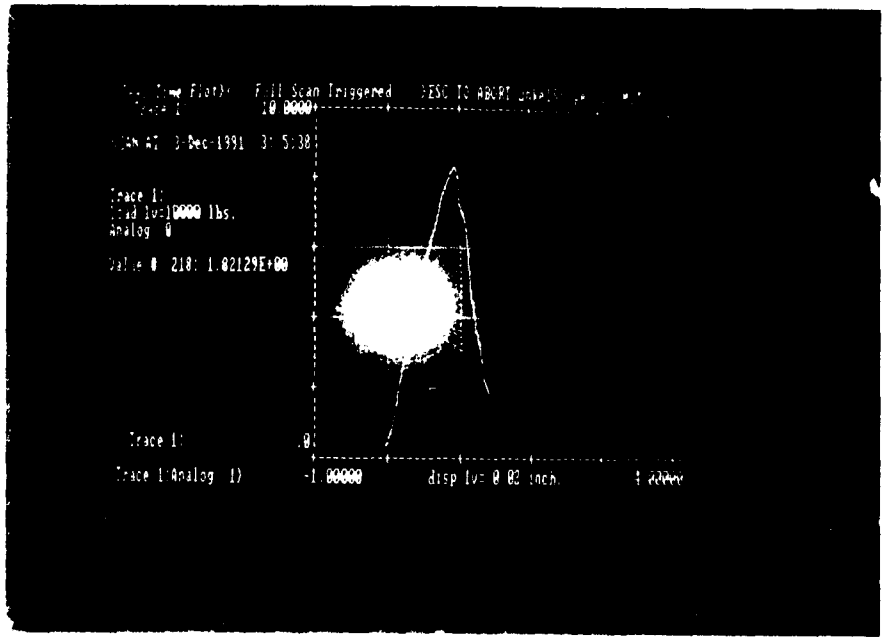

Figure A.8 Load vs. displacement recorded on computer during static test.

Reproduced with permission of the copyright owner. Further reproduction prohibited without permission.

APPENDIX "B"

Reproduced with permission of the copyright owner. Further reproduction prohibited without permission.

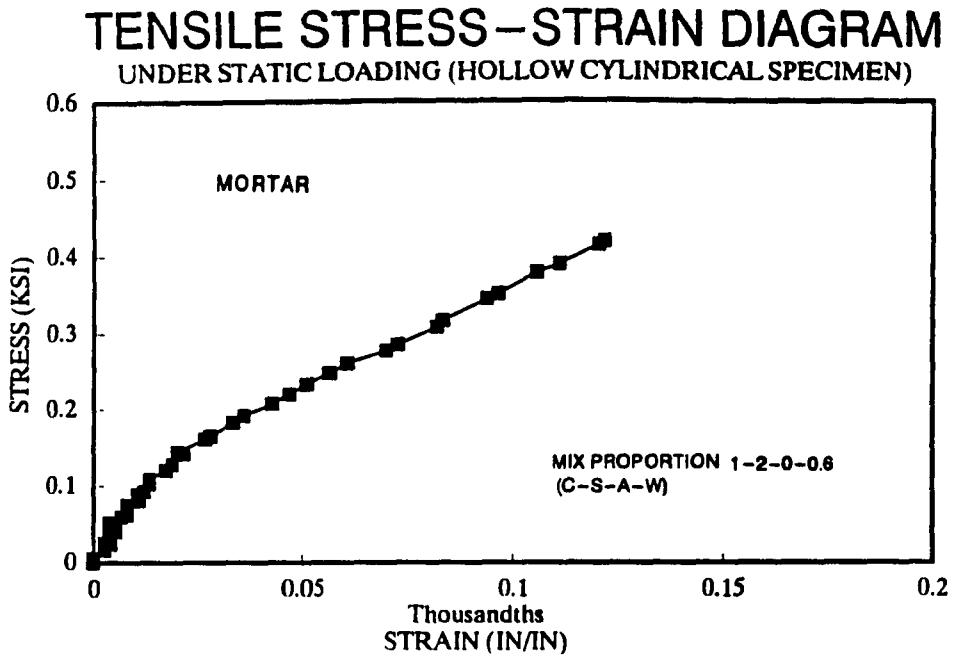

Figure B.1 Stress-strain relation of mortar hollow cylindrical specimen under static tensile load.

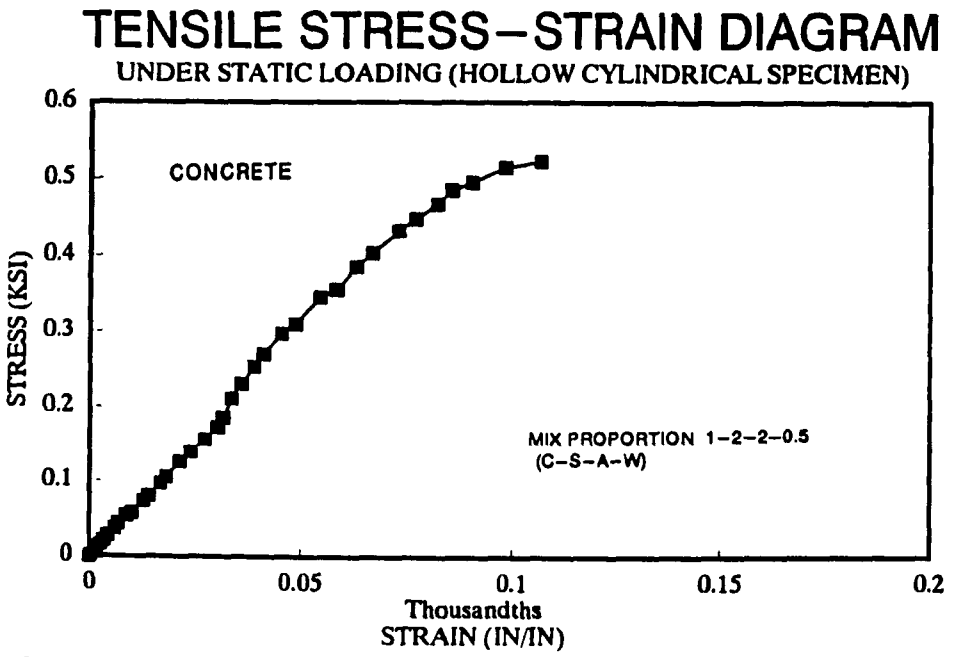

Figure B.2 Stress-strain relation of concrete hollow cylindrical specimen under static tensile load.

Reproduced with permission of the copyright owner. Further reproduction prohibited without permission.

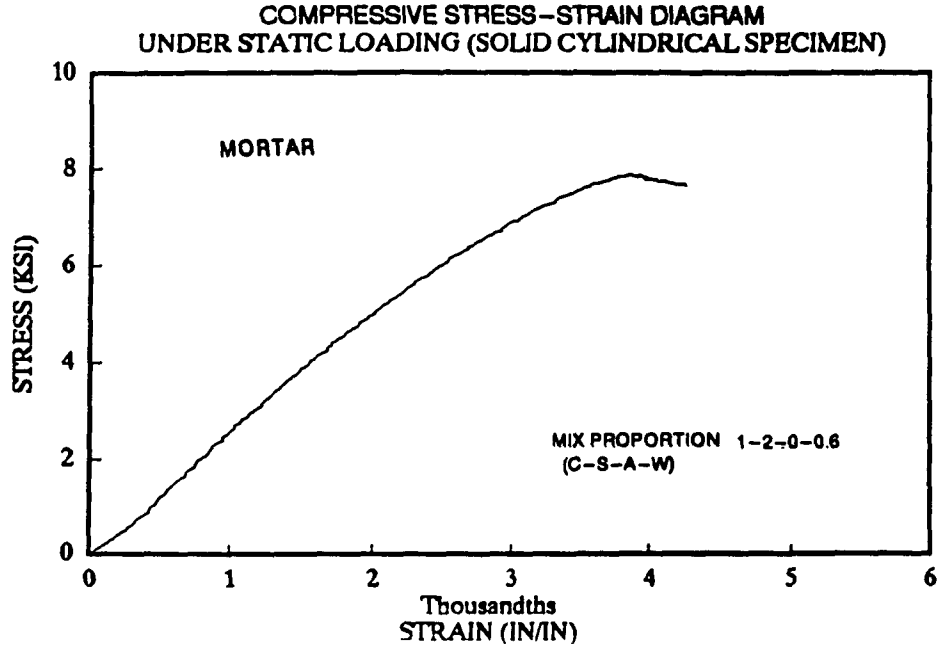

Figure B.3 Stress-strain relation of mortar solid cylindrical specimens under static compression load.

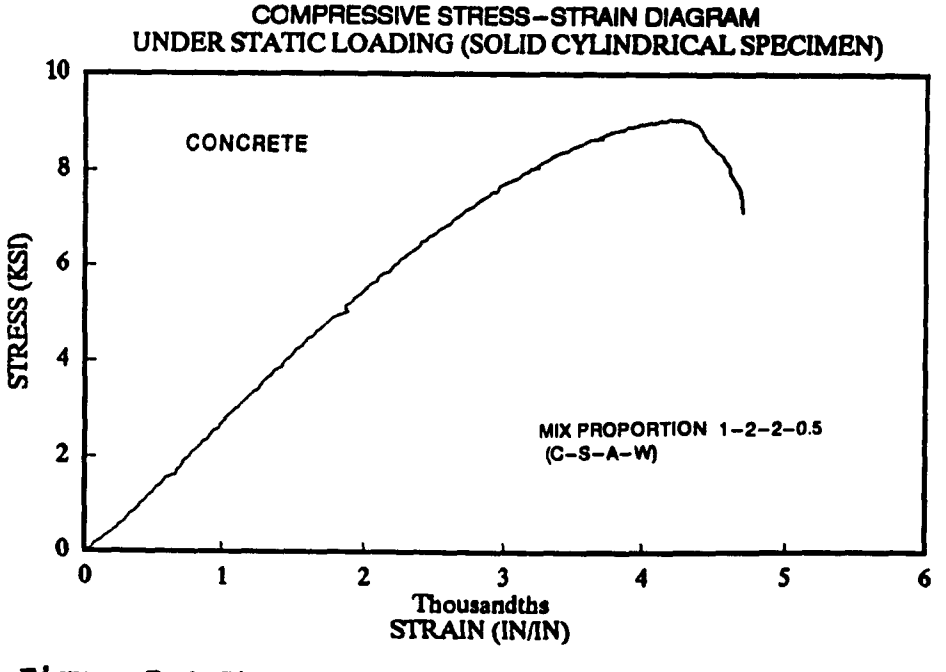

Figure B.4 Stress-strain relation of concrete solid cylindrical specimens under static compression load.

Reproduced with permission of the copyright owner. Further reproduction prohibited without permission.

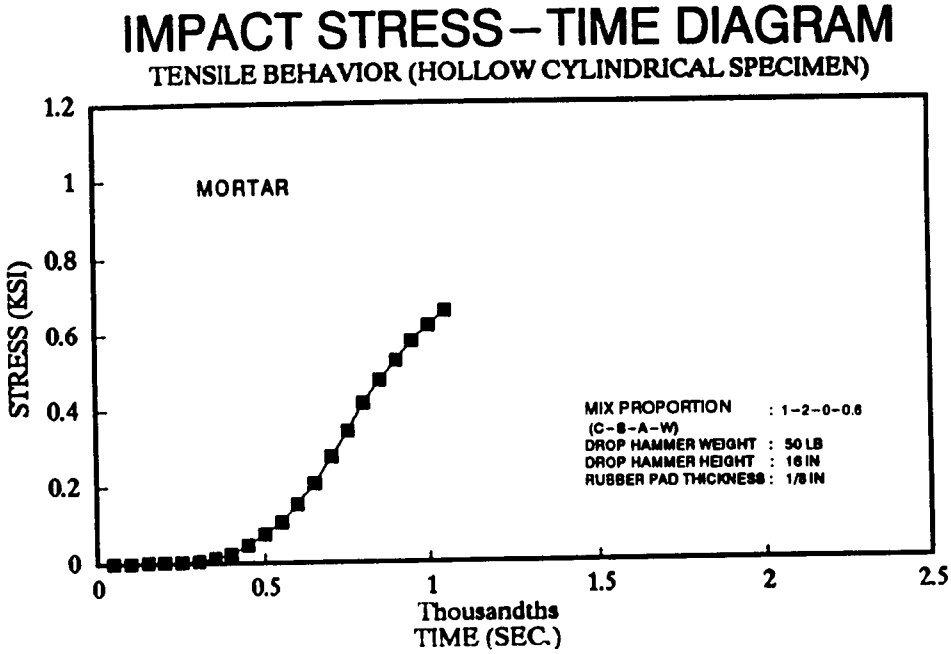

Figure B.5 Stress history of mortar specimen with 50 Lb hammer weight, 16 in hammer height, and 1/8 in rubber-pad thickness under impact tensile load.

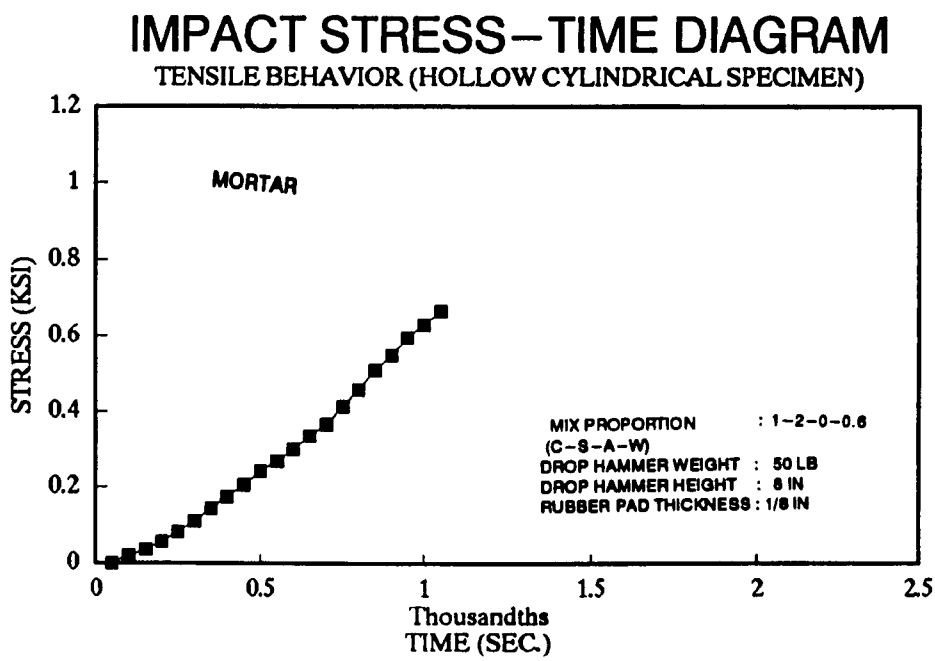

Figure B.6 Stress history of mortar specimen with 50 Lb hammer weight, 8 in hammer height, and 1/8 in rubber-pad thickness under impact tensile load.

Reproduced with permission of the copyright owner. Further reproduction prohibited without permission.

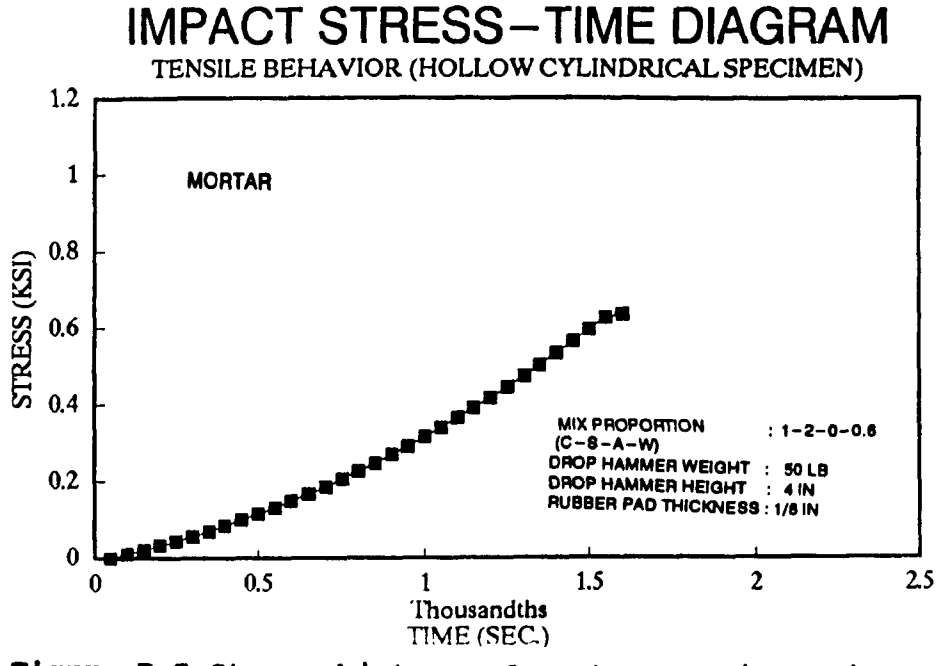

Figure B.7 Stress history of mortar specimen with 50 Lb hammer weight, 4 in hammer height, and 1/8 in rubber-pad thickness under impact tensile load.

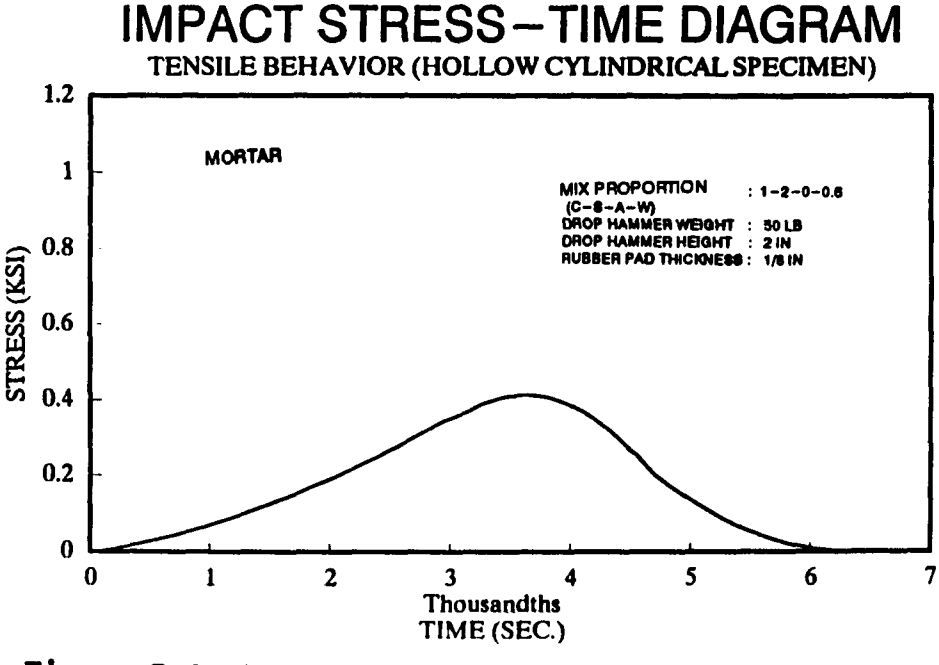

Figure B.8 Stress history of mortar specimen with 50 Lb hammer weight, 2 in hammer height, and 1/8 in rubber-pad thickness under impact tensile load.

Reproduced with permission of the copyright owner. Further reproduction prohibited without permission.

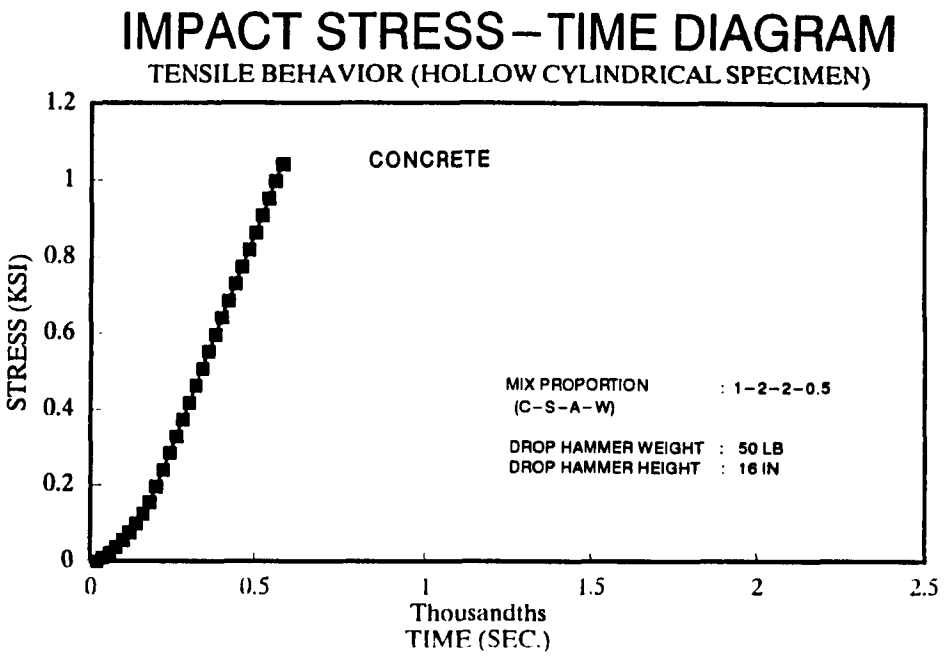

Figure B.9 Stress history of concrete specimen with 50 Lb hammer weight, 16 in hammer height, and no rubber-pad under impact tensile load.

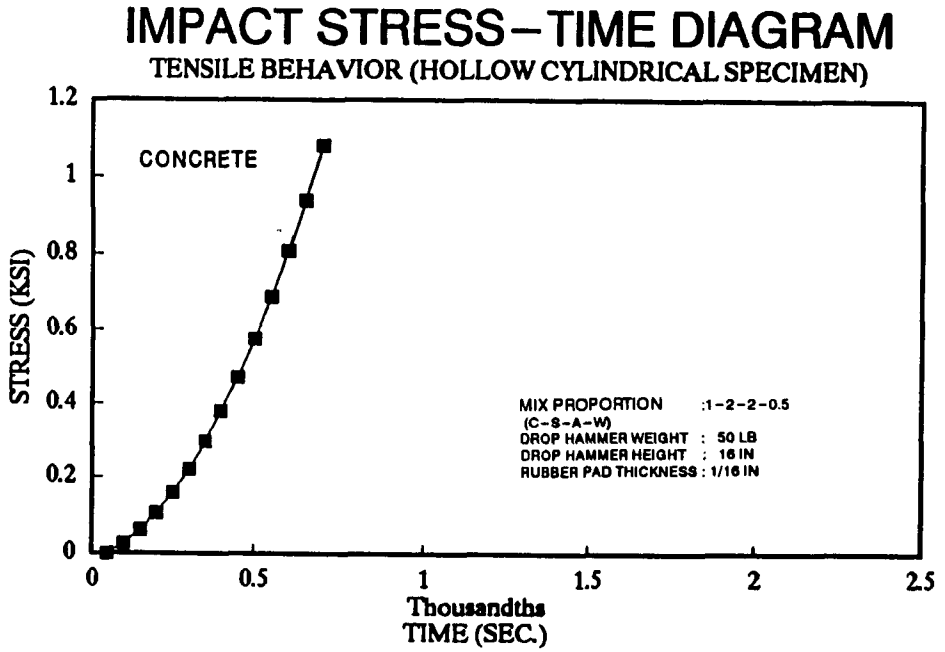

Figure B.10 Stress history of concrete specimen with 50 Lb hammer weight, 16 in hammer height, and 1/16 in rubber-pad thickness under impact tensile load.

Reproduced with permission of the copyright owner. Further reproduction prohibited without permission.

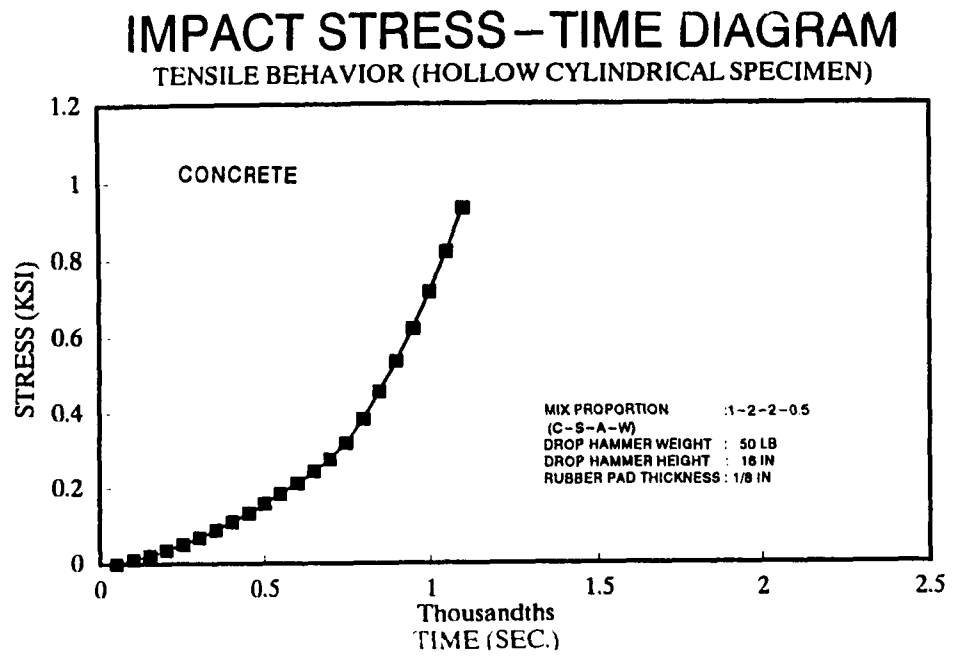

Figure B.11 Stress history of concrete specimen with 50 Lb hammer weight, 16 in hammer height, and 1/8 in rubber-pad thickness under impact tensile load.

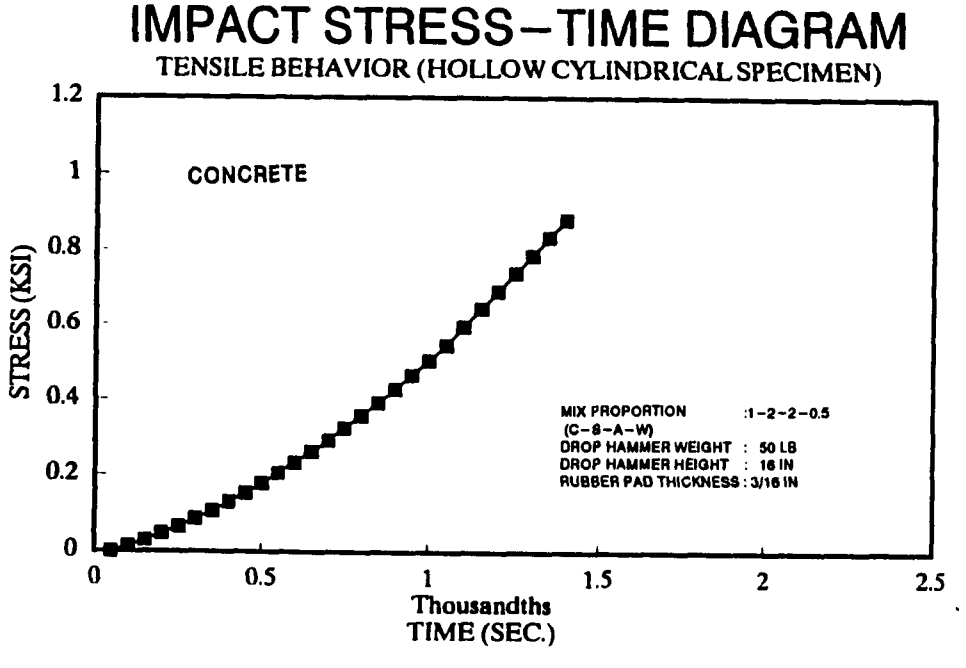

Figure B.12 Stress history of concrete specimen with 50 Lb hammer weight, 16 in hammer height, and 3/16 in rubber-pad thickness under impact tensile load.

Reproduced with permission of the copyright owner. Further reproduction prohibited without permission.

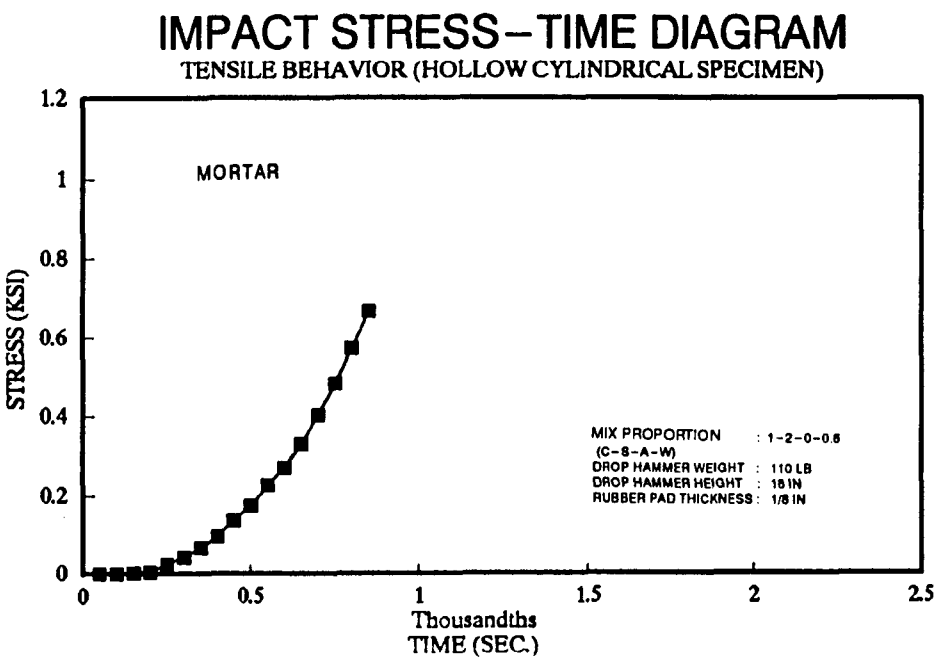

Figure B.13 Stress history of mortar specimen with 110 Lb hammer weight, 16 in hammer height, and 1/8 in rubber-pad thickness under impact tensile load.

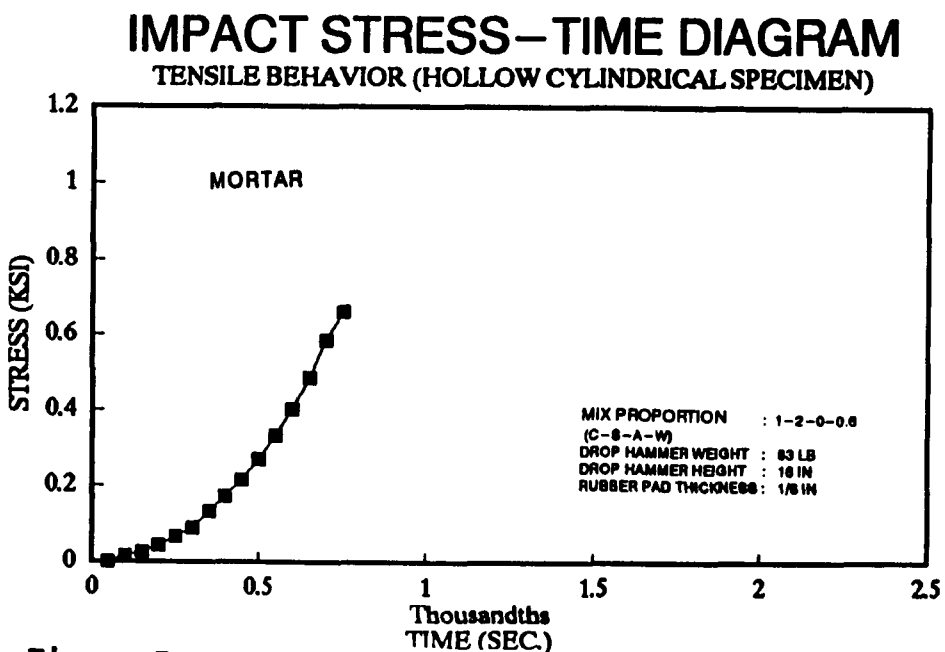

Figure B.14 Stress history of mortar specimen with 83 Lb hammer weight, 16 in hammer height, and 1/8 in rubber-pad thickness under impact tensile load.

Reproduced with permission of the copyright owner. Further reproduction prohibited without permission.

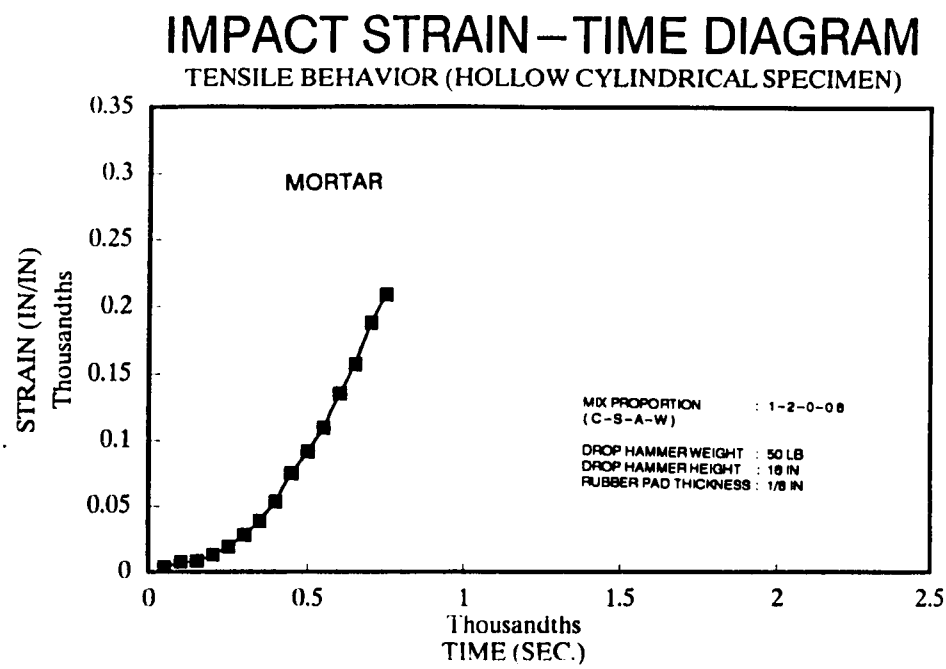

Figure B.15 Strain history of mortar specimen with 50 Lb hammer weight, 16 in hammer height, and 1/8 in rubber-pad thickness under impact tensile load.

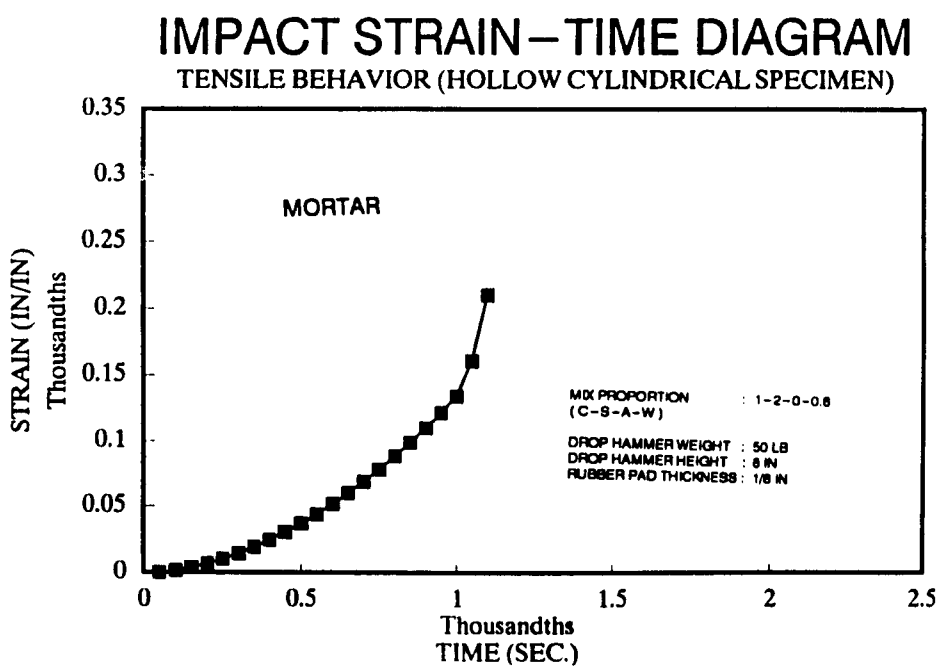

Figure B.16 Strain history of mortar specimen with 50 Lb hammer weight, 8 in hammer height, and 1/8 in rubber-pad thickness under impact tensile load.

Reproduced with permission of the copyright owner. Further reproduction prohibited without permission.

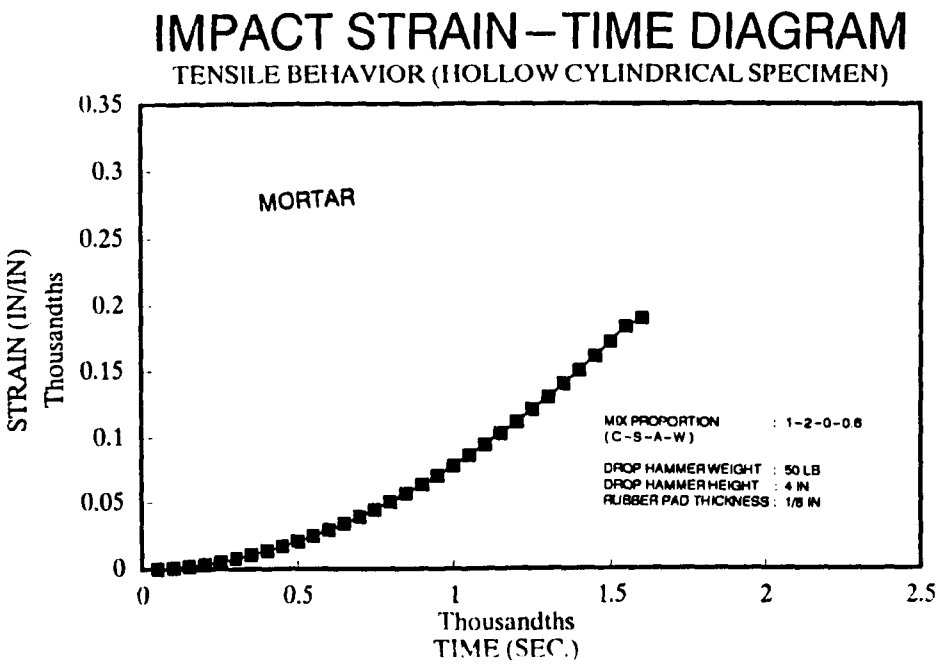

Figure B.17 Strain history of mortar specimen with 50 Lb hammer weight, 4 in hammer height, and 1/8 in rubber-pad thickness under impact tensile load.

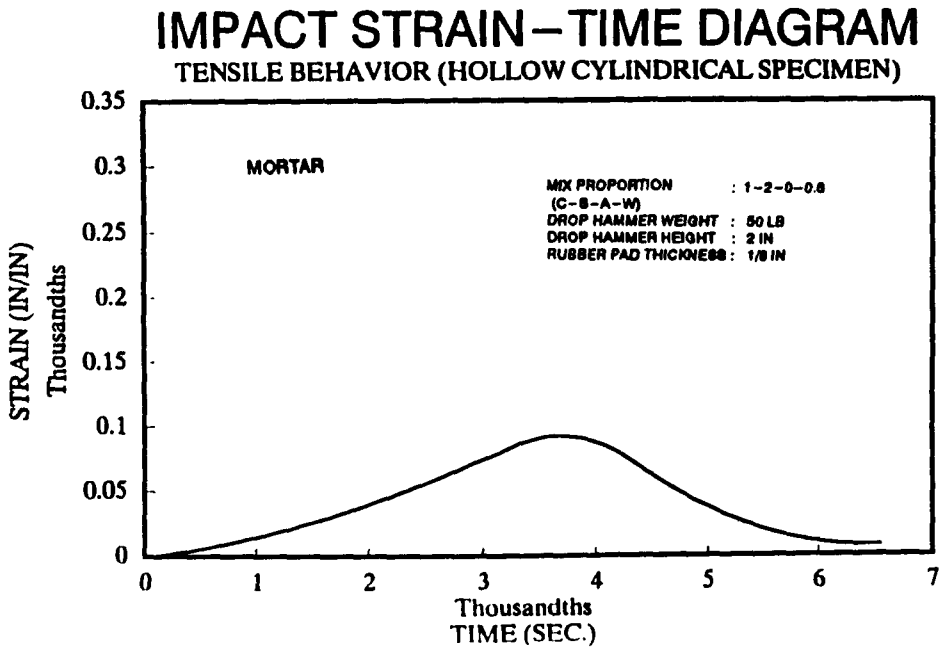

Figure B.18 Strain history of mortar specimen with 50 Lb hammer weight, 2 in hammer height, and 1/8 in rubber-pad thickness under impact tensile load.

Reproduced with permission of the copyright owner. Further reproduction prohibited without permission.

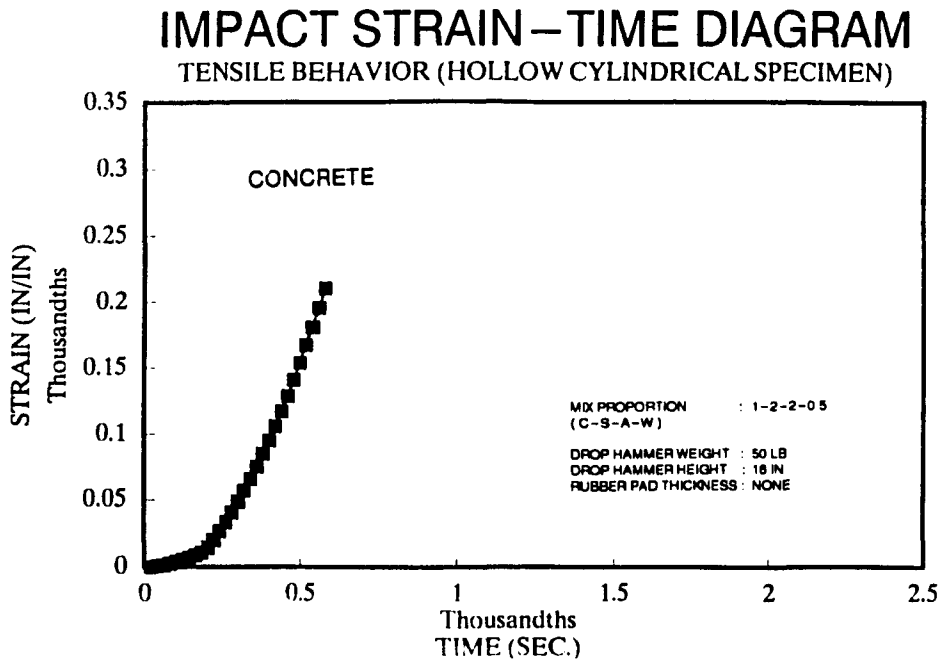

Figure B.19 Strain history of concrete specimen with 50 Lb hammer weight, 16 in hammer height, and no rubber-pad under impact tensile load.

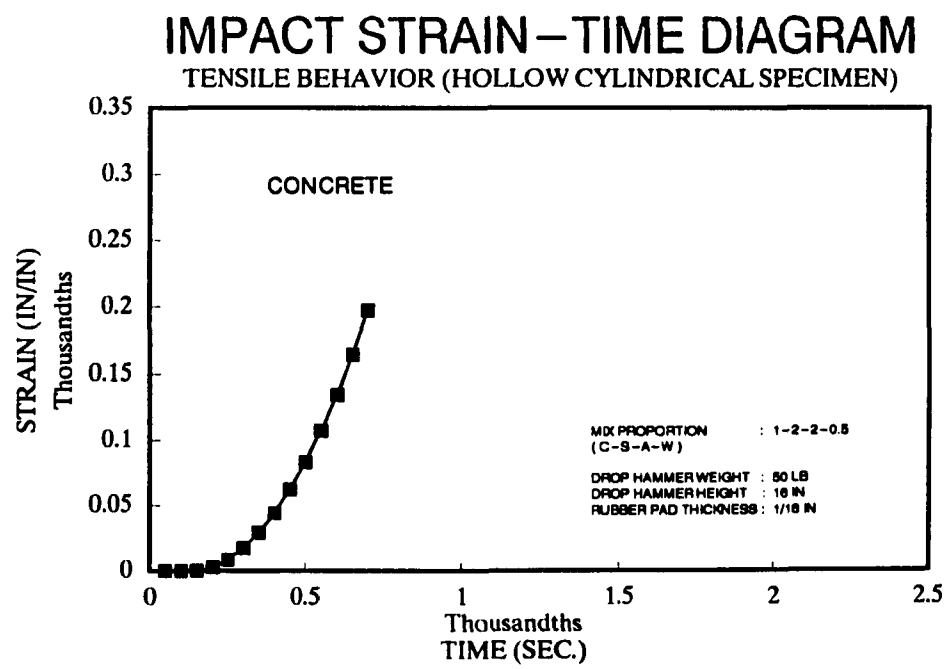

Figure B.20 Strain history of concrete specimen with 50 Lb hammer weight, 16 in hammer height, and 1/16 in rubber-pad thickness under impact tensile load.

Reproduced with permission of the copyright owner. Further reproduction prohibited without permission.

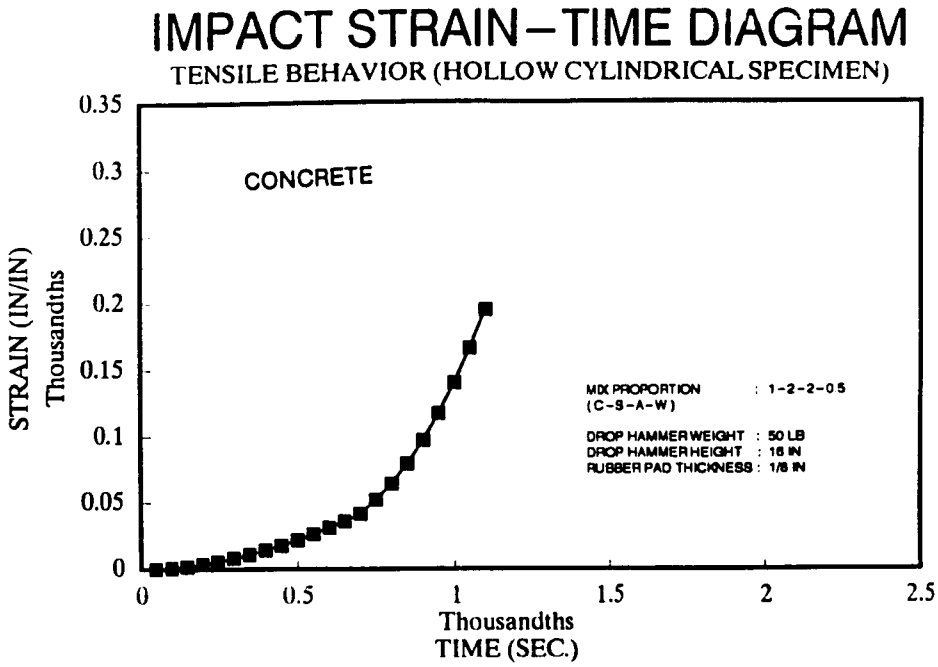

Figure B.21 Strain history of concrete specimen with 50 Lb hammer weight, 16 in hammer height, and 1/8 in rubber-pad thickness under impact tensile load.

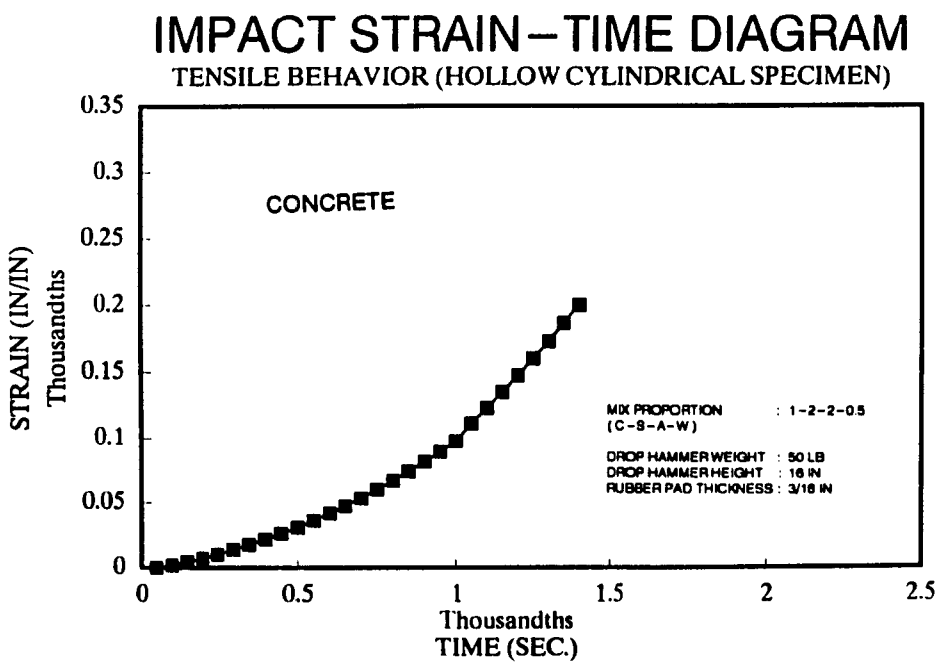

Figure B.22 Strain history of concrete specimen with 50 Lb hammer weight, 16 in hammer height, and 3/16 in rubber-pad thickness under impact tensile load.

Reproduced with permission of the copyright owner. Further reproduction prohibited without permission.

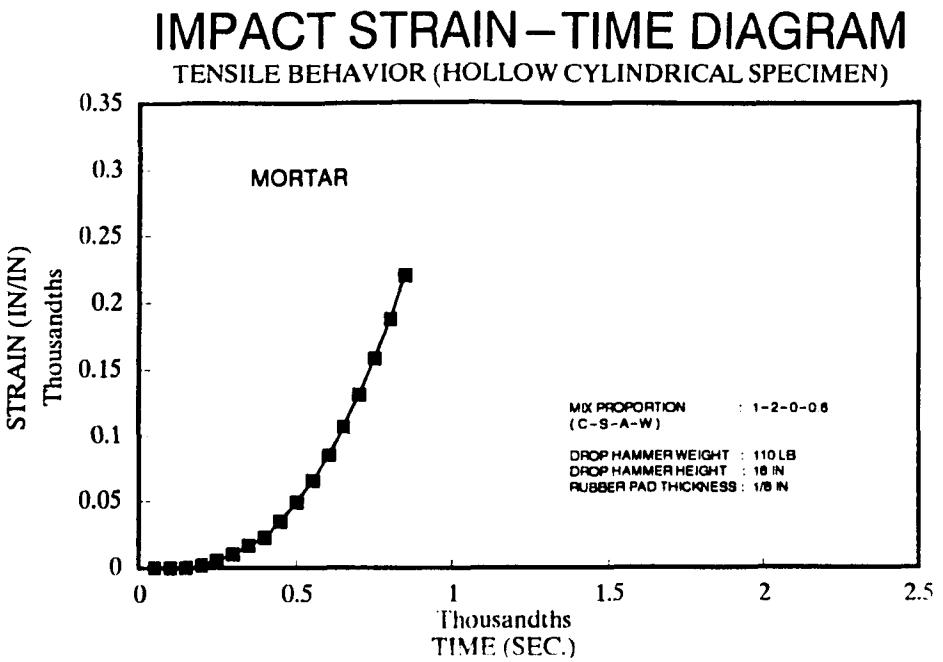

Figure B.23 Strain history of mortar specimen with 110 Lb hammer weight, 16 in hammer height, and 1/8 in rubber-pad thickness under impact tensile load.

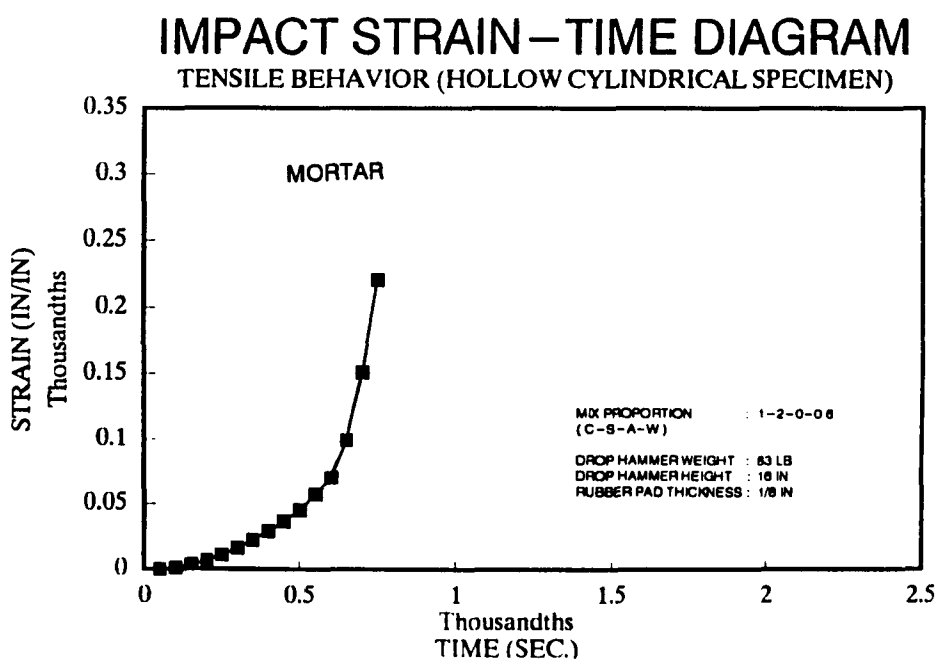

Figure B.24 Strain history of mortar specimen with 83 Lb hammer weight, 16 in hammer height, and 1/8 in rubber-pad thickness under impact tensile load.

Reproduced with permission of the copyright owner. Further reproduction prohibited without permission.

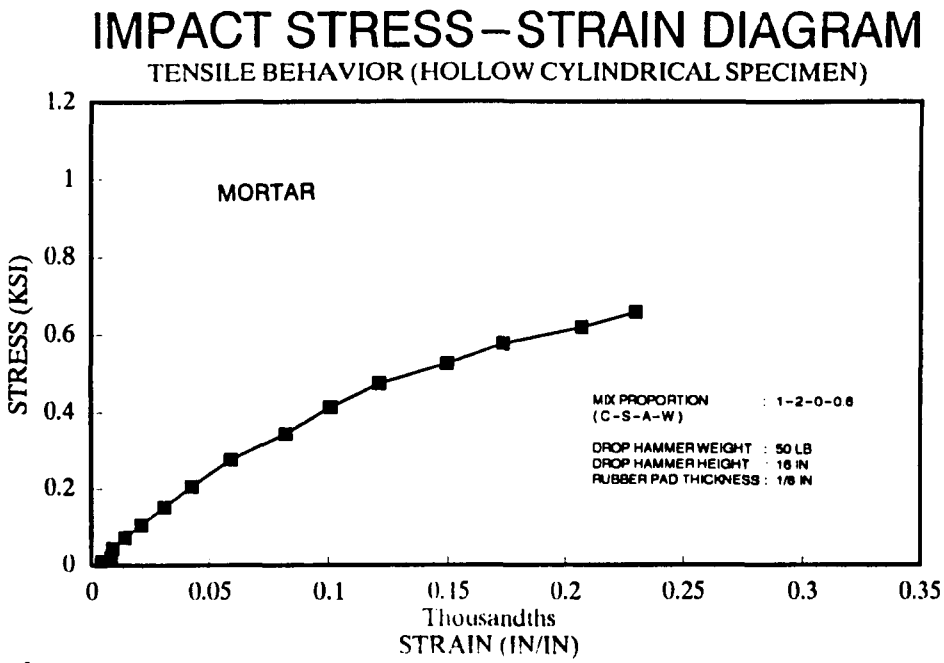

Figure B.25 Stress-strain relation of mortar specimen with 50 Lb hammer weight, 16 in hammer height, and 1/8 in rubber-pad thickness under impact tensile load.

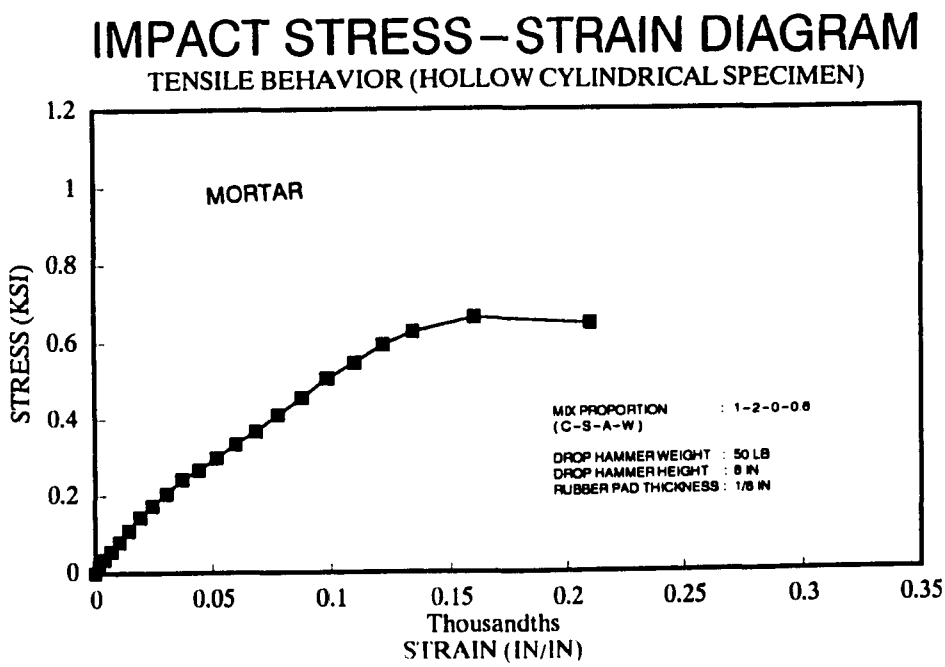

Figure B.26 Stress-strain relation of mortar specimen with 50 Lb hammer weight, 8 in hammer height, and 1/8 in rubber-pad thickness under impact tensile load.

Reproduced with permission of the copyright owner. Further reproduction prohibited without permission.

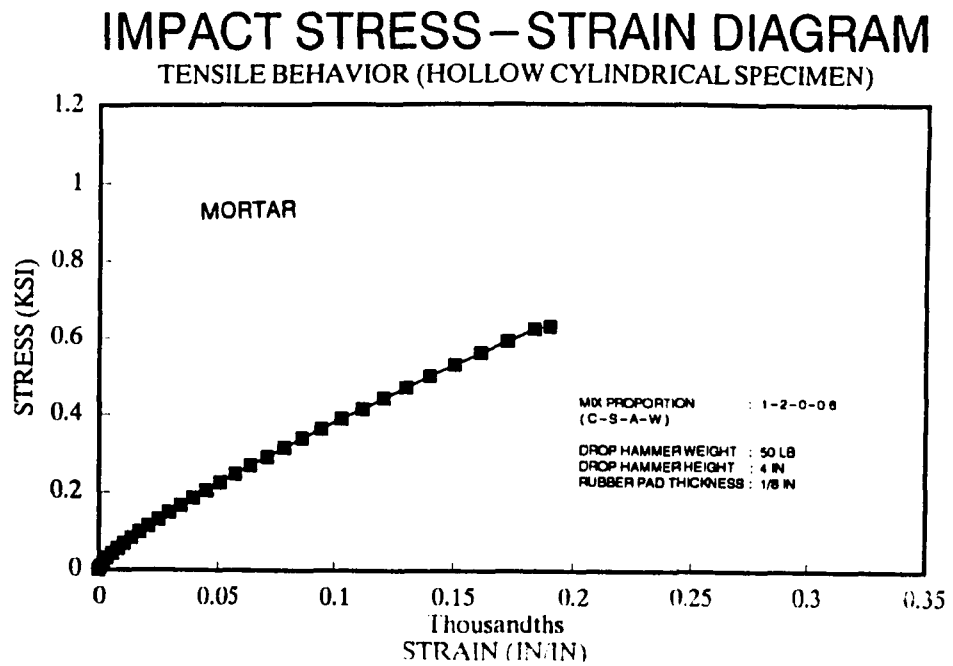

Figure B.27 Stress-strain relation of mortar specimen with 50 Lb hammer weight, 4 in hammer height, and 1/8 in rubber-pad thickness under impact tensile load.

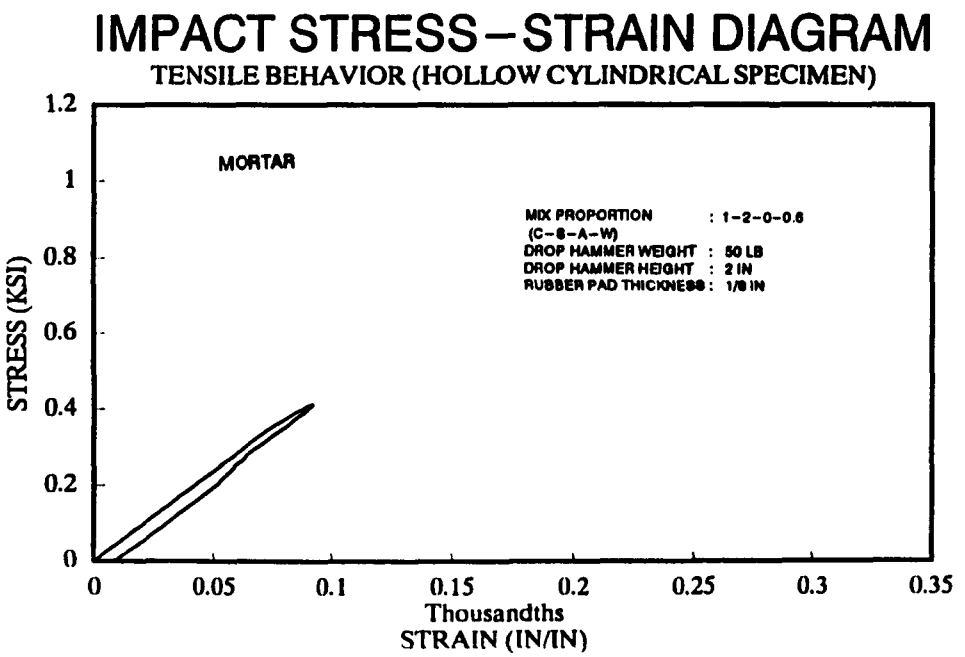

Figure B.28 Stress-strain relation of mortar specimen with 50 Lb hammer weight, 2 in hammer height, and 1/8 in rubber-pad thickness under impact tensile load.

Reproduced with permission of the copyright owner. Further reproduction prohibited without permission.

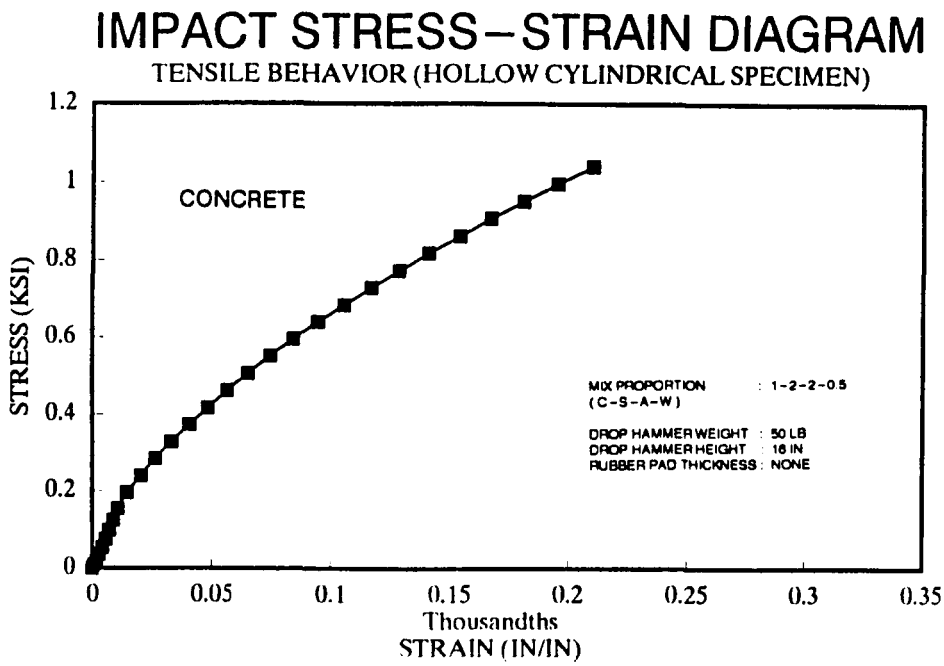

Figure B.29 Stress-strain relation of concrete specimen with 50 Lb hammer weight, 16 in hammer height, and no rubber-pad under impact tensile load.

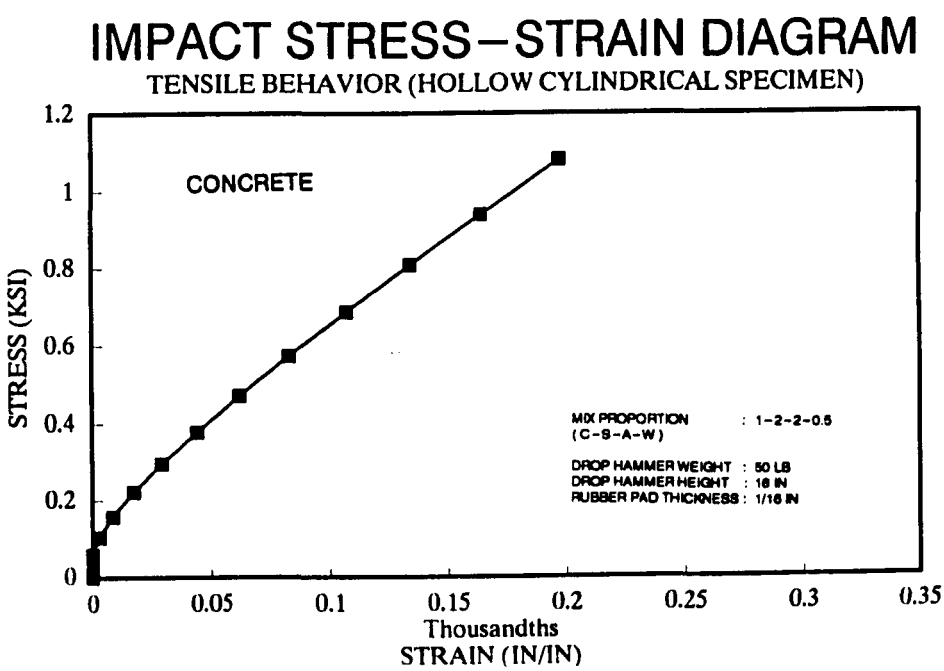

Figure B.30 Stress-strain relation of concrete specimen with 50 Lb hammer weight, 16 in hammer height, and 1/16 in rubber-pad thickness under impact tensile load.

Reproduced with permission of the copyright owner. Further reproduction prohibited without permission.

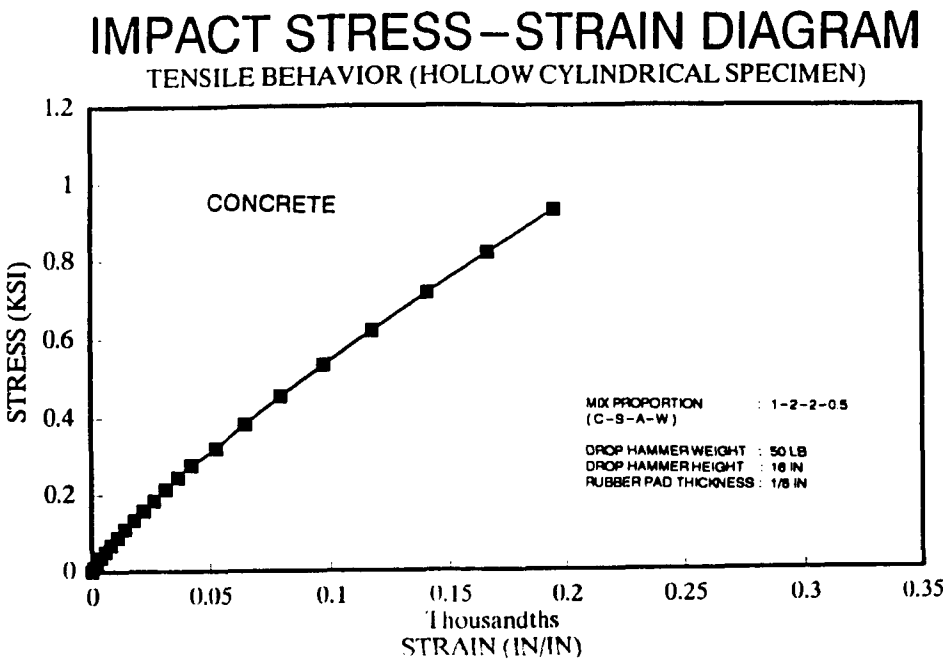

Figure B.31 Stress-strain relation of concrete specimen with 50 Lb hammer weight, 16 in hammer height, and 1/8 in rubber-pad thickness under impact tensile load.

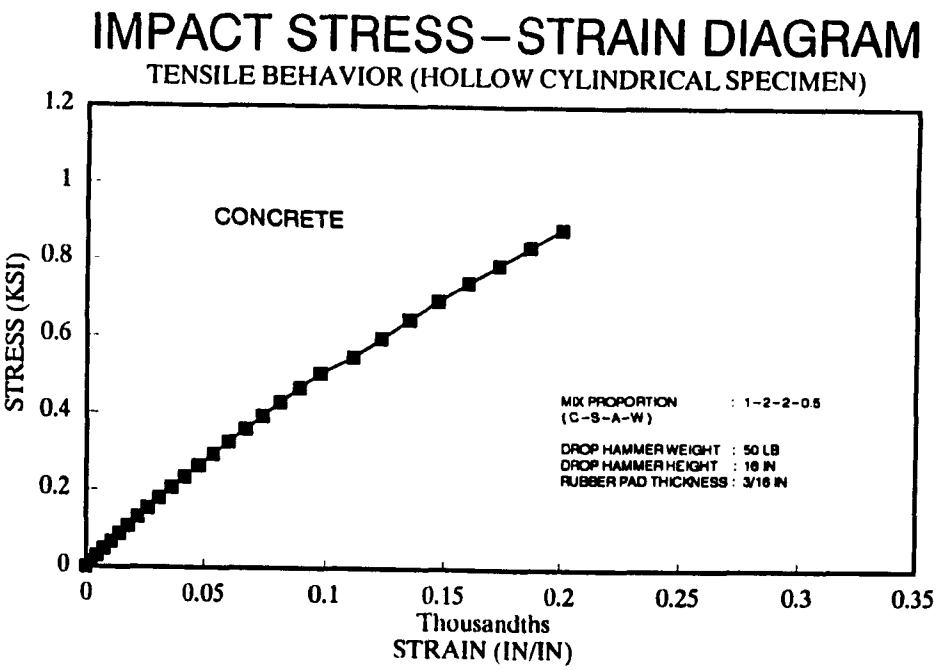

Figure B.32 Stress-strain relation of concrete specimen with 50 Lb hammer weight, 16 in hammer height, and 3/16 in rubber-pad thickness under impact tensile load.

Reproduced with permission of the copyright owner. Further reproduction prohibited without permission.

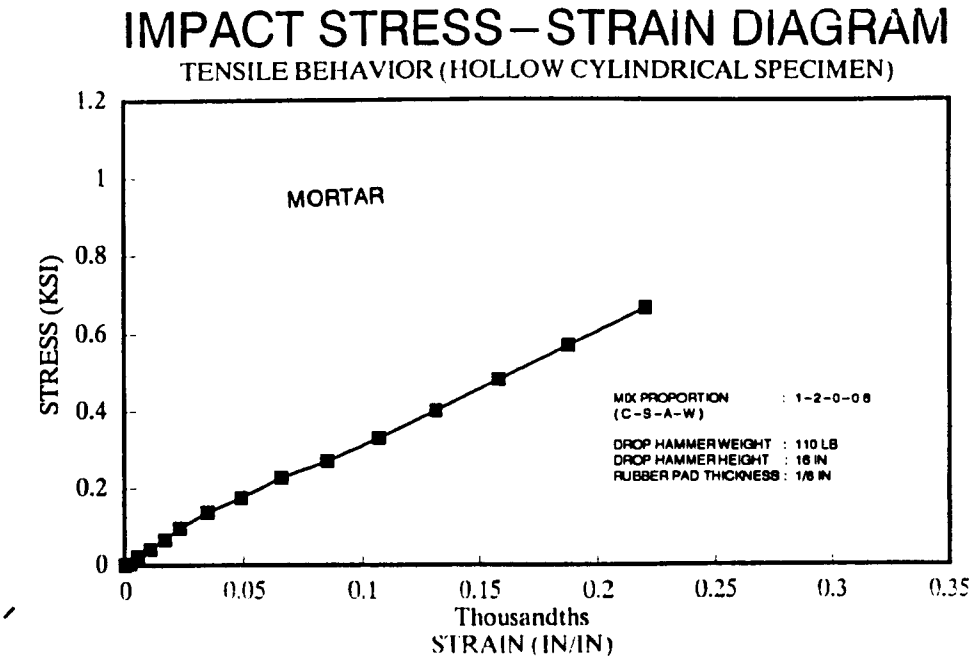

Figure B.33 Stress-strain relation of mortar specimen with 110 Lb hammer weight, 16 in hammer height, and 1/8 in rubber-pad thickness under impact tensile load.

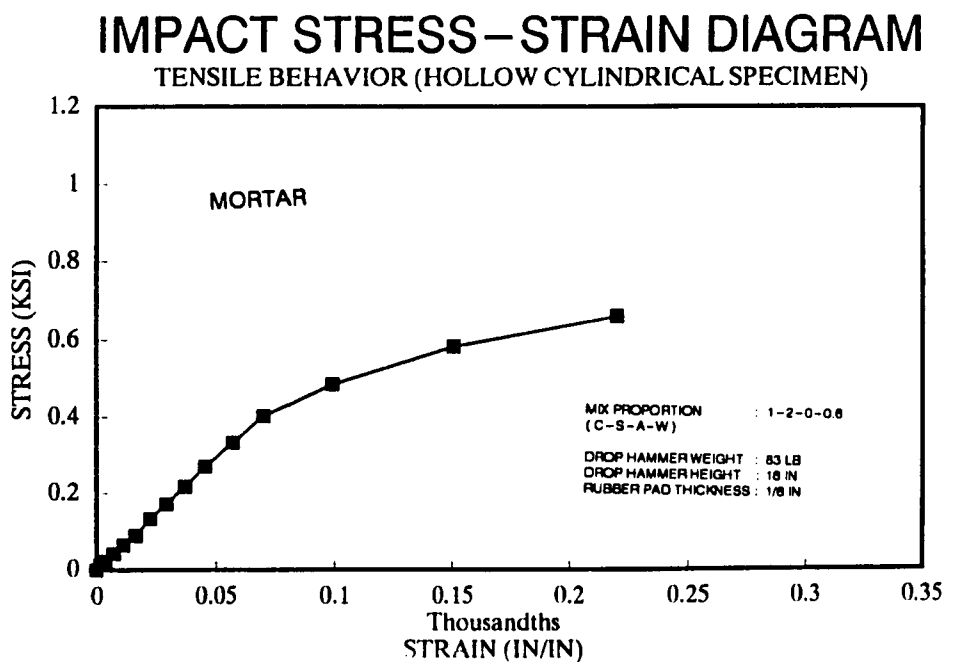

Figure B.34 Stress-strain relation of mortar specimen with 83 Lb hammer weight, 16 in hammer height, and 1/8 in rubber-pad thickness under impact tensile load.

Reproduced with permission of the copyright owner. Further reproduction prohibited without permission.

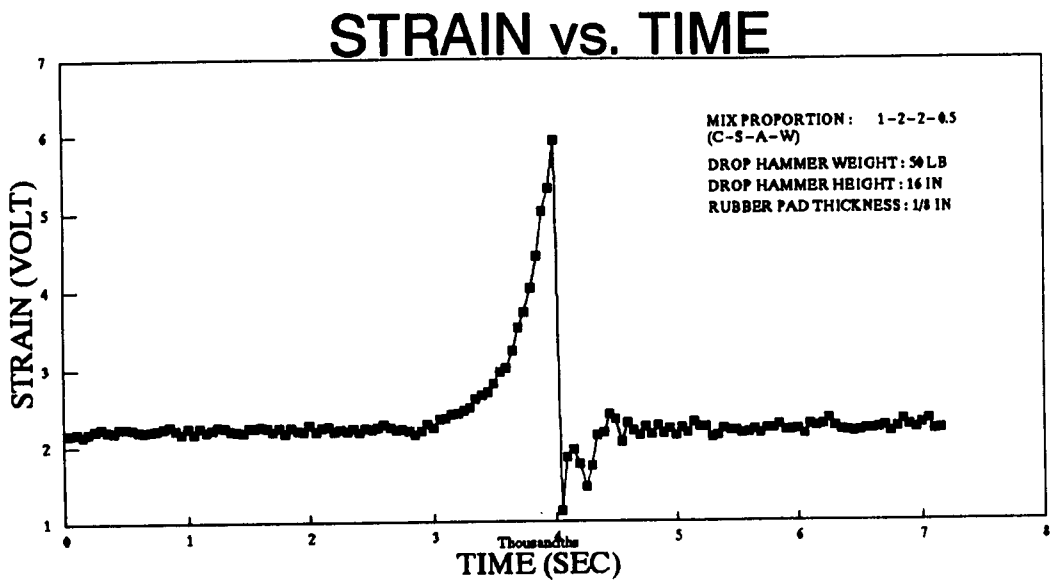

Figure B.35 Typical strain-time response of proposed hollow cylindrical specimen.

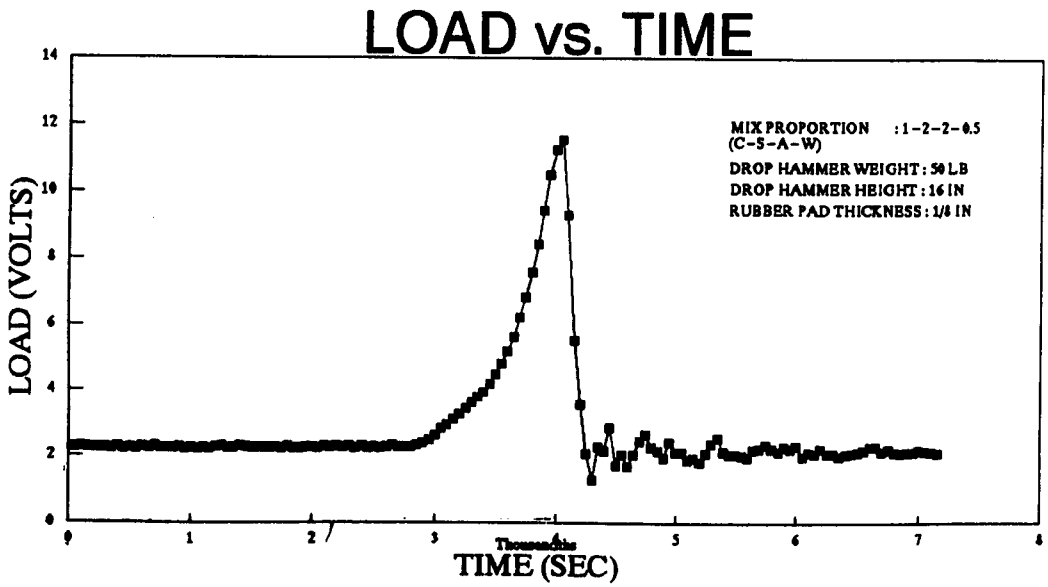

Figure B.36 Typical load-time response of proposed hollow cylindrical specimen.

Reproduced with permission of the copyright owner. Further reproduction prohibited without permission.